



Review of Critical Heat Flux (CHF) in Jet Impingement Boiling

V.S. Devahdhanush, Issam Mudawar*

Boiling and Two-Phase Flow Laboratory (PU-BTPFL), School of Mechanical Engineering, Purdue University, 585 Purdue Mall, West Lafayette, IN 47907, USA

ARTICLE INFO

Article history:

Received 13 November 2020

Revised 26 December 2020

Accepted 29 December 2020

Available online 6 February 2021

Keywords:

jet impingement

critical heat flux (CHF)

flow boiling

thermal management

ABSTRACT

Jet impingement boiling is a popular thermal management technique that caters to applications demanding very high heat dissipation rates. Like other boiling schemes, critical heat flux (CHF) is arguably the most important safety parameter for two-phase jet cooling, and determining CHF is often the starting point in a system's thermal design process. This article presents a systematized review of articles addressing jet impingement CHF. A very comprehensive search for studies is conducted, which includes research spanning over five decades and jets of various fluids, operating conditions, and geometrical configurations. Comprehensive lists of experimental jet CHF studies are given with detailed information on fluid, geometrical parameters, operating conditions, and notable conclusions. Parametric effects on CHF are also discussed in a systematic manner. Various techniques for increasing CHF, such as surface modification (including surface curvature, extended surface structures, surface coatings, or combinations thereof), specialized spent fluid removal schemes, and nanofluids, are discussed. An exhaustive list of CHF correlations is provided, along with the development rationale and applicability range for each. Also discussed are CHF trends for hybrid cooling schemes which combine jet impingement with other boiling schemes such as channel flow. The review is concluded with major conclusions and recommendations for future work.

© 2021 Elsevier Ltd. All rights reserved.

1. Introduction

1.1. Two-phase Thermal Management of High Heat Flux Devices

Thermal management is of utmost importance to all heat-dissipating devices, providing reliable and safe operation and prolonged lifespan. Several decades ago, cooling technologies employing natural and forced convection of air and single-phase liquids met the requirement of safely removing the heat. However, recent improvements in device performance, coupled with a constant pursuit of more compact and lightweight packaging has led to alarming increases in rate of heat dissipation per device surface area and per volume of cooling package. For example, heat dissipation from supercomputing chips began to exceed 100 W/cm^2 as early as the mid-1980s [1]. And, by the early 2000s, specialized high-performance devices emerged with heat dissipation requirements in excess of 1000 W/cm^2 [2]. Thermal management of these devices, unfortunately an after-thought in electronic system design in most cases, was no longer possible with single-phase cooling technologies. This trend shifted emphasis to two-phase thermal management solutions, which employ a closed cooling loop wherein boiling is used to remove heat from the devices and condensa-

tion to reject the heat from the loop to ambient air (or water in naval applications). Like their single-phase counterparts, two-phase technologies can take advantage of the coolant's sensible heat, but their effectiveness is rooted mostly in utilization of the coolant's latent heat.

Various schemes for implementing phase change in thermal management systems exist. Since the mid-1980s, investigators at the Purdue University Boiling and Two-Phase Flow Laboratory (PU-BTPFL) have explored as well as developed several such schemes, including ones utilizing capillary flow [3], pool boiling thermosyphons [4], falling film [5], macro-channel flow boiling [6], micro-channel flow boiling [2,7,8], spray cooling [9–11], and jet impingement cooling [11–18]. Of these different schemes, three are considered most effective for high heat flux applications: micro-channels heat sinks, sprays, and impinging jets [19]. Each of the three offers fundamental performance merits but also suffers from well-known disadvantages. For example, micro-channel heat sinks, typically containing an array of parallel channels in a highly conductive substrate or within the device itself, can yield very high heat transfer coefficients and both compact and lightweight packaging. However, they are prone to high pressure drop (which might lead to high compressibility and flashing, and even choking), large temperature gradients along the flow direction, and two-phase flow instabilities (e.g., severe pressure oscillation and parallel channel instability) [20]. Sprays offer high heat transfer coefficients and a more uniform surface temperature for relatively large surfaces.

* Corresponding author.

E-mail address: mudawar@ecn.purdue.edu (I. Mudawar).

URL: <https://engineering.purdue.edu/BTPFL> (I. Mudawar)

Nomenclature

A	area
A_r	ratio of total nozzle area to heated surface area
C, C_1, C_2, \dots	coefficients/constants in correlations
c_p	specific heat at constant pressure
D	diameter
Fr	Froude number
G	mass velocity
G_r	crossflow-to-jet mass velocity ratio
g	gravitational acceleration
g_c	Newton constant
H	jet height (jet nozzle-to-surface distance)
h	enthalpy; heat transfer coefficient
h_{fg}	latent heat of vaporization
Ja	Jakob number (definition varies between studies)
k	thermal conductivity
L	length
M	molecular weight; molar mass
\dot{m}	total mass flow rate
N	number of jets
n	number of datapoints
P	pressure
P_R	reduced pressure, $P_R = P/P_{crit}$
Pe	Peclet number
Q_v	volumetric flow rate
q''	heat flux
q''_{CHF}	critical heat flux
r	surface roughness factor
R	universal gas constant
R_a, R_q	average surface roughness parameters (arithmetic, root-mean-square)
R_s	radius of curvature of surface
Re	Reynolds number
T	temperature
ΔT_{sat}	surface superheat, $\Delta T_{sat} = T_s - T_{sat}$
ΔT_{sub}	fluid subcooling, $\Delta T_{sub} = T_{sat} - T_f$
U	velocity
V	voltage
W	width
W_w	half-width of microchannel walls
We	Weber number
x_e	thermodynamic equilibrium quality

Greek symbols

α	thermal diffusivity
Γ	jet radius reduction coefficient
δ	liquid sublayer thickness
ε	effectiveness
θ	impingement angle for oblique jets
θ_{CA}	solid-liquid contact angle
λ_c	capillary length, $\lambda_c = \sqrt{\sigma/g(\rho_f - \rho_g)}$
μ	dynamic viscosity
ν	kinematic viscosity
ρ	density
σ	surface tension
ϕ_s	solid fraction
ψ	empirical constant in Helmholtz instability criterion
ω	Pitzer's acentric factor

Subscripts

amb	ambient
c	unit jet cell

ch	channel
$char$	characteristic
$crit$	critical
f	liquid
g	vapor
in	inlet
n	jet nozzle exit; each nozzle
out	outlet
$pool$	liquid pool; pool boiling
s	surface; solid
sat	saturation
sc	subcooled
sub	subcooling
tot	total
$trans$	transition
z	local

Acronyms

CHF	Critical Heat Flux
DHLM	Developing Homogeneous Layer Model
DNB	Departure from Nucleate Boiling
EHD	Electrohydrodynamic
ONB	Onset of Nucleate Boiling
ONBD	Onset of Nucleate Boiling Degradation

But cooling system designers are often reluctant to use sprays due to their complexity of implementation and dependence of performance on an unusually large number of parameters [21]. Additionally, both corrosion and erosion effects in spray nozzles can compromise long-term repeatability of cooling performance. The present review article is concerned entirely with jet impingement cooling.

1.2. Jet Impingement Cooling Schemes

Jet impingement refers to the injection of a fluid onto a heated surface, through one or multiple nozzles. Jets are characterized by a uniform velocity high-speed central region called *potential core*, which is surrounded by a lower speed *free jet zone*. At the point where they strike the surface, they form a *stagnation zone*, which is surrounded by a *wall jet zone*, the latter is the result of fluid spreading on the surface. The earliest studies on jet impingement focused on gases (mostly air), which were either introduced from a compressed gas cylinder/line or directly from the atmosphere using a blower or compressor [22]. But attention later shifted to using liquids such as water and dielectric coolants to take advantage of their superior thermophysical properties. Pursuit of enhanced cooling performance to cater to high heat flux applications led researchers to combine the use of liquid jet impingement and boiling in the early 1970s [23].

Jet impingement boiling has numerous applications in both heat-flux-controlled and temperature-controlled cooling applications. Some examples of the former include electronic chips, power electronics, electrical actuators, avionics, and lasers, while the latter includes metal alloy processing and heat treatment processes such as forging, extrusion, and casting.

Some well-known advantages of jet impingement boiling compared to other high-performance cooling schemes are (i) comparatively low pressure drop, (ii) negligible dependence of pressure drop on heat flux, (iii) ability to maintain fairly uniform surface temperature for large surface areas by use of multiple jet arrays, (iv) ability to cool complex device shapes and multiple devices using a single cooling system, and (v) suitability for both microgravity [24,25] and high-body-force environments [16,17] due to their reliance on high flow inertia. On the other hand, jet impingement

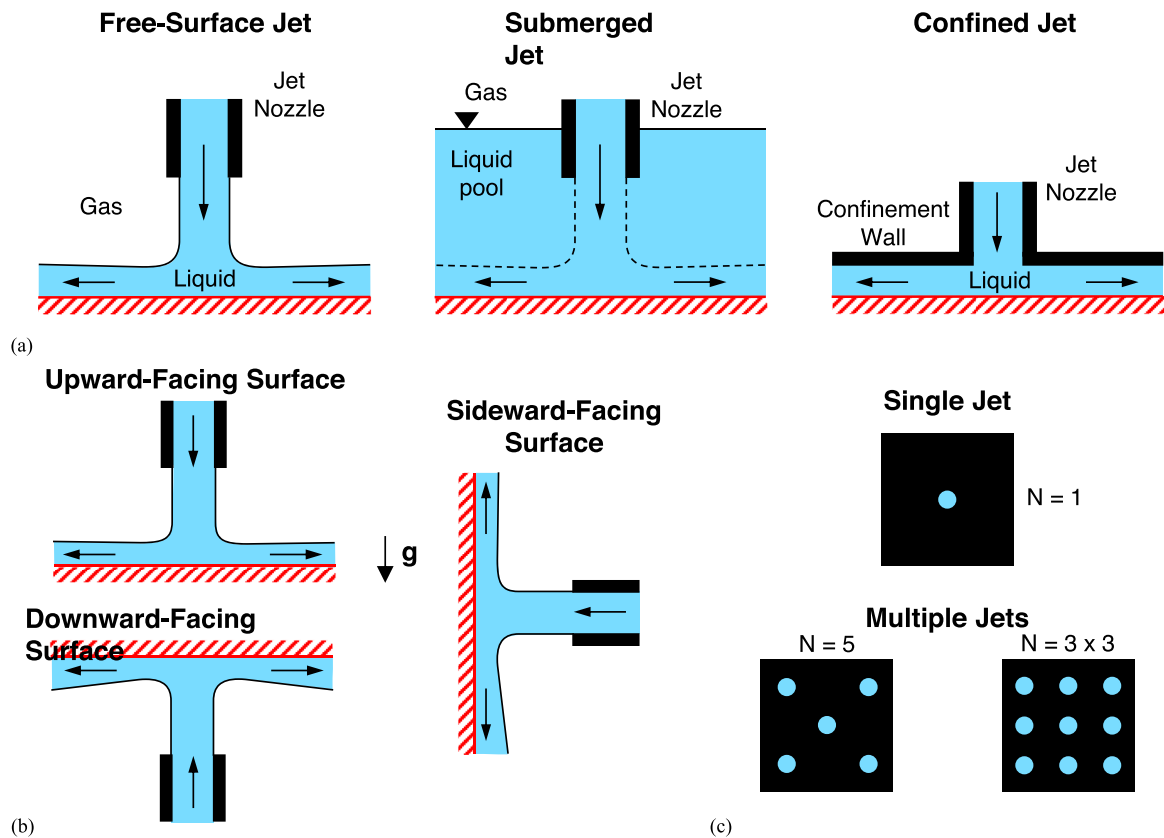


Fig. 1. Schematics of jet impingement geometrical configurations: (a) free-surface, submerged and confined jets, (b) upward-, downward- and sideward-facing heated surface orientations, and (c) examples of both single and multiple jets.

poses important drawbacks, including (i) need for a high-flow-rate pumping system, (ii) potential for device damage due to high impact and frictional shear stresses at the surface, and (iii) potential for flow instabilities caused by wall jet interactions when using multiple jets.

1.3. Jet Impingement Geometrical Classifications

Liquid impinging jets can be classified into three categories: *free-surface* [26], *submerged* [27], and *confined* [12], as illustrated in Fig. 1(a). *Free-surface jets* are the most common and for which heat transfer literature is abundant; they involve the introduction of liquid onto a heated surface amidst a gaseous medium (typically air). *Submerged jets* (or *immersed jets*) have the jet nozzle immersed under a pool of the same liquid, the top surface of which could be exposed to a gas or vapor. Submerged jets are subject to higher shear stresses than free-surface jets. *Confined jets* involve the injection of fluid into a confined space above the heating surface. The confinement wall is typically part of the jet nozzle plate and is generally parallel to the heating surface. For confined jets, far away from the stagnation zone, wall jets within the confinement region display characteristics similar to those for channel flow.

Denotation of flow orientation with respect to gravity is important in two-phase flows owing to the large density difference between the two phases and therefore buoyancy effects. In channel flow, the fluid flow is unidirectional, making it easier to define the flow orientation as vertically-upward, vertically-downward or horizontal [28]; whereas in jet impingement, defining flow orientation is more difficult, given the different possibilities for jet orientations, which are different from orientations of the spent fluid. Most jet studies are focused on normal (90°) impinging jets [29],

although a few are on oblique (or inclined) jets [30] and wall jets (fluid introduced parallel to the heated surface) [31]. Therefore, it is better to denote the flow geometry based on the heated surface itself. Illustrated in Fig. 1(b) are different orientations of the heating surface with respect to gravity. The surface could either be *upward-facing* or *downward-facing* (both horizontally oriented) [26] or *sideward-facing* (vertically oriented) [32].

As for the number of jets, most studies have focused on single jets, a key drawback of which is non-uniformity of surface temperature, especially for large surfaces. Multiple jets can help alleviate this problem as well as enhance the heat transfer performance. Examples of both single and multiple jets are illustrated in Fig. 1(c); with a typical single jet ($N=1$) at the center and multiple jets as both staggered ($N=5$) and regular ($N=3 \times 3$) arrays of equal spacing. It is noted that various other jet locations and configurations have also been studied.

1.4. Critical Heat Flux

The above-mentioned benefits of boiling flows are only valid in the nucleate boiling regime, which is characterized by formation, growth, and departure of vapor bubbles, while a significant portion of the heating surface maintaining contact with bulk liquid. The upper limit of this flow regime is termed Critical Heat Flux (CHF), marked by a serious degradation in heat transfer coefficient due to loss of liquid access to the heating surface. CHF is detected when a small increase in surface heat flux results in an unsteady and uncontrollable increase in surface temperature, which may lead to burnout and potential permanent damage to the device. Exceeding CHF leads to a transition to the film boiling regime wherein the entire surface is encased in vapor, which precludes any further liq-

uid essential to maintaining the nucleate boiling. During film boiling, liquid-to-vapor phase change occurs at the interface between the vapor film and liquid. Owing to poor thermal conductivity of the vapor, heat transfer in this regime is quite poor and surface temperature highly elevated. Therefore, CHF is the most important design parameter for a phase change cooling system involving heat-flux-controlled devices. In fact, determining the magnitude of CHF is typically the starting point in designing a two-phase thermal management system. From a design standpoint, best cooling performance is realized by maintaining cooling performance well within the nucleate boiling regime but safely below CHF.

Boiling CHF can be classified as either *saturated* or *subcooled*, based on the state of fluid exit condition (*i.e.*, thermodynamic equilibrium exit quality, $x_{e,out}$). A saturated CHF occurs when the fluid exits the heat sink in a saturated state ($0 \leq x_{e,out} \leq 1$), irrespective of whether the fluid enters the heat sink in a subcooled or saturated state. This is generally encountered with operating conditions such as low flow rate or low inlet subcooling.

It is interesting to note that micro-channels are more prone to saturated CHF owing to their large length-to-diameter ratio; CHF here manifests as *complete dryout* of liquid film along the channel walls [33]. On the other hand, subcooled CHF occurs when the fluid exits the heat sink in a subcooled state ($x_{e,out} < 0$), which implies that the fluid enters in a subcooled state as well. This is generally encountered in operating conditions such as high flow rate and high inlet subcooling and is manifest as *localized dryout* patches on the heating surface; this is especially the case with heat sinks with small length-to-diameter ratio.

Both types of CHF also manifest in jet impingement boiling depending on operating conditions (*e.g.*, pressure, inlet subcooling, jet velocity) and geometry (*e.g.*, jet diameter, number of jets, surface size), as detailed in the present authors' prior experimental study [18]. Subcooled CHF is generally preferred because of (i) better heat transfer performance in the nucleate boiling regime, (ii) higher CHF values resulting from strong condensation effects in the bulk fluid, and (iii) with subcooled fluid conditions at both inlet and outlet, ability to employ a rather simple single-phase liquid flow loop.

1.5. Objectives of the Present Review

Some past review articles on jet impingement are listed in Table 1 along with their foci. It is apparent that most of these articles are focused on single-phase gas and liquid jets, and some discuss both single- and two-phase jets with an emphasis on the former. There are very few articles that discuss two-phase jets in detail. And there are none (that we know of) that discuss exclusively research progress related to CHF in jet impingement boiling, for which research findings have been published since the 1970s. With around five decades of research on this specific heat transfer problem, the authors believe that the heat transfer community can greatly benefit from a systematized review. A comprehensive and exhaustive search for studies on jet CHF is conducted. This includes studies of jets of various fluids and different operating conditions and geometrical configurations. Both conventional gravity-head-driven and pumped jets are included, along with electrohydrodynamic (ionic) jets and vapor compression cycle adaptations. Various techniques of enhancing CHF, such as surface modification and specialized spent fluid removal, are discussed. Also included are CHF observed in *hybrid cooling* schemes that jet impingement is a part of. It is noted that only steady state CHF is discussed in this article, while CHF encountered during rapid transient quenching processes is excluded.

To aid the reader, comprehensive lists of studies on CHF for round and slot jets are given in Tables 2 and 3, respectively, along with detailed information concerning individual ex-

periments; these are further categorically discussed in sections 2, 3 and 4. An exhaustive list of jet CHF correlations is given in Table 4 with a gist in section 5. Section 6 and Table 5 include CHF for hybrid cooling schemes. Finally, the review is concluded with some noteworthy remarks on experimental jet impingement CHF measurement, and overall observations and recommendations.

2. CHF for Typical Round and Slot Jets

Critical heat flux for typical (conventional) jet configurations are discussed in this section. These include both round (circular) and slot (planar, rectangular) jets impinging normally onto a flat heated surface. All jet types such as free-surface, submerged, and confined jets as well as both single jets and jet arrays are considered. The liquid jets are forced by a pressure differential created by either a pump or a large gravitational head. Although the effects of each parameter are discussed separately in different sub-sections, it is noted that CHF is combinedly affected by one or many parameters simultaneously (*i.e.*, effects of one parameter on CHF might be affected by those of other parameters).

2.1. Submerging and Confinement Effects

Amongst the three commonly used types of jet impingement (free-surface, submerged, and confined), confined jets typically give the highest CHF values. Illustrations of fluid behavior during boiling of free-surface and confined jets are given in Fig. 2. During free-surface jet boiling, the upwards momentum created by vapor bubble production and growth at the wall leads to serious splashing of liquid [26,29,34–36]. Splashing has been seen to increase with increasing surface heat flux, slowly depleting the surface of fresh liquid supply. CHF is triggered when liquid film contact with the heated surface is locally removed, leading to dryout patches. This is typically seen at points farthest from the stagnation zone. Using direct surface heating by alternating current, Katto and Monde [35,36] devised a 'droplet catcher' to measure the mass of liquid lost to splashing and found that the fraction of mass flow rate lost to splashing increased almost linearly with increasing heat flux until ~ 0.4 – 0.5 after which it remained constant until burnout was observed. They also noted that the amount of liquid vaporized at the surface was negligible compared to splashing. In their subsequent study [26,34] using indirectly heated surface (electric heating elements embedded within a copper heating block), they noticed the splashing mass fraction reached ~ 0.8 – 1.0 near CHF and attributed the differences in values between their studies to the method of heating. Directly heating with alternating current was thought to induce periodic fluctuation in q'' and affected the splashing fraction; however, both nucleate boiling data and CHF remained unaffected. In either case, it can be concluded that free-surface jets are prone to splashing and this decreases CHF significantly.

But, for confined jet boiling, the typically parallel confinement wall resists liquid movement away from the wall and enforces liquid contact for a longer downstream distance from the impingement center, as shown in Fig. 2. Farther away from the stagnation zone, the confined wall jets behave like channel flow, where increased void fraction causes flow acceleration towards the outlet plenum.

Submerged jets lie between free-surface and confined jets, with the submerged jet boiling often described as pool boiling with jets helping remove the produced vapor from the heated surface. Many studies [29,37,38] have demonstrated the effectiveness of submerged jets at enhancing pool boiling CHF. Results from most studies [29,39,40] also show submerged jets yield higher CHF values than free-surface. For example, Katto and Kunihiro [29] compared the performances of free-surface and submerged jets with

Table 1
Foci of some past review articles on jet impingement.

Author(s)	Year	Focus
Single-phase gas and liquid jets		
Martin [145]	1977	Heat and mass transfer of single-phase gas jets; both single and multiple jets
Polat <i>et al.</i> [146]	1989	Numerical studies of both laminar and turbulent single-phase jets
Jambunathan <i>et al.</i> [147]	1992	Single-phase gas single circular turbulent jets
Viskanta [148]	1993	Single-phase isothermal turbulent air and flame jets; both single and multiple jets
Webb & Ma [149]	1995	Single-phase liquid jets
Han & Goldstein [150]	2001	Single-phase jets related to gas turbine systems; both single and multiple jets
Zuckerman & Lior [151]	2005	Single-phase jets related to gas turbine systems; emphasis on numerical simulation techniques
Zuckerman & Lior [152]	2006	Single-phase jets; both experimental and numerical studies with emphasis on the latter
Weigand & Spring [153]	2011	Multiple single-phase air jets; both experimental and numerical
Dewan <i>et al.</i> [154]	2012	Computational studies of turbulent single-phase jets
Sarkar <i>et al.</i> [155]	2014	Single-phase air jets related to food processing; both single and multiple jets
Carlomagno & Ianiro [156]	2014	Single-phase submerged jets with short nozzle-to-plate distances; both experimental and numerical
Both single- and two-phase jets		
Ma <i>et al.</i> [157]	1993	Both single-phase and liquid jets, with an emphasis on round jets
Lienhard [158]	1995	Both laminar and turbulent single-phase liquid jets; few boiling studies
Cho <i>et al.</i> [159]	2011	Single-phase gas and liquid jets; two-phase jets; both single and multiple jets
Molana & Banooni [160]	2013	Liquid jets (including nanofluids); mostly single-phase, but some two-phase studies; both single and multiple jets; both experimental and numerical
Mohammadpour & Lee [161]	2020	Nanofluid jets with and without boiling; both experimental and numerical
Two-phase jets		
Wolf <i>et al.</i> [162]	1993	Nucleate boiling, CHF, transition boiling, and film boiling
Qiu <i>et al.</i> [163]	2015	Nucleate boiling, ONB, and CHF; emphasis on experimental studies with some theoretical and numerical ones; review of 1993-2014 studies
Fan & Duan [164]	2020	Two-phase submerged and confined jets related to electronics cooling; pool boiling also discussed

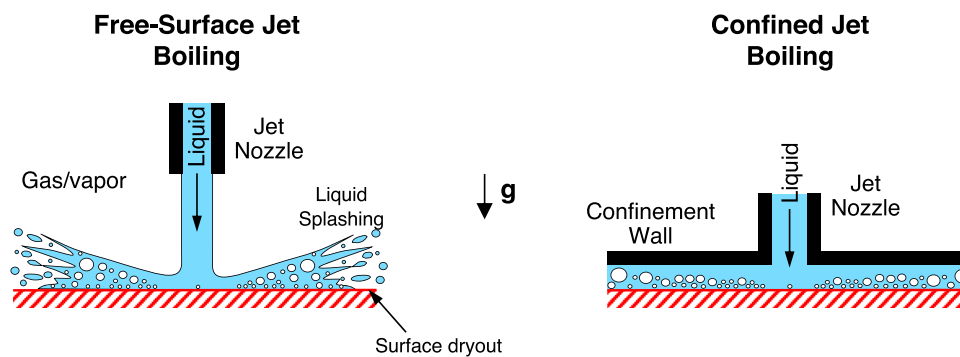


Fig. 2. Schematics illustrating advantages of confined jet impingement boiling over free-surface jets.

$D_n = 0.71 - 1.60$ mm and equal jet-to-surface distance of $H = 1 - 30$ mm impacting a circular heated surface of $D_s = 10$ mm. The submerged jets yielded higher CHF, especially for $H = 1 - 3$ mm, and differences increased for faster jets. Monde and Furukawa [39,40] experimented with single round jets of fixed nozzle-to-surface distance of $H = 5$ mm, but the liquid pool depth, H_{pool} , was varied from 0 to 8 mm. Highest CHF was obtained with the largest H_{pool} of 8 mm, clearly exceeding free-surface jet values. But this might not be true for all geometries. For example, Robidou *et al.* [41] conducted experiments with single slot jets ($A_n = 1 \times 9$ mm²) of water impinging onto a $\sim 80 \times 10$ mm² surface at an asymmetrical location ~ 15 mm from one edge of the surface. Localized stagnation line CHF was found to decrease when a 100-mm-deep liquid pool was used, which they attributed to deep pool decreasing impact velocity due to dissipation of momentum to surrounding fluid. However, heat transfer performance did increase in regions far away from the stagnation line.

2.2. Effects of Jet Velocity

Jet velocity is perhaps the most widely studied parameter that affects CHF. Almost all studies [18,29,35,36] point to CHF augmentation with increasing jet velocity for all jet types. This can be attributed to faster liquid jets more effectively piercing the vapor layer atop the heated surface. Continued liquid access to the sur-

face yields a broader nucleate boiling range by delaying CHF. However, some studies [18,42] which included broad ranges of jet velocity showed the CHF augmentation with increasing jet velocity is remarkable only at lower velocities but tapers off at high velocities.

Several studies by Katto, Monde and their co-workers [42–47] showed the existence of four different jet CHF regimes: V-, I-, D-, and HP-regimes, demarcated mostly by jet velocity, U_n . The D-regime was observed at very low velocities, where CHF was primarily the result of deficiency of liquid supply leading to complete vaporization with no splashing. This D-regime [42] was referred to as L-regime in a later study by Monde and Okuma [43], who pointed out its prevalence for very large heated surface to jet diameter ratios (D_s/D_n) in addition to very low velocities, and considered the fraction of liquid lost to splashing in their CHF prediction model. The V-regime was prevalent at lower velocities, albeit higher than those of the D-regime, where CHF was observed to increase with increasing jet velocity. I-regime was prevalent at higher velocities and/or moderate pressures, where CHF became almost or fully independent of jet velocity. Finally, the HP-regime was prevalent at high pressures where CHF regained dependence on jet velocity. Both D- and V- regimes were observed in experiments at atmospheric pressures, whereas the I- and HP- regimes at elevated pressures. Variation of CHF with velocity for different saturation pressures and heated surface areas is shown in Fig. 3. These plots include data for free-surface single round jets of R-

Table 2
Summary of experimental studies on CHF in round jet impingement boiling.

Author(s)	Fluid(s)	Jet Geometry ^a	Heated Surface Geometry ^b	Operating Conditions	Remarks and Major Conclusions
Copeland (1970) [23]	Water	F* $D_n = 0.279, 0.394$ mm $L_n/D_n = 70$ $H/D_n = 23 - 28$	▼ Copper plated with 25- μ m nickel $D_s = 19.1$ mm Sides of heater block not insulated	$U_n = 0.91 - 7.22$ m/s $\dot{m} = 0.227 - 3.674$ kg/hr $P_{sat} \approx 1$ atm $T_{in} = 20 - 96.11^\circ\text{C}$ $T_{amb} \approx 22.22^\circ\text{C}$	$q''_{CHF} \approx 59.94 - 315.46$ W/cm ² ; two burnout types: oversupply and thermal; oversupply due to more heat input than that could be removed by complete vaporization of jet; thermal characterized by a peak heat flux of 189.28 W/cm ² ; both burnout mechanisms interact with each other, leading to lower q''_{CHF}
Katto & Kunihiro (1973) [29]	Water	F*, S* $D_n = 0.71, 1.165, 1.60$ mm $H = 1 - 30$ mm $H_{pool} = 0 - 30$ mm	▲ Copper $D_s = 10$ mm Polished with emery #0	Gravity-head-driven flow $U_n \leq 3$ m/s $\dot{m} = 0, 58 - 270$ g/min $P_{sat} = 1$ atm $\Delta T_{sub,in} \leq 3^\circ\text{C}$	CHF of pool boiling is augmented with jets; burnout occurs due to liquid splashing caused by blowing up of generated vapor at the surface; CHF increases with increasing U_n
Ishigai & Mizuno (1974) [165]	Water	F* $D_n = 5.7 - 17$ mm	▲ Stainless-steel $A_s = 8 \times 12$ mm ² Directly heated	$U_n = 1.3 - 9.0$ m/s $\Delta T_{sub,in} = 45 - 80^\circ\text{C}$	Details from Wolf <i>et al.</i> [162]
Katto & Monde (1974, 1975) [35,36]	Water	F* $D_n = 2$ mm	▲ 14%-Cr stainless steel $A_s = 8 \times 8$ mm ² 80- μ m-thick foil directly heated by AC	$U_n = 5 - 60$ m/s $Re_{Dn} \leq 4040$ $P_{sat} = 1$ atm $\Delta T_{sub,in} \approx 3^\circ\text{C}$	CHF relates to separation of liquid flow from heated surface; CHF increases with increasing U_n
Katsuta (1977) [166]	R-113	F* $D_n = 1.99, 2.40, 3.81$ mm	▲ Copper $D_s = 15, 20, 25$ mm	$U_n = 0.54 - 3.84$ m/s $Q_v = 0.37 - 2.63$ L/min $\Delta T_{sub,in} = 0.82 - 12.54^\circ\text{C}$	
Monde & Katto (1977, 1978) [26,34]	Water, R-113	F* $D_n = 2.0, 2.5$ mm $H = 0.3, 0.5$ mm	▲▼ Copper $D_s = 10 - 21$ mm polished with emery #0	$U_n = 1 - 30$ m/s $P_{sat} = 1$ atm $\Delta T_{sub,in} = 3 - 30^\circ\text{C}$	Dryout starts at outermost edges of heated surface
Katto & Shimizu (1979) [42]	Water, R-22, R-113	F* $D_n = 2$ mm	▼ Copper $D_s = 10$ mm	$U_n < 20$ m/s $P_{sat} = 6.0 - 27.9$ bar (R-22), 1 atm (others) $\Delta T_{sub,in} \approx 0^\circ\text{C}$	Explained presence of 4 CHF regimes: V-regime (CHF dependent on velocity, seen at lower velocities), I-regime (CHF independent of velocity, seen at higher velocities), D-regime (CHF due to deficiency of liquid supply leading to complete vaporization with no splashing, seen at very low velocities), and HP-regime (seen at elevated pressures)
Monde (1980) [167,168]	Water	F* $D_n = 0.7 - 4.15$ mm	▲ Copper $D_s = 11.9, 20.7, 25.5$ mm ($D_s/D_n = 5 - 36.4$) Impingement at center or at eccentric positions	$U_n = 0.3 - 15$ m/s $P_{sat} = 1$ atm $\Delta T_{sub,in} = 10^\circ\text{C}$ (for $D_n = 0.7$ mm), $3 - 5^\circ\text{C}$ (others)	CHF is strongly influenced by location of impingement on heated surface, and weakly affected by diameter ratio, D_s/D_n
Monde <i>et al.</i> (1980) [66,67]	Water, R-113	F** $N = 2 - 4$ (combination of 11 impingement locations)	▲▼ Copper $D_s = 25.2$ mm	$U_n = 1 - 20$ m/s $P_{sat} = 1$ atm $\Delta T_{sub,in} = 3 - 5^\circ\text{C}$	Burnout takes place at locations within the jet cell farthest away from the jet center
Katsuta & Kurose (1981) [123]	Water, R-113, R-11	F* $D_n = 1.99 - 3.81$ mm	▲ Copper $D_s = 15, 20, 25$ mm Polished with emery #800 - #0/6	$U_n = 0.50 - 3.84$ m/s $Q_v = 0.31 - 2.63$ L/min $\Delta T_{sub,in} = 0.82 - 12.5^\circ\text{C}$ (R-113), $\approx 0^\circ\text{C}$ (others)	0.02% wt. Rapisool B-80 surfactant added to water ($\sigma = 3.55 \times 10^{-2}$ N/m)
Ma & Bergles (1983) [89]	R-113	S* $D_n = 1.067$ mm $H = 2$ mm	► Constantan $A_s = 5 \times 5$ mm ² 10- μ m-thick foil directly heated by DC power	$U_n = 1.08 - 2.72$ m/s $P_{sat} = 1$ atm $\Delta T_{sub,in} = 0 - 29.5^\circ\text{C}$	When jet is directed at heated surface center, burnout occurs at edges; when it is directed at one edge, burnout occurs at the opposite edge; CHF varies as cube root of U_n ; CHF weakly affected by subcooling for high subcoolings
Monde & Okuma (1985) [43]	Water, R-113	F* $D_n = 0.7 - 4.12$ mm $H = 3$ mm	▼ Copper $D_s = 40, 60$ mm ($D_s/D_n = 9.6 - 57.1$)	$U_n = 0.33 - 13.7$ m/s $P_{sat} = 1$ atm $\Delta T_{sub,in} < 3^\circ\text{C}$	Focused on L-regime of CHF, prevalent at very large D_s/D_n , in addition to very small velocities; same as D-regime by Katto and Shimizu [42]
Monde & Furukawa (1987, 1988) [39,40]	R-113	F*, S* $D_n = 1.1$ mm $H = 5$ mm $H_{pool} = 0, 1, 2, 4, 8$ mm	▲ Copper $D_s = 59.8$ mm	$U_n = 1.5 - 3.9$ m/s $P_{sat} = 1$ atm $\Delta T_{sub,in} \approx 0^\circ\text{C}$	Co-existence of pool boiling and jets was studied; below a pool height of 1 mm, jet CHF is not affected by the pool and predicted well by Monde's [87] correlation

(continued on next page)

Table 2 (continued)

Author(s)	Fluid(s)	Jet Geometry ^a	Heated Surface Geometry ^b	Operating Conditions	Remarks and Major Conclusions
Monde (1987) [44], Monde <i>et al.</i> (1986, 1987) [45,46]	Water, R-22, R-113	F* $D_n = 2$ mm $H = 10$ mm	▼ Copper $D_s = 10, 20, 40$ mm	$P_{sat} = 6 - 28$ bar (R-22), 1 - 6 bar (water), 1 - 3 bar (R-113) $\Delta T_{sub,in} \approx 0^\circ\text{C}$ $\rho_l/\rho_g = 5.3 - 1603$ $Q_v = (3.8, 6.3) \times 10^{-5}$ m ³ /s $\Delta T_{sub,in} \approx 0^\circ\text{C}$	I- and HP-regimes of CHF established from the data; I-regime: velocity independent CHF, seen at moderate pressures; HP-regime: CHF increases with increasing U_n , seen at high pressures
Kamata <i>et al.</i> (1987, 1988) [82,83]	Water	C* $D_n = 2.2$ mm $H = 0.3 - 0.6$ mm Nozzle plate (confinement wall) parallel to heated surface; free-flow at edges to atmosphere	▲ Copper $D_s = 20.0$ mm Polished with emery #1500	$Q_v = (4.4 - 7.5) \times 10^{-5}$ m ³ /s $\Delta T_{sub,in} \approx 0^\circ\text{C}$	Conducted both steady-state and transient experiments using same heater block (with former heated using electric heater and gas burner, and latter only using a gas burner till 400°C); most transient pool boiling curves match steady state curves, but CHF seems to be a bit higher than transient maximum heat flux; maximum heat flux of jets higher for lower H at fixed Q_v and for higher Q_v at fixed H
Kamata <i>et al.</i> (1987, 1988) [169,170]	Water	C* $D_n = 2.2$ mm $H = 0.3 - 0.6$ mm Nozzle plate (confinement wall) parallel to heated surface and has a 0.2-mm high circumferential brim; free-flow at the edges to atmosphere	▲ Copper $D_s = 20.0$ mm Polished with emery #1500	$Q_v = (4.4 - 7.5) \times 10^{-5}$ m ³ /s $\Delta T_{sub,in} \approx 0^\circ\text{C}$	Only transient boiling curves shown; maximum heat flux increases by ~45% with addition of circumferential brim; surface scale formation is smaller with a brim; other conclusions similar to [82,83]
Cho & Wu (1988) [171]	R-113	F* $D_n = 0.76$ mm $H = 13$ mm	► Copper $D_s = 20.5$ mm	$U_n = 0.7 - 8.2$ m/s $Q_v = 0.3 - 3.8$ cc/s	$q''_{CHF} = 21.7 - 54.1$ W/cm ² ; $n = 6$; CHF increases with increasing U_n
Nonn <i>et al.</i> (1988) [32]	FC-72	F*, F _s * $N = 1, 2 \times 2, 3 \times 3$ $D_n = 0.5, 1.0$ mm $H = 0.1 - 5.0$ mm	► Brass $A_s = 12.7 \times 12.7$ mm ² Single and arrays of 3 heat sources aligned horizontally or vertically	$U_n = 1.6 - 12.7$ m/s $T_{sat} = 56^\circ\text{C}$ $\Delta T_{sub,in} = 20 - 37^\circ\text{C}$	CHF is mainly influenced by velocity; jet array helps with T_s uniformity; suggestion of jet array combined with smaller jets is made; reducing jet plate-to-heated surface distance beyond a certain limit enhances CHF due to submerging/confinement effects; crossflow effects due to heat source array do not have a significant effect on boiling curve or CHF
Nonn <i>et al.</i> (1989) [61]	50-50% vol. FC-72/FC- 87 mixture	F*, F _s * $N = 1, 2 \times 2, 3 \times 3$ $D_n = 0.5, 1.0$ mm $H/D_n = 0.2 - 5.0$	► Brass $A_s = 12.7 \times 12.7$ mm ²	$U_n = 1.6 - 12.7$ m/s $T_{sat} = 41^\circ\text{C}$ (57°C for FC-72; 30°C for FC-87) $\Delta T_{sub,in} = 20 - 30^\circ\text{C}$	Data compared with pure FC-72 of Nonn <i>et al.</i> [32]; higher CHF at higher jet velocities; higher CHF is attained with smaller jet diameters than with increasing number of jets; CHF for this fluid mixture is lower than for pure FC-72 for similar conditions; CHF correlation for flow boiling in short channels gives good predictions of jet CHF
Maceika & Skema (1990) [56]	Water	S* $D_n = 3, 9, 18$ mm $H/D_n = 2 - 4$ $H_{pool} = 200$ mm	▲ Copper $W_s = 6$ mm $L_s/D_n = 0.5 - 8$ 30 μm-thick foil heated by DC	$U_n = 1 - 35$ m/s $T_f = 15 - 20^\circ\text{C}$	As L_s/D_n is increased from 0 (stagnation point), CHF peaks at 2 and then decreases monotonically because wall jet velocity is maximum at that point
McGillis & Carey (1990) [122]	R-113	C* single jet for each heater $D_n = 1$ mm $H = 1$ mm	► Copper $A_s = 6.4 \times 6.4$ mm ² 10 heat sources in vertical channel of width 12.7 mm; spacing between heat sources = 6.4 mm; 2 configurations: flush and 0.8-mm-protruding	$U_n = 0.46 - 3.08$ m/s $P_{sat} \approx 1$ atm $T_{sat} \approx 47.6^\circ\text{C}$ $\Delta T_{sub,in} = 1 - 40^\circ\text{C}$	Heater protrusion does not affect jet impingement CHF; CHF of heat source array increases with increasing U_n and $\Delta T_{sub,in}$; as U_n is reduced, CHF asymptotically approaches Kutateladze's [172] pool boiling CHF; good predictions with Nonn <i>et al.</i> 's [32] correlation for moderate to high U_n
Skema & Slanciauskas (1990) [57]	Water	S*, S _s * Staggered (X) and regular (+) jet arrays $D_n = 3, 9, 18$ mm Jet spacing = (3 - 11) D_n $H/D_n = 2 - 4$ $H_{pool} = 200$ mm	▲ Copper $W_s = 6 - 20$ mm $L_s = 9 - 20$ mm ($L_s/D_n = 0.5 - 8$) Directly heated by DC	$U_n = 1 - 35$ m/s $P_{sat} = 1$ atm + $\rho_f U_n^2/2$ $T_f = 15 - 20^\circ\text{C}$	CHF increases with increasing L_s/D_n until 2, after which, it monotonically decreases; CHF is lower at the interaction point of jet arrays than the stagnation point of a single jet for jet spacings > 4 D_n , but differences between the two are much smaller for spacings of (3-4) D_n ; CHF is higher for staggered arrays than regular

(continued on next page)

Table 2 (continued)

Author(s)	Fluid(s)	Jet Geometry ^a	Heated Surface Geometry ^b	Operating Conditions	Remarks and Major Conclusions
Ishimaru <i>et al.</i> (1991) [173]	Liquid nitrogen	S* (tube-in-tube) $D_n = 0.6$ mm $H = 0.6$ mm	► $D_s = 1.5$ mm Polished with emery #3000	$U_n = 0.22 - 1.34$ m/s $\dot{m} = 0.05 - 0.30$ g/s $\Delta T_{sub,in} \approx 0^\circ\text{C}$	Max. $q''_{CHF} = 1.2$ MW/m ²
Aihara <i>et al.</i> (1991, 1993) [78,79]	Liquid nitrogen	S* (tube-in-tube) $D_n = 0.8$ mm $H = 0.5 - 2.2$ mm	► Oxygen-free copper $D_s = 2.3$ mm 3 types: flat, concave with $R_s = 1.15$ mm, and flat with 3-mm-tall needle of base diameter 0.5 mm 3 surface finishes: machine, mirror, and emery #500	$U_n \approx 0.75 - 1.75$ m/s $\dot{m} = 0.30 - 0.64$ g/s $Re_{Dn} = 3500 - 8000$	Application in surgical cryoprobes; CHF increases with increasing U_n and decreasing H ; CHF is highest for concave surface, followed by flat surface with a needle for similar operating conditions; CHF for rougher surfaces (machine and emery #500) is slightly higher than for mirror finish
Copeland (1992, 1998) [59,60]	FC-72	C*, C** $N = 1 - 100$ $D_n = 0.25 - 1.0$ mm ($NA_n = 1.25 - 20$ mm ²) $L_n = 20$ mm (single), $5D_n$ (arrays)	▲ Silicon $A_s = 10 \times 10$ mm ²	$U_n = 0.25 - 8$ m/s $Q_v = 0.3 - 1.2$ L/min $T_{in} = 24^\circ\text{C}$ $\Delta T_{sub,in} = 32^\circ\text{C}$	$q''_{CHF} = 48 - 168$ W/cm ² ; CHF increases with increases in U_n and nozzle area; CHF is affected negligibly by N ; at very low velocities, CHF becomes a function of Q_v alone
Pais <i>et al.</i> (1993) [121]	Water	F** (rotating nozzle plate) $N = 4 - 9$ $D_n = 127 - 368$ μm $H = 11 \pm 1$ mm Speed = 0 - 2100 rpm	▲ OHFC copper $D_s = 11.3$ mm ($A_s = 1$ cm ²) Polished with emery #1/0; $R_q = 4.4$ μm	$U_n = 1.2 - 21$ m/s $Q_v = 1.1 - 4.7$ L/hr $P_{sat} \approx 1$ atm $T_{in} = 20 - 95^\circ\text{C}$	Max. $q''_{CHF} = 600$ W/cm ² ; heat flux (and hence CHF) increases appreciably with increases in both flow rate and inlet subcooling; no significant change is seen with respect to U_n , N or rotation speed for a fixed Q_v
Monde <i>et al.</i> (1994) [75,76]	Water, R-113, R-22	F* $D_n = 2$ mm	▼ Stainless steel $L_s = 40, 60$ mm $W_s = 7$ mm Foil directly heated by DC	$U_n = 4.2 - 33.9$ m/s $P_{sat} = 1 - 25$ bar $\Delta T_{sub,in} = 0 - 115^\circ\text{C}$ $\rho_l/\rho_g = 8.8 - 1605$	High subcooling achieved by varying both fluid temperature and P_{sat} (using nitrogen gas); flow model for jet subcooled boiling is proposed, and fully-developed nucleate boiling within the saturation zone is found to be identical to saturated boiling Discussed in Johns and Mudawar [16]
Johns (1994) [15]	FC-72	C* C** $N = 2 \times 2, 3 \times 3$ $D_n = 0.40, 0.79, 2.06$ mm $L_n/D_n = 1.91$ mm $H = 2.03$ mm	► Oxygen-free copper $A_s = 12.7 \times 12.7$ mm ² Vapor blasted with 10- μm slurry particles	$U_n = 0.056 - 4$ m/s $P_{sat} = 1.24$ bar $T_{sat} = 62.8^\circ\text{C}$ $\Delta T_{sub,in} = 10, 25, 40^\circ\text{C}$	L_n restricted by available space; CHF of jet arrays increases with increases in $\Delta T_{sub,in}$ and U_n ; CHF decreases with increasing N for fixed Q_v and D_n
Nakayama & Copeland (1994) [174]	FC-72				Jet data adapted from Copeland [59,60]
Estes & Mudawar (1995) [11]	FC-72	F* $D_n = 0.660 - 1.14$ mm	▲ Oxygen-free copper $A_s = 12.7 \times 12.7$ mm ² Polished	$U_n = 5.17 - 16.9$ m/s $Q_v = 3.03 - 17.3 \times 10^{-6}$ m ³ /s (0.048 - 0.275 gal/min) $P_{in} = 1.03$ bar $T_{sat} = 57.3^\circ\text{C}$ $\Delta T_{sub,in} = 13, 23, 33^\circ\text{C}$ $Q_v \approx 0.01 - 0.18$ L/min $P_{sat} = 101.3 - 276$ kPa $T_f = 77 - 78$ K $\Delta T_{sub,in} = 0.1 - 9.3$ K	$q''_{CHF} = 37 - 177$ W/cm ² ; increases in U_n and D_n enhance CHF; subcooling greatly increases CHF; recommend confined configurations over free-surface; premature dryout occurs when heat flux is increased too quickly; compared jets with spray cooling
Vader <i>et al.</i> (1995) [73]	Liquid nitrogen	C* $D_n = 0.52$ mm $H = 2.60$ mm	► Actual silicon chip $A_s = 6.5 \times 6.5$ mm ²	$U_n = 1.4, 5.6$ m/s (water), 7.3 m/s (R-113) $\Delta T_{sub,in} = 70^\circ\text{C}$	Subcooling achieved by pressurizing with helium gas; jets significantly increase CHF of pool boiling for all subcoolings
Lay & Dhir (1995) [116]	Water, R-113	F* $D_n = 1.1, 2.2$ mm $H = 8.7$ mm	► Copper $D_s = 17.6$ mm ~0.5 mm heater block protrusion; bare surface, 3 macro-structured (grooves and ridges) surfaces, 1 micro-structured (sintered) surface, 4 surfaces with both macro- and micro-structuring		Structured surfaces augment CHF; amount of enhancement depends on actual geometry of structuring; highest augmentation (~125% increase) is observed for surface with both macro- and micro-structuring; simple oxidation of bare copper surface enhances CHF by 5-10%

(continued on next page)

Table 2 (continued)

Author(s)	Fluid(s)	Jet Geometry ^a	Heated Surface Geometry ^b	Operating Conditions	Remarks and Major Conclusions
Monde & Mitsutake (1996) [175], Monde et al. (1995) [176]	Water	F _{**} N = 2, 4 D _n = 2 mm	▼ Stainless steel 2L _{char} = 45.1, 46.5 mm W _s = 15 mm Foil directly heated by DC	U _n = 5 – 25 m/s P _{sat} = 1, 3 bar ΔT _{sub,in} = 0 – 80°C ρ _f /ρ _g = 658 – 1605	Characteristics of multiple jets within each jet cell similar to single standalone jets; single jet correlation by Monde et al. [75,76] gives equally good predictions for multiple jets; n = 121
Copeland (1996) [58]	FC-72	C*, C _s * N = 1, 5 × 5, 10 × 10 D _n = 2.5 – 5.0 mm (single jet), 0.25 – 1.0 mm (arrays) (NA _n = 5 – 20 mm ²) L _n = 20 mm (single), 5D _n (arrays) H = 1 – 4 mm	▲ Copper A _s = 10 × 10 mm ² Bare flat surface and pin-fin arrays pin-fin thickness = 0.1, 0.2 mm Pin-fin height = 0.1 – 1.0 mm	U _n = 0.125 – 2 m/s Q _v = 0.15 – 0.6 L/min ΔT _{sub,in} = 36 – 44°C	q ^{CHF} = 45 – 395 W/cm ² ; pin-fin arrays enhance CHF compared to flat surfaces; both flat surfaces and pin-fin arrays show similar enhancements in CHF on varying operating parameters; CHF is independent of pin-fin width for a fixed pin-fin aspect ratio
Johns & Mudawar (1996) [16]	FC-72	C* D _n = 0.40, 0.79, 2.06 mm H = 0.51, 1.02, 2.03 mm L _n /D _n = 1.91 mm	► Oxygen-free copper A _s = 12.7 × 12.7, 6.35 × 6.35, 4.23 × 4.23 mm ² Vapor blasted with 10-μm slurry particles	U _n = 0.5 – 6 m/s P _{sat} = 1.24 bar T _{sat} = 62.8°C ΔT _{sub,in} = 10, 25, 40°C	Max. q ^{CHF} = 185 W/cm ² ; CHF increases with increases in ΔT _{sub,in} and U _n ; CHF is negligibly affected by H; CHF is high for smaller surface areas; implemented in avionics cooling clamshell modules
Kamata (1997, 1999) [177,178]	Water	F* D _n = 2.2 mm	▲ Copper D _s = 80 mm Polished with emery #1200	U _n = 0.6 – 2.1 m/s P _{sat} = 1 atm T _{in} = 369 – 371 K U _n = 2.9, 4.7, 6.7 m/s	Conducted both steady- and unsteady-state experiments; datapoints in boiling curves are too dense to interpret CHF trends
Cheng et al. (2001) [49]	FC-72	F* D _n = 2, 3 mm H = 5 mm	Thick film resistor A _s = 12.7 × 8 mm ²	P _{sat} = 1 atm T _{sat} = 56°C T _{in} = 28 – 54°C U _n = 2.9, 4.7, 6.7 m/s	CHF increases with increases in U _n , D _n , and ΔT _{sub,in}
Tay et al. (2002) [179]	FC-72	F* D _n = 1 mm (thermal test die), 2, 3 mm (film resistor) H = 5 mm	Thick film resistor A _s = 12.7 × 8 mm ² 6 × 6 mm ² thermal test die 4.5 × 4.5 mm ² measurement area made of a 9 × 9 array of 500 × 500 μm ² polysilicon resistors	P _{sat} = 1 atm T _{sat} = 56°C T _{in} = 28 – 54°C	Same CHF conclusions as from their previous study [49]; test die made of discrete heating elements shows non-uniform T _s due to phase change occurring only over smaller portion of surface
Liu & Zhu (2002) [129]	Water	F* D _n = 2, 6, 10 mm H = 10 mm	▲ Ni-Cr alloy A _s = 2 × 4, 6 × 6, 10 × 10 mm ² 0.1- or 0.05-mm-thick foil heated by DC	U _n = 0.5 – 6 m/s P _{sat} = 1 atm ΔT _{sub,in} ≈ 0°C	Higher CHF for higher U _n and smaller D _n
Mitsutake & Monde (2003) [74]	Water	F* D _n = 2.0 mm H = 5 mm	▲ Nickel L _s = 5, 10 mm W _s = 4 mm √L _s ² + W _s ² /D _n = 3.20, 5.39 Foil thickness = 0.03, 0.05, 0.1, 0.3 mm	U _n = 5, 17, 35, 60 m/s P _{sat} = 1 – 10 bar T _{in} = 20°C ΔT _{sub,in} = 80 – 170°C	Max. q ^{CHF} = 211.9 MW/m ² ; CHF is strongly affected by heater thickness, but this effect disappears when heat capacity of unit area of heated surface > 0.8 kJ/m ² /K, which corresponds to 2 mm thickness for nickel; CHF increases with increasing U _n and decreasing L _s ; comparisons made with theoretical maximum heat flux proposed by Gambill and Lienhard [180]
Mitsutake et al. (2003) [181]			W _s = 4, 6 mm		All parameters and conclusions same as those of Mitsutake and Monde [74], except for experiments with two heated surface widths
Zhou & Ma (2004) [182]	R-113	S* D _n = 0.96, 1.01 mm L _n = 30, 35 mm H/D _n = 5	► Constantan A _s = 5 × 5 mm ² 10-μm-thick foil	U _n = 0 – 11.355 m/s P _{sat} = 1 atm ΔT _{sub,in} = 18.5, 27.6°C	When jet impinges at center of heated surface, highest temperatures are observed around edges, which is where burnout occurs
Liu et al. (2004) [52]	Water	F* D _n = 3, 6, 8, 12 mm H = 5 mm	▲ Copper D _s /D _n = 1	U _n = 0.5 – 6 m/s P _{sat} = 1 atm ΔT _{sub,in} = 15 – 80°C	Higher CHF is obtained for higher U _n and smaller D _n ; linear relationship between CHF and ΔT _{sub,in}

(continued on next page)

Table 2 (continued)

Author(s)	Fluid(s)	Jet Geometry ^a	Heated Surface Geometry ^b	Operating Conditions	Remarks and Major Conclusions
Qiu & Liu (2005) [53]	R-113	F* $D_n = 8, 4 \text{ mm}$ $H = 5 \text{ mm}$	▲ Copper $D_s/D_n = 1$	$U_n = 0.5 - 8 \text{ m/s}$ $P_{sat} = 1 \text{ atm}$ $\Delta T_{sub,in} = 0 - 33^\circ\text{C}$	Conclusions similar to those of Liu <i>et al.</i> [52]
Qiu & Liu (2005) [54]	Water, ethanol, R-113, R-11	F* $D_n = 3 - 12 \text{ mm}$ $H = 5 \text{ mm}$	▲ Copper $D_s/D_n = 1$	$U_n = 0.5 - 10 \text{ m/s}$ $P_{sat} = 1 \text{ atm}$ $\Delta T_{sub,in} \approx 0^\circ\text{C}$	Conclusions similar to those of Liu and Zhu [129]
Qiu & Liu (2005) [55]	Water, ethanol, R-113	F* $D_n = 3 - 12 \text{ mm}$ $H = 5 \text{ mm}$	▲ Copper $D_s/D_n = 1$	$U_n = 0.5 - 8 \text{ m/s}$ $P_{sat} = 1 \text{ atm}$ $\Delta T_{sub,in} = 0 - 80^\circ\text{C}$	Conclusions similar to those of Liu <i>et al.</i> [52]
Liu & Qiu (2006) [112]	Water	F* $D_n = 4.0 \text{ mm}$ $H = 5.0 \text{ mm}$	▲ Copper $D_s = 20 \text{ mm}$ Coated with $\sim 1\mu\text{m TiO}_2$ (with and without 275 - 315 nm ultraviolet light irradiation)	$U_n = 0.5 - 6.5 \text{ m/s}$ $Re_{Dn} \approx 25000 - 400000$ $P_{sat} = 1 \text{ atm}$ $\Delta T_{sub,in} = 0 - 74^\circ\text{C}$	$R_a = 194.01 \text{ nm}$ (bare copper), 106.61 nm (coated copper); $\theta_{CA} = 0^\circ$ (coated and UV radiated), $20-40^\circ$ (just coated), $40-70^\circ$ (bare copper); same conclusions as those of Qiu and Liu [114]
Liu & Qiu (2006) [113]	Water	F* $D_n = 4, 8 \text{ mm}$ $H = 5 \text{ mm}$	▲ Copper $D_s/D_n = 1$ Coated with $\sim 1\mu\text{m TiO}_2$ (with and without 275 - 315 nm ultraviolet light irradiation)	$U_n = 0.5 - 8 \text{ m/s}$ $P_{sat} = 1 \text{ atm}$ $\Delta T_{sub,in} = 0 - 80^\circ\text{C}$	CHF on coated surface is $\sim 50\%$ higher than that on bare copper; parametrical effects similar to those of Liu <i>et al.</i> [52]
Liu & Qiu (2007) [119]	0.1 - 2% wt. CuO/water nanofluid	F* $D_n = 4 \text{ mm}$ $H = 5 \text{ mm}$	▲ Copper $D_s = 20 \text{ mm}$	$U_n = 0.5 - 6.5 \text{ m/s}$ $P_{sat} = 1 \text{ atm}$ $\Delta T_{sub,in} = 0 - 74^\circ\text{C}$	CHF for nanofluid increases with particle concentration up to 1% wt., but becomes insensitive to concentration above 1% wt.; CHF using nanofluids is $\sim 25\%$ higher than for water
Qiu & Liu (2008) [114]	Water	F* $D_n = 4 \text{ mm}$ $H = 5 \text{ mm}$	▲ Copper $D_s = 20 \text{ mm}$ Coated with $\sim 1\mu\text{m TiO}_2$ (with and without 275 - 315 nm ultraviolet light irradiation)	$U_n = 0.5 - 6.5 \text{ m/s}$ $P_{sat} = 1 \text{ atm}$ $\Delta T_{sub,in} = 0 - 74^\circ\text{C}$	Coated surfaces irradiated with ultraviolet light yield $\sim 30\%$ higher CHF than bare copper due to a large decrease in solid-liquid contact angle
Sarkar <i>et al.</i> (2009) [118]	FC-72	C** $N = 4 \times 4$ $D_n = 1.6 \text{ mm}$ $H = 0.254 - 0.635 \text{ mm}$ 5×5 array spent fluid removal holes of $D = 1.32 \text{ mm}$ at corners of jet cells	▲ $A_s = 20 \times 20 \text{ mm}^2$	$Q_v = 1.05 - 2.0 \text{ L/min}$ $T_{sat} = 53^\circ\text{C}$ $T_{in} = 22.5 - 41.0^\circ\text{C}$	Max. $q''_{CHF} = 101 \text{ W/cm}^2$ (for $T_{in} = 23^\circ\text{C}$, $Q_v = 2 \text{ L/min}$, and $H = 0.381 \text{ mm}$); CHF increases with increases in Q_v and $\Delta T_{sub,in}$; highest CHF is achieved for medium H of 0.381 mm , meaning system has optimum H value
Browne <i>et al.</i> (2010) [62]	R-134a	C** Staggered with hexagonal jet cells $N = 17$ $D_n = 112 \mu\text{m}$ $H = 200 \mu\text{m}$ jet spacing = $360 \mu\text{m}$	▲ Thin-film titanium heater $A_s = 1 \times 1 \text{ mm}^2$	$U_n = 4, 7, 10 \text{ m/s}$ $\Delta T_{sub,in} = 10, 20, 30^\circ\text{C}$ Nitrogen was mixed with fluid to study effects of non-condensable gases	CHF occurs at much lower surface superheats with increasing non-condensable gas content; inlet subcooling does not affect the superheat at which CHF occurs
Cardenas <i>et al.</i> (2010) [183]	Water				Study seems to be a subset of that of Cardenas and Narayanan [27]; $n = 15$
Cardenas (2011) [184]	Water, FC-72				Data seem to be a subset of that of Cardenas and Narayanan [27,185]
	Water	F* $D_n = 1.16 \text{ mm}$ $H = 6D_n$	Oxygen-free copper $D_s = 27.64 \text{ mm}$ $R_a = 33 \text{ nm}$	$U_n = 0.79 - 5.88 \text{ m/s}$ $Re_{Dn} = 1641 - 15859$ $P_{sat} = 0.176, 0.276 \text{ bar}$ $T_{sat} = 57.3, 67.2^\circ\text{C}$ $\Delta T_{sub,in} = 0^\circ\text{C}$	$q''_{CHF} = 34 - 185.4 \text{ W/cm}^2$; $n = 11$
Cardenas & Narayanan (2011) [186]	Water				Study seems to be a subset of that of Cardenas and Narayanan [37]

(continued on next page)

Table 2 (continued)

Author(s)	Fluid(s)	Jet Geometry ^a	Heated Surface Geometry ^b	Operating Conditions	Remarks and Major Conclusions
Grassi & Testi (2011) [98]	FC-72, HFE-7100	S*, S* _* ionic jets N = 1, 7 (in-line separated by 4 mm) H = 8 mm	▲ Stainless-steel A _s = 20 × 20 mm ² q" and T measurements made over only a part of surface that is heated 40-μm-thick plate directly heated	V _{EHD} = 12, 18, 24 kV P _{sat} ≈ 1 atm T _{sat} = 56°C (FC-72), 61°C (HFE-7100)	Jets created due to potential difference between high-voltage negative DC polarity electrodes (regular tailor's steel pin) and electrically grounded heated plate; ionic jets augment CHF compared to pool boiling; CHF improves with increasing number of jets
Zhang et al. (2011) [80]	Liquid nitrogen	S* (tube-in-tube) D _n = 2.0 mm H = 1.5, 3.5 mm	▲ Oxygen-free copper D _s = 5 mm 3 surfaces: flat surface, concave surface with R _s = 2.5 mm, flat surface with 5-mm-tall needle of base diameter 1 mm	U _n = 0.34 – 1.11 m/s P _{sat} = 101.3 – 160.0 kPa	CHF increases with increasing U _n ; concave surface yields highest CHF for similar operating conditions
Browne et al. (2012) [63]	R-134a	C* _* Staggered with hexagonal jet cells N = 17 D _n = 112 μm Jet spacing = 230, 360 μm H = 200 μm	▲ Thin-film titanium heater A _s = 1 × 1 mm ² (A _r = 8.9, 21.4%)	U _n = 4, 7 m/s ΔT _{sub,in} = 10, 20, 30°C Nitrogen partial pressure = 0, 103, 241 kPa	Nitrogen mixed with fluid to study effects of non-condensable gases; increasing inlet subcooling increases CHF; contrary to their hypothesis in Browne et al. [62], nitrogen content does not affect CHF mechanism
Mahmoudi et al. (2012) [77]	HFE-7100	F* D _n = 1.37, 0.41 mm H = 5 – 50 mm	▲ Nickel-plated copper D _s = 8 mm	Free-falling Q _v = 20 – 60 cc/min P _{sat} = 1 bar; T _{sat} = 61°C T _{in} ≈ 59°C ΔT _{sub,in} ≈ 2°C	For low velocities, increasing H decreases cross-sectional jet diameter near impingement point due to surface tension; this thinner liquid film causes pre-mature CHF
Cardenas & Narayanan (2012) [185]	FC-72	S* D _n = 1.16, 2.29, 3.96 mm H = 6D _n	Oxygen-free copper D _s = 27.64 mm (D _s / D _n = 23.8, 12.1, 7) R _a = 33 nm	U _n = 0 – 3.4 m/s Re _{D_s} = 0 – 14000 P _{sat} = 1 atm	q"CHF = 14.4 – 21.9 W/cm ² ; n = 22; CHF increases with increasing Re and decreasing D _n ; data is predicted well by Monde and Katto's [26] correlation for Re _{D_s} > 4000
Cardenas & Narayanan (2012) [27]	Water	S* D _n = 1.16 mm H = 6D _n	▲ Oxygen-free copper D _s = 27.64 mm R _a = 123 nm and 33 nm	U _n = 0 – 4.18 m/s Re _{D_n} = 0 – 12634 P _{sat} = 0.176, 0.276, 0.477 bar T _{sat} = 57.3, 67.2, 80.2°C ΔT _{sub,in} = 0, 17°C	q"CHF = 43.2 – 190.6 W/cm ² ; n _{sat} = 20; n _{sc} = 5; CHF increases with increases in P _{sat} , surface roughness, subcooling, and Re
Cardenas & Narayanan (2012) [37]	Water	S* D _n = 1.16 mm H = 6D _n	▲ Oxygen-free copper D _s = 23.8 D _n R _a = 123 nm and 33 nm	U _n = 0 – 4.9 m/s Re _{D_s} = 0 – 14000 P _{sat} = 0.176, 0.276, 0.477 bar T _{sat} = 57.3, 67.2, 80.2°C ΔT _{sub,in} = 0, 17°C ρ _l /ρ _g = 8502, 5544, 3295	
Cardenas & Narayanan (2012) [38]	Water	S* D _n = 1.16 mm H = 6D _n	▲ Oxygen-free copper D _s = 27.64 mm R _a = 33 nm	U _n = 0 – 3.03 m/s Re _{D_n} = 0 – 6757 P _{sat} = 0.176 bar T _{sat} = 57.3°C ΔT _{sub,in} = 0°C	q"CHF = 54.6 – 88.5 W/cm ² (n _{water} = 5); q"CHF = 15.2 – 21.9 W/cm ² (n _{FC-72} = 8); Water yields higher CHF than FC-72 for pool boiling and for submerged jets of similar Re; enhancement of jet CHF over pool boiling CHF is more pronounced for water; data seems to be a subset of those of Cardenas and Narayanan [27,185]
		FC-72		U _n = 0 – 3.38 m/s Re _{D_n} = 0 – 14216 P _{sat} = 1.01 bar T _{sat} = 56.6°C ΔT _{sub,in} = 0°C	
Mikielewicz et al. (2012) [187]	Water	F* D _n = 71, 101 μm L _n = 2 mm; H = 25 mm	▲ Silver-plated copper D _s = 10 mm	G = 4700 – 15600 kg/m ² s P _{sat} = 1 atm ΔT _{sub,in} = 40, 60, 80°C	CHF increases with increasing subcooling; jet CHF is lower than pool boiling CHF predicted by Kutateladze's [172] correlation

(continued on next page)

Table 2 (continued)

Author(s)	Fluid(s)	Jet Geometry ^a	Heated Surface Geometry ^b	Operating Conditions	Remarks and Major Conclusions
Buchanan & Shedd (2013) [30]	R-245fa	C _s * Oblique; $\theta = 45^\circ$ $N = 14 - 51$ $D_n = 0.25, 0.43, 0.58$ mm $L_n = 1.8, 3.9, 8.4$ mm $L_{jet} = 2.3 - 8.9$ mm	▲ Copper $A_s = 3.63$ cm ² square $H = 3.5, 6.7$ mm	$Q_v = 0.14 - 0.41$ L/min/cm ² $Re = 1400 - 14000$ $T_{in} = 10, 20, 30^\circ\text{C}$	$q''_{CHF} \approx 35 - 110$ W/cm ² ; CHF is strongly influenced by T_{in} and Q_v
Li et al. (2013) [115]	Water	F* $D_n = 3$ mm $H = 5$ mm	▲ Copper $D_s = 3$ mm Nano-characteristic surfaces $\theta_{CA} = 5$ (hydrophilic), 60 (bare copper), 105° (hydrophobic)	$U_n = 5 - 40$ m/s $P_{sat} = 1$ atm $\Delta T_{sub,in} = 0 - 50^\circ\text{C}$	At low U_n , CHF is proportional to $U_n^{1/3}$; at high U_n , velocity has a complex effect on CHF; CHF increases with decreasing contact angle, θ_{CA}
Bin et al. (2013) [188]	Water	F _s * $N = 25$ in a single row $D_n = 0.4$ mm $H = 50$ mm	▲ Cast industrial copper	$U_n = 0.95 - 1.59$ m/s $\Delta T_{sub,in} = 30 - 83^\circ\text{C}$	CHF increases with increases in Q_v and $\Delta T_{sub,in}$ as well as with use of multiple jets
Hong et al. (2013) [50]	43% mass conc. aqueous ethylene glycol	C _s * $N = 4 \times 8$ $D_n = 1$ mm $H/D_n = 1$ Jet spacing = $5D_n$	▲ 0.03-mm-thick metal $A_s = 20 \times 40$ mm ²	$U_n = 0.2, 0.31, 0.5$ m/s $P_{sat} = 1$ atm $T_{sat} = 106^\circ\text{C}$ $\Delta T_{sub,in} = 36 - 96^\circ\text{C}$	$q''_{CHF} = 60.8 - 127.5$ W/cm ² ; $n = 9$; CHF increases with increasing U_n and $\Delta T_{sub,in}$; highest T_s is observed at heater edges
Hong et al. (2014) [64]	43% mass conc. aqueous ethylene glycol	C _s * $N = 4 \times 8, 5 \times 10$ $D_n = 1$ mm $H/D_n = 1, 1.5, 3$ Jet spacing = $(5,4) D_n$	▲ Ni-Cr $A_s = 20 \times 40$ mm ² 0.03-mm-thick thin film heater polished with emery #2000	$U_n = 0.2, 0.31, 0.5$ m/s $P_{sat} = 1$ atm $T_{sat} = 106^\circ\text{C}$ $\Delta T_{sub,in} = 36 - 56^\circ\text{C}$	CHF increases with increasing N ; highest CHF is achieved with optimum combination of H and jet spacing
Werneke (2015) [65]	HFE-7000	C _s * Staggered and regular arrays $N = 9 - 23$ $D_n = 98$ μm $H = 192$ μm Jet spacing = $230 - 360$ μm	▲ Thin-film titanium heater $A_s = 1 \times 1$ mm ² ($A_r = 0.065 - 0.164$)	$U_n = 0.9 - 15.0$ m/s $T_{sat} \approx 58.2^\circ\text{C}$ $\Delta T_{sub,in} = 11.9 - 35^\circ\text{C}$	Flow loop pressurized either using nitrogen or by heating fluid; CHF is higher for jet impingement than for micro-channel flow boiling; CHF increases with increasing A_r , but is independent of array pattern
Zhang et al. (2016) [107]	air-dissolved FC-72	C* $D_n = 3.0$ mm $H = 3.0, 6.0$ mm	▲ P-doped N-type silicon chip $A_s = 10 \times 10$ mm ² Bare flat and 4 micro-pin-finned surfaces (pin-fin width \times thickness \times height = $30 \times 30 \times 60, 50 \times 50 \times 60, 30 \times 30 \times 120, 50 \times 50 \times 120$ μm ³) Fin spacing = thickness	$U_n = 0.5, 1.0, 1.5$ m/s $P_{sat} = 1$ atm $T_{sat} = 56^\circ\text{C}$ $\Delta T_{sub,in} = 25, 35^\circ\text{C}$	Max. $q''_{CHF} = \sim 157$ W/cm ² ; for all surfaces, CHF increases with increasing Re and $\Delta T_{sub,in}$; smaller H yields higher CHF enhancement with Re ; CHF for micro-pin-finned surfaces is higher than for flat surface
Grassi et al. (2016) [99]	FC-72	S* ionic jets $H = 5$ mm $D_{n,EHD} = 3$ mm	▲ Copper $A_s = 12 \times 12$ mm ²	$U_{n,EHD} = 0.25 - 0.55$ m/s $Re_{EHD} \approx 0 - 4300$ $P_{sat} \approx 1$ atm $T_{sat} = 56^\circ\text{C}$	Jets from high-voltage negative DC polarity platinum electrode to grounded heated plate; equivalent D_n and U_n based on [132]; ionic jets augment CHF by $\sim 40\%$ over pool boiling
de Oliveira & Barbosa (2016) [100]	R-134a	F* (based on their module design) $D_n = 300, 500$ μm $H = 9.75, 28.84$ mm	▲ Copper $D_s = 28.54$ mm ($A_s = 6.36$ cm ²)	Vapor compression cycle T_f (condenser) = $15, 25^\circ\text{C}$ \dot{m} (condenser) = 180 kg/hr $T_{amb} = 25^\circ\text{C}$ $\Delta T_{superheat}$ (compressor) = 10°C Compressor piston displacement = $50, 75, 100\%$ full stroke	Results are presented for entire loop in refrigeration application terms; findings similar to de Oliveira and Barbosa [101]

(continued on next page)

Table 2 (continued)

Author(s)	Fluid(s)	Jet Geometry ^a	Heated Surface Geometry ^b	Operating Conditions	Remarks and Major Conclusions
de Oliveira & Barbosa (2017) [101]	R-134a	F* (based on their module design) $D_n = 300 \mu\text{m}$ $H = 9.75, 28.84 \text{ mm}$	▲ Copper $D_s = 28.54 \text{ mm}$ ($A_s = 6.36 \text{ cm}^2$)	Vapor compression cycle T_f (condenser) = 15, 25°C \dot{m} (condenser) = 180 kg/hr $T_{amb} = 25^\circ\text{C}$ $\Delta T_{superheat}$ (compressor) = 10°C Compressor piston displacement = 50, 75, 100% full stroke	Results are presented for entire loop in refrigeration application terms; CHF decreases by reducing H for 75% and 100% strokes, but is unaffected by H for 50% stroke; the CHF decrease is attributed to increased jet splattering and droplet breakup at low H ; CHF is higher for higher condenser secondary fluid temperature
de Oliveira & Barbosa (2017) [102]	R-134a	F*, F** (based on their module design) $D_n = 300 - 1000 \mu\text{m}$ Staggered array of 13 holes covering $20 \times 20 \text{ mm}^2$ area that can be opened/closed $N = 1, 5$ (3 symmetrical configurations) $H = 28.84 \text{ mm}$	▲ Copper $D_s = 28.54 \text{ mm}$ ($A_s = 6.36 \text{ cm}^2$)	Vapor compression cycle T_f (condenser) = 25°C \dot{m} (condenser) = 180 kg/hr $T_{amb} = 25^\circ\text{C}$ $\Delta T_{superheat}$ (compressor) = 10°C	Results are presented for entire loop in refrigeration application terms; multiple jets enhance CHF due to less abrupt transition from fully wetted to partially wetted surface regime
Joshi & Dede (2017) [117]	R-245fa	C** (Non-uniform jet cells; concentrated at center) $N = 5 \times 5$ $D_n = 0.75 \text{ mm}$ jet spacing = 3 mm $H = 2.5 \text{ mm}$	▲ Oxygen-free copper $58.5 \times 58.5 \text{ mm}^2$ heat spreader attached to $19 \times 19 \text{ mm}^2$ nichrome resistance heater 4 surface types (all coated with microporous copper): flat, with open tunnels, with closed tunnels, and pin-finned; 0.25 mm thick porous coating by sintering 75-100- μm copper particles. Coating area = $25 \times 25 \text{ mm}^2$	$T_{sat} = 45^\circ\text{C}$ $\Delta T_{sub,in} = 5^\circ\text{C}$	Application in wide band-gap power semiconductor devices; CHF increases in following order: flat surface (145 W/cm^2), closed tunnel (194 W/cm^2), open tunnel (202 W/cm^2), pin-finned surface ($>218 \text{ W/cm}^2$); $n = 4$
de Brun et al. (2017) [189]	Water	C** $N = 2 \times 2, 3 \times 3, 5 \times 5$ $D_n = 1.0 \text{ mm}$ $H = 2 \text{ mm}$	▲ Copper $35 \times 35 \text{ mm}^2$ surface mates with $15 \times 15 \text{ mm}^2$ heat source underneath $A_r = 0.014, 0.031, 0.087$	$U_n = 0.28 - 3.54 \text{ m/s}$ $Q_v = 0.33 - 0.67 \text{ L/min}$ $Re_{Dn} = 900 - 11800$ $P_{sat} = 1 \text{ atm}$ $T_{in} = 92^\circ\text{C}$; $\Delta T_{sub} = 8^\circ\text{C}$	CHF for jet arrays is stronger function of U_n than Q_v ; data is predicted well by Buchanan and Shedd's [30] correlation; $n = 8$
Cui et al. (2018) [109]	HFE-7000	C** $N = 4 \times 2$ (normal and distributed jet plates) $D_n = 1 \text{ mm}$ $H = 3 \text{ mm}$ $L_n = 1.5 \text{ mm}$ Nozzle spacing = 5 mm	▲ Copper Bare and pin-finned surfaces $A_s = 10 \times 20 \text{ mm}^2$ Pin-fins: 0.5 mm width, 1 mm height, 0.5 mm spacing	$Q_v = 0.5, 0.8, 1.0 \text{ L/min}$ $T_{sat} = 60^\circ\text{C}$ $T_{in} = 35^\circ\text{C}$	'Normal' has a single large exit at one end of confinement area; 'distributed' has exit holes of diameter D_n at 4 corners of each jet cell; CHF increases with increasing Q_v for all configurations; pin-finned surfaces augment CHF for both nozzle plates; CHF is higher for distributed jet plate because of better flow uniformity in each jet cell

(continued on next page)

Table 2 (continued)

Author(s)	Fluid(s)	Jet Geometry ^a	Heated Surface Geometry ^b	Operating Conditions	Remarks and Major Conclusions
Zhang <i>et al.</i> (2018) [108]	air-dissolved FC-72	C ^{*,*} N = 2 × 2 D _n = 3.0 mm H = 3.0, 6.0, 9.0 mm	P-doped N-type silicon chip A _s = 10 × 10 mm ² Bare flat and 4 micro-pin-finned surfaces (pin-fin width × thickness × height = 30 × 30 × 60, ΔT _{sub,in} = 35°C 50 × 50 × 60, 30 × 30 × 120, 50 × 50 × 120 μm ³) Fin spacing = thickness	U _n = 0.5, 1.0, 1.5 m/s Re _{Dn} = 2853, 5707, 8560 P _{sat} = 1 atm T _{sat} = 56°C	CHF for micro-pin-finned surfaces is higher than for flat surface
Naidu & Khandekar (2018) [190]	Water	F [*] D _n = 481.2 μm H = 5.0 mm	▲ Aluminum 6061 D _s = 10 mm Ground to R _a = 0.45 μm	Re _{Dn} = 2186, 3499, 4374 P _{sat} = 0.095, 0.180 bar T _{sat} = 45, 58°C ΔT _{sub,in} = 3 – 25°C	q ^{''} _{CHF} = 140 – 168 W/cm ² ; no other CHF data or discussion given
Zhang & Chen (2019) [110]	Water	S [*] D _n = 4 mm H = 50 mm	▲ Copper D _s = 30 mm Surfaces: bare, brass beads porous layer of bead diameters of 4, 6, and 8 mm Number of layers = 1, 2, 3	Q _v = 300, 600, 900 mL/min P _{sat} = 1 atm T _{sat} = 100°C ΔT _{sub,in} = 8, 20, 40°C	An optimal number of layers and bead diameter exists for maximum CHF
Zhang & Chen (2020) [111]	Water	F [*] D _n = 4 mm H = 50 mm	▲ Copper D _s = 30 mm Ground by emery wheel of mesh #200 per in ² and particle size 75 μm Surfaces: bare, brass beads porous layer of bead diameters of 4, 6, 8, and 10 mm Number of layers = 1, 2, 3	Q _v = 300, 600, 900 mL/min P _{sat} = 1 atm T _{sat} = 100°C ΔT _{sub,in} = 10°C	An optimal number of layers and bead diameter exists for maximum CHF; CHF increases with increasing Q _v for all surfaces
Devahdhanush & Mudawar (2020) [18]	R-134a	C [*] , C ^{*,*} N = 1, 3 × 3, 6 × 6 D _n = 0.40, 0.79, 2.06 mm H = 4.724 mm	▲ Oxygen-free copper A _s = 25.4 × 25.4, 12.7 × 12.7, 4.23 × 4.23 mm ²	U _n = 0.50 – 10.08 m/s Q _v = 0.009 – 2.314 gal/min ṁ = 7.057 × 10 ⁻⁴ – 0.179 kg/s P _{in} = 612.7 – 870.2 kPa P _{sat} = 612.2 – 837.2 kPa T _{sat} = 22.23 – 32.94°C ΔT _{sub,in} = 1.50 – 13.03°C x _{e,in} = -0.112 – -0.012	q ^{''} _{CHF} = 16.88 – 222.84 W/cm ² ; T _s at CHF = 36.45 – 128.20°C; x _{e,out} = -0.077 – 0.846; higher CHF is achieved by increasing U _n , increasing D _n and N for fixed U _n , and decreasing D _n and N for fixed Q _v ; higher CHF at higher P _{sat} for fixed T _{in} ; both subcooled and saturated CHF are achieved; underlying mechanisms for two types of CHF transients (sharp sudden and mild gradual) propounded; burnout patterns on heated surface examined to interpret wall jet interactions

^a F: free-surface jets, S: submerged jets, C: confined jets, *: single jet, **: jet array (multiple jets); jets normally impinging (θ = 90°) on surface center unless noted otherwise

^b ▲: upward-facing surface, ▼: downward-facing surface, ►: sideward-facing surface; bare flat surface flush with housing unless noted otherwise; A_s denotes planform area for non-flat surfaces; circular surface only where D_s is given

Table 3
Summary of experimental studies on CHF in slot jet impingement boiling.

Author(s)	Fluid(s)	Jet Geometry ^a	Heated Surface Geometry ^b	Operating Conditions	Remarks and Major Conclusions
Andrews & Rao (1974) [81]	Water	S* H = 12.7 – 50.8 mm 13 different locations of nozzle over surface	▲ Stainless-steel A _s = 3.175 mm × L _s (not given) 203-μm-thick ribbon directly heated by DC Not insulated at bottom Mill finish of 16-32 rms	U _n = 0, 0.3 – 2.0 m/s P _{sat} = 1 atm ΔT _{sub,in} ≈ 0 – 56°C	CHF increases with increases in ΔT _{sub} and U _n ; CHF decreases with increasing H
Ishigai <i>et al.</i> (1978) [191], Nakanishi <i>et al.</i> (1980) [192]	Water	F* A _n = 56.2 × 6.2 mm ² with rounded corners H = 15 mm	▲ Stainless-steel A _s = 50 × 12 mm ² 0.1-mm-thick; directly heated by AC 3 surfaces: polished with emery #100, unpolished, grooved	U _n = 1.0, 2.1 m/s P _{sat} = 1 atm ΔT _{sub,in} = 35, 75°C	Conducted both steady state and transient (quenching from 1000 – 1200°C) experiments; CHF values obtained from steady state experiments is higher than from transient due to poorer accuracy of the latter; CHF increases with increases in ΔT _{sub,in} and U _n
Katto & Ishii (1978) [97]	Water, R-113, Trichloro-ethane	F* Oblique wall jet W _n = 0.56, 0.77 mm θ = 15°, 60°	▼ L _s = 10, 15, 20 mm Jet introduced at edge of heated surface	U _n = 1.5 – 15 m/s P _{sat} = 1 atm ΔT _{sub,in} ≈ 0°C	
Katto & Kurata (1980) [31]	Water, R-113	S* Parallel wall jet W _n = 5, 10 mm Nozzle depth = 15 mm	► Copper L _s = 10, 15, 20 mm W _s = 10 mm Jet introduced upwards at bottom edge of heated surface	U _n = 0.5 – 10 m/s P _{sat} = 1 atm ΔT _{sub,in} < 3°C	q [*] _{CHF} = 1.59 – 4.95 MW/m ² (Water); q [*] _{CHF} = 0.306 – 0.897 MW/m ² (R-113); CHF is independent of W _n
Miyasaka & Inada (1980) [69]	Water	F* A _n = 10 × 30 mm ² H = 15 mm	▲ Platinum A _s = 4 × 8 mm ² 0.1-mm-thick foil directly heated by AC Rubbed with emery #5/0	U _n = 1.5 – 15.3 m/s P _{sat} = 1 atm + ρ _f U _n ² /2 T _{in} = 15°C	Pressure measured at stagnation point; CHF increases with increasing U _n
Miyasaka <i>et al.</i> (1980) [70]	Water	F* W _n = 10 mm H = 15 mm	▼ Platinum D _s = 1.5 mm 0.05-mm-thick foil diffusion-bonded to a copper block Rubbed with emery #5/0	U _n = 1.5 – 15.3 m/s P _{sat} = 1 atm + ρ _f U _n ² /2 T _{in} = 15°C	Testing continued into transition boiling regime; CHF increases with increasing U _n ; n = 3
Katto & Haramura (1981) [91]	Water, R-113	F* Parallel wall jet W _n = 0.4 – 1.5 mm	▼ Stainless-steel Directly heated by DC L _s = 10 – 40 mm	U _n = 1.8 – 65 m/s ΔT _{sub,in} ≈ 0°C	Details from Wolf <i>et al.</i> [162]
Baines <i>et al.</i> (1984) [92]	Water	F* Parallel wall jet from top W _n = 1.33 mm	Oxygen-free copper A _s = 114 × 66 mm ² Placed 45° or 90° to horizontal Cleaned with wire wool	U _n = 0.85 – 4.9 m/s P _{sat} = 1 atm ΔT _{sub,in} = 0°C	q [*] _{CHF} = 1188 – 1766 kW/m ² ; CHF increases with increasing U _n , but this effect is weaker for U _n > 2.5 m/s
Wadsworth & Mudawar (1990) [12]	FC-72	C* W _n = 0.254 mm L _n = 5 W _n ; H = 5.08 mm 3 nozzle profiles: flat, Vee, curved	► Oxygen-free copper A _s = 12.7 × 12.7 mm ²	U _n = 5 m/s T _{in} = 46.0°C	Nozzle geometry does not affect CHF; flat and Vee profiles result in 15% and 5% higher pressure drops than curved, respectively; Vee-profile chosen because of moderate ΔP and ease of fabrication
Mudawar & Wadsworth (1991) [13]	FC-72	C* W _n = 0.127 – 0.508 mm H = 0.508 – 5.08 mm	► Oxygen-free copper A _s = 12.7 × 12.7 mm ² blasted with air/water/silica slurry to yield approximately 15-μm-diameter cavities	U _n = 1 – 13 m/s P _{sat} = 1.2 – 1.6 bar ΔT _{sub,in} = 0 – 40°C	Max. q [*] _{CHF} = 249 W/cm ² ; two different CHF regimes discovered: CHF increases with increasing U _n in medium velocity regime, but levels off and ultimately decreases with increasing U _n in high velocity regime; decreasing H promotes transition to high velocity regime at jet lower velocities; CHF in medium velocity regime increases with increases in ΔT _{sub,in} and W _n , but is fairly insensitive to H

(continued on next page)

Table 3 (continued)

Author(s)	Fluid(s)	Jet Geometry ^a	Heated Surface Geometry ^b	Operating Conditions	Remarks and Major Conclusions
Wadsworth & Mudawar (1992) [14]	FC-72	C* $W_n = 0.254$ mm $L_n = 5 W_n$ $H = 2.54$ mm	► Oxygen-free copper $A_s = 12.7 \times 12.7$ mm ² 3 surfaces: flat bare, micro-stud, and micro-groove height, width, and in-between spacing of features are 1.02 mm, 0.305 mm, and 0.305 mm, respectively Blasted with air/water/silica slurry to yield approximately 10 – 15- μ m-radius cavities	$U_n \approx 2 - 10.5$ m/s $\Delta T_{sub,in} = 10 - 40^\circ\text{C}$	Micro-studs and micro-grooves provide surface area enhancements of 4.255 and 4.444 over the flat bare surface, respectively; CHF increases with increasing U_n for all surfaces; CHF based on planform area is highest for micro-groove, followed by micro-studded and flat surfaces for all U_n ; CHF monotonically increases with increasing $\Delta T_{sub,in}$ for micro-stud surface; for micro-groove surface, CHF first decreases then increases with increasing $\Delta T_{sub,in}$
Furuya <i>et al.</i> (1995) [104,193]	Water	F* $W_n = 2.2 - 4.4$ mm Nozzle depth = 50 mm	▲ Copper $W_s = 7, 35$ mm $L_s = 55$ mm ($L_s/W_n = 0 - 25$) Both flat and concave surfaces $R_s = 24.8, 62.1$ mm, ∞ 12- μ m-thick foil directly heated by DC	$U_n = 1.3 - 3.2$ m/s $P_{sat} \approx 1$ atm $\Delta T_{sub,in} = 1.1 - 60^\circ\text{C}$	Primarily proposed to cool diverter surfaces of ITER Fusion Engineering Reactors; for the velocities tested, curvature has only small effect on CHF
Inoue <i>et al.</i> (1995) [103]	Water	F* $W_n = 2.5$ mm $L_n = 200$ mm Nozzle depth = 50 mm $H = 46$ mm	▲ Copper $W_s = 6$ mm $L_s \leq 63$ mm Both flat and concave surfaces $R_s = 24.8, 62.1$ mm, ∞ 12- μ m-thick foil directly heated by DC	$U_n = 6.3, 10.3, 14.6$ m/s $P_{sat} \approx 1$ atm $\Delta T_{sub,in} = 30, 60, 80^\circ\text{C}$	Max. $q''_{CHF} = 38$ MW/m ² for $U_n = 14.6$ m/s and $\Delta T_{sub,in} = 80^\circ\text{C}$; CHF increases near heated surface edges because of surface curvature; the curvature effect is more pronounced for $Fr_{Rs} > 100$
Copeland (1995) [106]	FC-72	Alternate nozzle jet impingement and suction nozzles C_{**} $A_n = 2.5$ mm ²	Copper $A_s = 10 \times 10$ mm ² Arrays of pin-fins (width = 0.1, 0.2 mm; height = 0.1 – 1.0 mm)	$U_n = 0.05 - 4$ m/s $Q_v = 0.075 - 0.6$ L/min $\Delta T_{sub,in} = 40^\circ\text{C}$	Maximum $q''_{CHF} = 369$ W/cm ² ; at these low velocities, CHF has a weaker dependence on Q_v and stronger dependence on pin-fin aspect ratio; CHF shows no dependence on pin-fin width
Wang & Monde (1997) [93], Monde <i>et al.</i> (1998) [94]	Water, R-22	F* Parallel wall jet $W_n = 1, 2$ mm $L_n = 20$ mm	▲ Stainless-steel $L_s = 40, 60, 80$ mm $W_s = 10, 20$ mm 0.2-mm-thick foil directly heated by DC	$U_n = 3 - 15$ m/s $P_{sat} = 1$ bar (water), 15 – 30 bar (R-22) $\Delta T_{sub,in} = 0 - 60^\circ\text{C}$ $\rho_l/\rho_g = 6.6 - 17.5, 1603$	Prior to CHF, subcooled region exists for a certain length, after which saturated nucleate boiling takes place; CHF is associated with evaporation of thin liquid layer near downstream heated surface edge; $n = 87$
Monde & Wang (2000) [95], Monde <i>et al.</i> (2000) [96]	R-113	F* Parallel wall jet $W_n = 1$ mm $L_n = 20$ mm	▲ Stainless-steel $L_s = 40, 80$ mm $W_s = 20$ mm foil directly heated by DC	$U_n = 3 - 15$ m/s $P_{sat} = 1, 2, 4$ bar $\Delta T_{sub,in} \approx 0^\circ\text{C}$ $\rho_l/\rho_g = 50 - 203$	Gravity does not influence CHF, be it for upward-facing or downward-facing surface orientations; $n = 46$
Inoue <i>et al.</i> (2000) [105]	Water	C* $W_n = 6$ mm $L_n = 20$ mm Nozzle depth = 25 mm 2 types of jet plates: normal (uniform confinement height, sharp 90°edges at nozzle exit) and improved (gradually decreasing confinement height from center, rounded nozzle exit edges)	▲ Copper $W_s = 6$ mm $L_s = 4.8 - 63$ mm Both flat and concave surfaces $R_s = 24.8, 62.1$ mm, ∞ 12- μ m-thick foil directly heated by DC	$U_n = 5.0, 8.0, 12.0$ m/s $\Delta T_{sub,in} = 30, 60, 80^\circ\text{C}$	CHF always occurs at outer edges of heated surface; local CHF measured by decreasing resistance of heater farthest from jet center; confinement enhances CHF by ~100% for flat surface; surface curvature has insignificant effect on CHF because confinement effects overshadow centrifugal force effects in resisting splashing; improved jet plate design helps prevent abnormal CHF occurrence and improves local CHF profiles

(continued on next page)

Table 3 (continued)

Author(s)	Fluid(s)	Jet Geometry ^a	Heated Surface Geometry ^b	Operating Conditions	Remarks and Major Conclusions
Robidou <i>et al.</i> (2002) [41]	Water	F*, S* $A_n = 1 \times 9 \text{ mm}^2$ Jet impinges at center of second heated section $H = 3, 6, 10 \text{ mm}$ $H_{pool} = 100 \text{ mm}$	▲ Copper electroplated with 0.5-mm-thick nickel Heated block divided into 8 in-line heating sections of $10 \times 10 \text{ mm}^2$ each	$U_n = 0.66 - 0.8 \text{ m/s}$ $P_{sat} = 1 \text{ atm}$ $\Delta T_{sub,in} = 7 - 17^\circ\text{C}$	Temperature-controlled experiments: q'' for each heating section automatically adjusted to ensure uniform T_s ; CHF strongly decreases with distance from stagnation line; CHF increases with increases in U_n and $\Delta T_{sub,in}$; increasing H increases CHF for free jets but decreases CHF for submerged jets; submerging decreases CHF
Robidou <i>et al.</i> (2003) [194]	Water	F* $A_n = 1 \times 9 \text{ mm}^2$ Jet impinges at center of second heated section $H = 6 \text{ mm}$	▲ Copper electroplated with 0.5-mm-thick nickel Heated block divided into 8 in-line heating sections of $10 \times 10 \text{ mm}^2$ each	$U_n = 0.5 - 1 \text{ m/s}$ $P_{sat} = 1 \text{ atm}$ $\Delta T_{sub,in} = 5 - 20^\circ\text{C}$	Temperature-controlled experiments: q'' for each heating section automatically adjusted to ensure uniform T_s ; CHF first reached in parallel flow region (away from impingement region); CHF decreases with distance from stagnation line until $\sim 10 \text{ mm}$ after which it becomes almost constant
Meyer <i>et al.</i> (2006) [17]	FC-72	C** $N = 3$ re-entrant jets $H = 5.60 \text{ mm}$ $W_n = 0.127 - 0.508 \text{ mm}$	▲ Oxygen-free copper $A_s = 30 \times 30 \text{ mm}^2$	$U_n = 1 - 8 \text{ m/s}$ $P_{in} = 1.06 - 1.88 \text{ bar}$ $P_{sat} = 1.03 - 1.18 \text{ bar}$ $T_{sat} = 57.1 - 61.2^\circ\text{C}$ $\Delta T_{sub,in} = 10.6, 20.6^\circ\text{C}$ $\Delta T_{sub,in} = 26, 44, 56^\circ\text{C}$	$q''_{CHF} = 35 - 139 \text{ W/cm}^2$ (for FC-72); specialized spent fluid removal jet nozzle plate with fluid allowed to exit between nozzles and at ends; CHF increases with increasing U_n and W_n ; CHF increases significantly with increasing $\Delta T_{sub,in}$; for fixed flow rate, CHF decreases with increasing W_n
Omar <i>et al.</i> (2007) [51]	Ethanol Water	$W_n = 1.00 \text{ mm}$ (ethanol) F* $A_n = 1 \times 8 \text{ mm}^2$	▲ Copper C110 $A_s = 8 \times 10 \text{ mm}^2$	$U_n = 0.75 - 1.7 \text{ m/s}$ $P_{sat} = 1 \text{ atm}$ $\Delta T_{sub,in} = 10 - 28^\circ\text{C}$	CHF increases with increasing U_n and $\Delta T_{sub,in}$; $n = 16$
Bogdanic <i>et al.</i> (2009) [195]	Water	F* Centered at heated part of surface $A_n = 1 \times 9 \text{ mm}^2$ $H = 8 \text{ mm}$	▲ Copper with 0.5-mm-thick electroplated nickel Total length = 104 mm $L_s = 9.5 \text{ mm}$ (heated; uncentered about total length) $W_s = 12 \text{ mm}$	$U_n = 0.4 \text{ m/s}$ $\Delta T_{sub,in} = 20^\circ\text{C}$	Boiling curve similar to those in Robidou <i>et al.</i> [41]; optical probe used to observe two-phase flow structure and obtain data of void fraction, contact frequencies, and distribution of liquid and vapor contact times at various locations atop surface
Shin <i>et al.</i> (2009) [84]	PF-5060	C* $A_n = 2.0 \times 10.0 \text{ mm}^2$ $H/W_n = 0.5, 1.0, 4.0$ $L_n/W_n = 20$	▲ Inconel $A_s = 8 \times 10 \text{ mm}^2$ 467- μm -thick heater Polished with emery #2000	$U_n = 0.20 - 0.52 \text{ m/s}$ $T_{in} = 31^\circ\text{C}$ $\Delta T_{sub,in} = 25^\circ\text{C}$	CHF for middle $H/W_n = 1.0$ is lower than other two
Li <i>et al.</i> (2014) [48]	Water	F* $A_n = 1 \times 12 \text{ mm}^2$ $H = 5 \text{ mm}$	▲ Nickel $A_s = 1 \times 10 \text{ mm}^2$; $\theta_{CA} = 90^\circ$ 0.08-mm-thick foil directly heated by DC	$U_n = 4 - 40 \text{ m/s}$ $P_{sat} = 1 \text{ atm} + \rho_f U_n^2/2$ $\Delta T_{sub,in} = 0 - 99^\circ\text{C}$	CHF increases proportional to $U_n^{1/3}$ for $U_n < 10 \text{ m/s}$, but slope changes for higher U_n (for high subcooling, the slope remains unchanged and for low subcooling, the slope increases); their correlation predicts CHF to decrease with increasing U_n when stagnation pressure approaches 1/3 of critical pressure
Chen <i>et al.</i> (2015) [71]	Water	F* $A_n = 1 \times 12 \text{ mm}^2$ $H = 5 \text{ mm}$	▲ Nickel $L_s = 1.5, 5 \text{ mm}$; $W_s = 1 \text{ mm}$ 0.08-mm-thick foil directly heated by DC	$U_n = 10 - 40 \text{ m/s}$ $P_{sat} = 1 \text{ atm} + \rho_f U_n^2/2$ $\Delta T_{sub,in} = 0 - 70^\circ\text{C}$	Max. $q''_{CHF} = 1.14 \times 10^8 \text{ W/m}^2$; stagnation line CHF increases with decreasing heater size
Wang <i>et al.</i> (2016) [72]	Water	F* $A_n = 1 \times 12 \text{ mm}^2$ $H = 5 \text{ mm}$	▲ Nickel $L_s = 1.5, 5 \text{ mm}$ $W_s = 1 \text{ mm}$ 0.08-mm-thick foil directly heated by DC 8 surfaces: bare nickel, 3 chemically treated, 4 electrochemically treated with nanocone array $\theta_{CA} = 5 - 90^\circ$ $R_a = 0.021 - 0.189 \mu\text{m}$; $r = 1 - 1.45$	$U_n = 10, 40 \text{ m/s}$ $P_{sat} = 1 \text{ atm} + \rho_f U_n^2/2$ $\Delta T_{sub,in} = 0, 70^\circ\text{C}$	Max. $q''_{CHF} = 1.62 \times 10^8 \text{ W/m}^2$; CHF is not affected by average nanoscale surface roughness, but increases with increasing solid-liquid contact angle and increasing roughness

^a F: free-surface jets, S: submerged jets, C: confined jets, *: single jet, **: jet array (multiple jets); jets normally impinging ($\theta = 90^\circ$) on surface center unless noted otherwise

^b ▲: upward-facing surface, ▼: downward-facing surface, ►: sideward-facing surface; bare flat surface flush with housing unless noted otherwise; A_s denotes planform area for non-flat surfaces; circular surface only where D_s is given

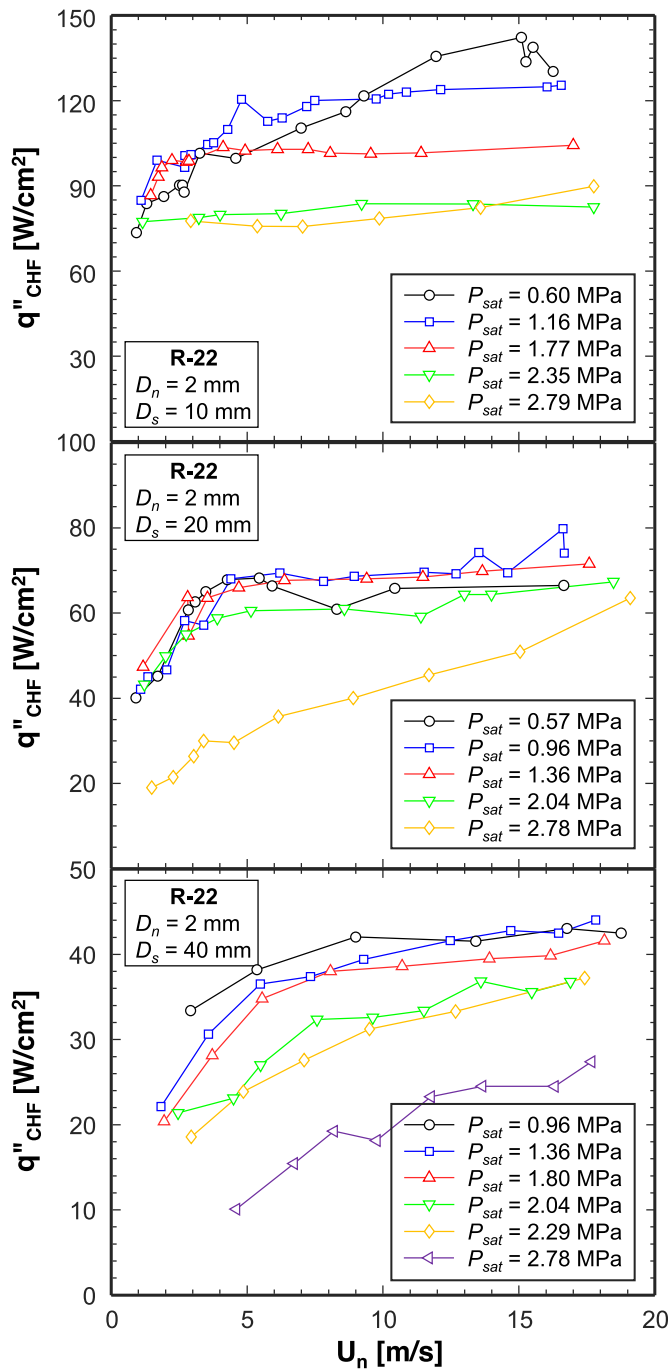


Fig. 3. Variation of CHF with jet velocity for different saturation pressures and heated surface areas. Data adapted from Katto and Shimizu [42] and Monde [44].

22 adapted from both Katto and Shimizu [42] and Monde [44]. It is clear that CHF does increase significantly with U_n for both lower U_n and lower P_{sat} . However, at moderate P_{sat} and higher velocities, CHF becomes almost independent of U_n for $D_s = 10$ mm, and weakly dependent on U_n for $D_s = 20$ and 40 mm. At the highest pressure tested, $P_{sat} \approx 2.78$ MPa, CHF for all three surface areas shows augmentation with increasing U_n throughout the velocity range. Criteria for demarcating between different regimes have been derived simply by equating CHF correlations for adjacent regimes. However, this classification of CHF regimes seems to have fallen out of use by researchers. This could be because neither the lines of transition between regimes nor the mechanisms for regimes or transitions are well understood, probably due to most

experiments not being conducted over sufficiently broad ranges of operating conditions. There is no study in literature that has observed all four regimes in the same set of experiments using the same fluid.

Interestingly, some studies [13,18] have noted a deterioration in CHF when velocity is increased beyond a certain limit, as shown in Fig. 4; this is also evident for the two top cases in Fig. 3. For single confined slot jets, Mudawar and Wadsworth [13] noted the presence of two CHF types, moderate velocity and high velocity, with the transition point depending on confinement height. Transition occurred at lower velocities for lower heights, probably due to an increase in void fraction above the heated surface for lower spacings. This points to existence of an upper velocity limit for maximum CHF for a particular geometry and fluid. The CHF correlation of Li *et al.* [48] (using thermophysical properties determined at stagnation pressure) predicts CHF to decrease with increasing velocity when stagnation pressure approaches one-third of critical pressure, although this decreasing CHF trend was not clearly observed in their experimental data for free-surface single water jets of $U_n = 4 - 40$ m/s. High-velocity jets significantly affect the local saturation pressure, which is further discussed in section 2.5.

The velocity limit at which the CHF trend with jet velocity changes seem to be different for different studies, which implies this limit is a function of fluid properties, operating conditions, or geometrical parameters. Further studies are needed to find relations for the velocity limit.

2.3. Effects of Nozzle and Heater Dimensions

Nozzle size plays a role in determining the portion of heated surface that the jets could sufficiently cover. For a fixed flow rate, nozzle size is one of the factors determining jet velocity at nozzle exit. Discussed here are effects of jet size in the form of diameter or width for round and slot jets, respectively.

For fixed jet nozzle velocity and heater size, nearly all studies [11,18,49] point to higher CHF for larger nozzles, as shown in Fig. 5(a) for round jets and Fig. 6(a) for slot jets. This is because of a higher mass of fluid available for heat transfer and a better coverage of heated surface with the jets. For confined jets and a fixed cross-sectional confinement area, this also increases the speed of the wall jets due to basic mass conservation. Augmentation of CHF for larger nozzles is higher for slower jets; this is the case for both single jets and jet arrays [18], as seen in Fig. 5(a).

When actual thermal management system design is concerned, total flow rate is more relevant than jet velocity. For a fixed flow rate, jet velocity decreases considerably as nozzle size is increased. When CHF data is plotted against total flow rate, as shown in Figs. 5(b) and 6(b) for round and slot jets, respectively, it becomes clear that smaller nozzles yield higher CHF for a fixed flow rate [17,18]. This proves that, at moderate velocities, jet velocity has a stronger effect on CHF than total flow rate. But it should also be noted that pressure drop increases with decreasing nozzle size.

Both heater geometry and size also affect critical heat flux. CHF for round jets has been tested on circular [43], square [18], and rectangular [50] surfaces. Similarly, planar jets have been tested on square [17] and rectangular [51] surfaces. The general consensus is that CHF is higher for smaller surfaces, but it is noted that most studies have been performed with jet nozzles that are smaller than the surface itself. This CHF trend can be explained by burnout typically occurring at locations farthest from the impingement zone. For example, for a circular jet, impingement at the center of a circular surface causes CHF to occur at the heater's outer circumference, and, for a square surface, at the four corners.

An interesting result to note is based on a series of studies by Liu and co-workers [52–55] on localized stagnation zone CHF, which involved use of single round jets of various fluids and jet

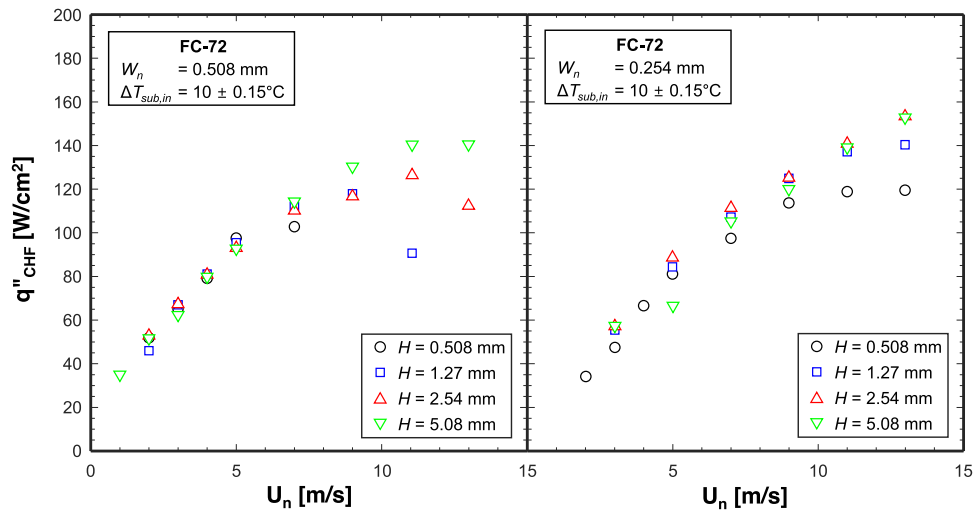


Fig. 4. Variation of CHF with jet velocity for two slot nozzle widths and four confinement heights. Data adapted from Mudawar and Wadsworth [13].

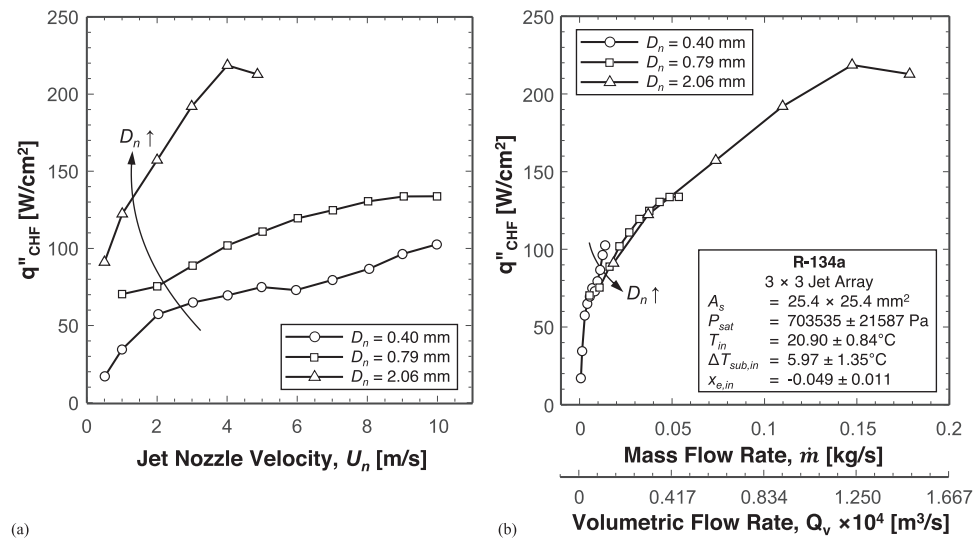


Fig. 5. Variation of CHF with (a) jet velocity and (b) flow rate for different round nozzle diameters. Adapted from Devahdhanush and Mudawar [18].

diameters of $D_n = 3 - 12$ mm impinging on circular heated surfaces of diameter equal to that of the nozzle ($D_s = D_n$). Both saturated and subcooled CHF were found to be inversely proportional to $\sim D_n^{1/3}$, meaning that, for a given set of operating conditions, CHF decreases as both nozzle and heater sizes are increased together.

Maceika and Skema [56] and Skema and Slanciauskas [57] used submerged round single jets and jet arrays of water impinging onto rectangular surfaces and noticed that, as surface length-to-jet diameter ratio, L_s/D_n was increased from 0 (corresponding to stagnation point), CHF increased up to $L_s/D_n = 2$, after which it monotonically decreased. This was attributed to the wall jets having a maximum local velocity at $L_s/D_n = 2$.

2.4. Single Jets versus Jet Arrays

Two problems commonly associated with single jet cooling are surface temperature non-uniformity and inability to adequately cool large surfaces. Using arrays of jets helps overcome these limitations. For round jets, the most commonly used arrangement is a regular ($\sqrt{N} \times \sqrt{N}$) array with equal jet cells [15,18,32,58–61], however other configurations have also been studied [50,57,62–64]. Between the different types of arrays, Skema and Slanci-

auskas [57] showed that staggered (\times) arrays yield higher CHF than regular (+) arrays (see Fig. 1(c)). On the other hand, Werneke [65] showed that array pattern does not influence CHF.

Monde *et al.* [66,67] were the first to investigate the effects of multiple jets impinging onto a single heated surface. Using 2 to 4 free-surface round jets impinging at various locations on a heated disk, they located burnout at places within each jet cell farthest away from the respective jet center. For a fixed jet velocity, higher CHF was obtained with jet arrays over single jets, and with larger than smaller arrays [18], Fig. 7(a). This was attributed to larger amount of fluid impinging in a uniform widespread fashion. For a fixed flow rate, increasing the number of jets led to CHF deterioration [15,18], mainly due to the decrease in jet velocity rendering the jets less effective at piercing through the produced vapor. For systems with stringent flow rate limits, Fig. 7(b) prompts use of single jets over jet arrays, provided the pumping system can tackle the higher pressure drop, and the surface is reasonably small.

Most of the early correlations [66–68] developed for multiple jets took forms similar to those of single jets, excepting the characteristic heated length being based on individual jet cell dimensions instead of heater size. Copeland’s correlations [58,59] for jet arrays also included jet number, N , as parameter to account for interactions between wall jets, but this effect was rather small. But the

more recently developed correlation by Devahdhanush and Mudawar [18] for jet arrays of R-134a and FC-72 and wider ranges of operating conditions and geometries included a stronger influence of N . Their correlation showed CHF is compromised with increasing N because of complex interactions among wall jets.

2.5. Choice of Fluid and Saturation Pressure Effects

As evident from Tables 2 and 3, CHF has been investigated for a wide variety of fluids that include water, refrigerants, dielectric heat transfer fluids, and cryogenics. The choice of fluid mainly depends on the actual thermal management system itself, but it affects CHF due to inherently different thermophysical properties. The effects of each property on CHF can be understood from the various correlations listed in Table 4. Jet CHF is found to be mainly dependent on saturation temperature, T_{sat} , densities of both phases, ρ_f and ρ_g , latent heat of vaporization, h_{fg} , surface tension, σ , and liquid specific heat, $c_{p,f}$ (or liquid enthalpy, h_f).

It is noted that these properties further vary with the saturation pressure within the jet-impingement cooling module. Most correlations point to CHF increasing with increases in ρ_f/ρ_g , h_{fg} , σ , and $c_{p,f}$. By investigating CHF for submerged circular single jets of water over $P_{sat} = 0.176 - 0.477$ bar, Cardenas and Narayanan [27] noted that CHF increased with increasing P_{sat} for both saturated and 17°C subcooled jets. It has already been noted that saturation pressure further affects how CHF varies with jet velocity (HP-regime of Katto and Shimizu [42] for saturated R-22; see Fig. 3), but a clear CHF augmentation with increasing P_{sat} is not observed in the data of Katto and Shimizu [42] and Monde [44] shown in Fig. 3.

Thermophysical properties for most studies have been estimated based on saturation pressure within the jet-impingement cooling module, which is approximately the outlet plenum pressure, P_{out} . This is justified by the pressure drop between the impingement zone and outlet plenum being negligibly smaller than the pressure drop across the jet nozzle. But some studies [48,57,69–72] have noted that properties should be estimated based on impingement stagnation pressure, $P_{sat} = P_{out} + \rho_f U_n^2/2$, to account for effects of fast moving jets (e.g., Skema and Slanciauskas [57]: $U_n = 1 - 35$ m/s, Miyasaka *et al.* [69,70]: $U_n = 1.5 - 15.3$ m/s, Li *et al.* [48]: $U_n = 4 - 40$ m/s, Chen *et al.* [71]: $U_n = 10 - 40$ m/s, Wang *et al.* [72]: $U_n = 10, 40$ m/s). Li *et al.* [48] mentioned that their correlation for $U_n = 4 - 40$ m/s showed $q''_{CHF} \propto U_n^{1/3}$ only for $U_n < 10$ m/s, and attributed departure of predictions above this velocity to large variations in thermophysical properties for fast moving jets.

2.6. Effects of Fluid Subcooling

Most studies [11,13,16,50] agree that fluid subcooling is one of the major parameters that augment CHF for all jet types. An example is shown in Fig. 6, where CHF for $\Delta T_{sub,in} = 20^\circ\text{C}$ is higher than that for 10°C for all jet nozzle widths, jet velocities, and flow rates. This can be attributed to the large condensing effects of subcooled liquid. The bubbles produced at the surface are quickly absorbed by the bulk fluid, leading to a reduction in void fraction and more effective utilization of the fluid's sensible in addition to latent heat. Depending on operating conditions, two main types of CHF can occur, subcooled and saturated. As noted earlier, subcooled CHF is typically higher, and the fluid could even exit the jet-impingement cooling module in subcooled liquid state, which greatly simplifies external flow loop design. Retrofitting a two-phase cooling module into an existing single-phase liquid conditioning loop would be possible, while also taking advantage of much enhanced heat transfer due to nucleate boiling.

It is noted that the exact augmentation of jet CHF with respect to fluid subcooling is slightly different for different studies, evi-

denced by the different forms and exponents of subcooling terms in the correlations listed in Table 4.

Fluid subcooling ($\Delta T_{sub} = T_{sat} - T_f$) can be increased by either increasing the saturation pressure or lowering the fluid temperature. Most of jet literature [11,13,16] involves investigating the effects of ΔT_{sub} by varying the fluid temperature at a fixed pressure (often slightly higher than atmospheric). T_f is typically varied by either heating the fluid using a pre-heater or cooling using a refrigerated chiller. These T_f control methods are possible for fluids with relatively high boiling points at atmospheric pressure (e.g., water, FC-72, HFE-7100), i.e., available in liquid state as they enter the cooling module. On the other hand, the second technique of increasing ΔT_{sub} by increasing the saturation pressure for a fixed fluid temperature is more suitable for low boiling point fluids (e.g., R-134a, liquid nitrogen). This method has been shown to be viable for liquid nitrogen jets by Vader *et al.* [73], who added a non-condensable gas – helium – to increase saturation pressure, for water jets by Mitsutake and Monde [74], who added a non-condensable gas – nitrogen – to increase saturation pressure, and for R-134a jets by Devahdhanush and Mudawar [18], who used a liquid reservoir system with immersion heaters to increase system pressure. Maintaining a constant T_f further eliminates the need for a separate subcooling refrigeration chiller that would greatly increase size, weight, and cost of the entire system [73]. It is obvious that this latter technique is applicable only for a closed loop, and it slightly changes fluid properties by virtue of the increased saturation pressure. Therefore, this second technique can be viewed as one involving the effects of saturation pressure for a fixed fluid temperature. Both Devahdhanush and Mudawar [18] and Vader *et al.* [73] have noted CHF augmentation by increasing P_{sat} for a fixed $T_{f,in}$. It is naturally possible to combine both techniques to vary fluid subcooling as shown by Monde *et al.* [75,76], who varied $T_{f,in}$ using a nozzle heater, and P_{sat} by adding a non-condensable gas – nitrogen – to achieve $\Delta T_{sub,in} = 0 - 115^\circ\text{C}$ for water, R-113, and R-22 jets.

2.7. Effects of Jet Height

Jet height, H , is defined as the distance between nozzle exit and heated surface. Literature has mixed results regarding the influence of H on CHF. Katto and Kunihiro [29] tested both free-surface and submerged single jets of $D_n = 0.71 - 1.60$ mm, $H = 1 - 30$ mm and $U_n < 3$ m/s, and found CHF to increase with decreasing H . In fact, the jet effect was essentially lost for submerged jets with $H = 30$ mm, and the system behaved like pool boiling. Nonn *et al.* [32] tested free-surface round single jets and jet arrays of $D_n = 0.5 - 1.0$ mm and $H/D_n = 0.2 - 5.0$, and showed that most jet heights did not influence CHF. However, when H/D_n was decreased below 0.5, CHF augmentation was reported, probably due to the wall jet starting to become confined.

Robidou *et al.* [41] studied both free-surface and submerged single slot jets for very large surfaces and found that, when H was increased, CHF increased for free jets and decreased for submerged jets. This was attributed to the free jets reaching a larger impinging velocity for higher H , but, for submerged jets, the impinging velocity would be lower due to momentum loss to surrounding fluid.

Mahmoudi *et al.* [77] studied CHF for free-surface free-falling round jets (i.e., very low velocities) over a wide range of jet heights, $H = 5 - 50$ mm, and noticed that, for the lowest nozzle velocity, increasing H decreased the cross-sectional jet diameter near the impingement point due to surface tension effects. The resulting thinner liquid film caused pre-mature CHF. However, the influence of H on CHF decreased upon increasing jet velocity.

Studies by Aihara *et al.* [78,79] for a submerged tube-in-tube jet configuration with $D_n = 0.8$ mm and $H = 0.5 - 2.2$ mm reveal that CHF does increase as H is decreased. Data from a study by

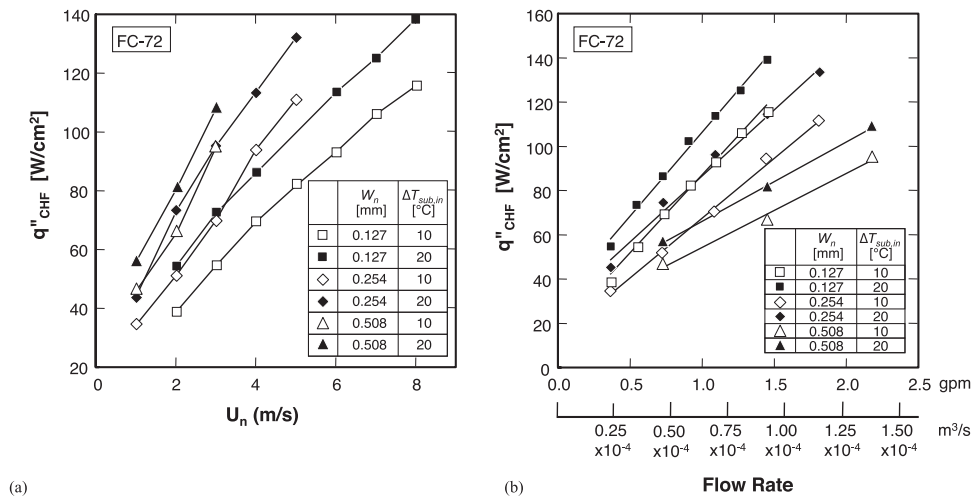


Fig. 6. Variation of CHF with (a) jet velocity and (b) flow rate for different slot nozzle widths and inlet subcoolings. Adapted from Meyer *et al.* [17].

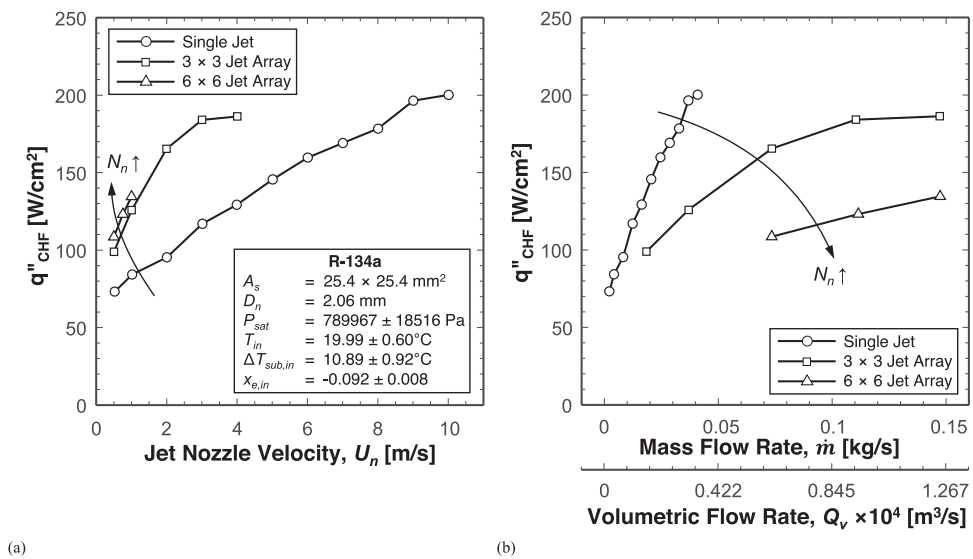


Fig. 7. Variation of CHF with (a) jet velocity and (b) flow rate for round single jets and jet arrays. Adapted from Devahdhanush and Mudawar [18].

Zhang *et al.* [80] for a similar configuration, with $H=1.5$ and 3.5 mm and $D_n=2.0$ mm, also showed that CHF is slightly higher for the smaller height, although the authors did not discuss this aspect in detail. The same trend is supported by Andrews and Rao [81] for submerged single slot jets of $H=12.7 - 50.8$ mm.

For confined jets, jet height is controlled by the confinement height, *i.e.* the spacing between the heated surface and confinement wall. Kamata *et al.* [82,83] studied CHF using confined single round jets of $D_n=2.2$ mm and $H=0.3 - 0.6$ mm, and showed that maximum heat flux was higher for lower H at a fixed Q_v . On the other hand, Johns and Mudawar [16] used confined single round jets of $D_n=0.40 - 2.06$ mm to show that confinement height has negligible effect on CHF for $H=0.51 - 2.03$ mm. Mudawar and Wadsworth [13] studied the effects of height for a much wider range of $H=0.508 - 5.08$ mm using confined single slot jets and found that CHF is unaffected by H for medium velocities of $U_n \approx 1.5 - 7$ m/s (see Fig. 4). For higher velocities, CHF started deteriorating with increasing U_n , especially for smaller H ; however, this effect diminished for smaller nozzle widths. Using confined single slot jets of $W_n=2$ mm, $H/W_n=0.5, 1.0$ and 4.0 , and $U_n=0.2 - 0.52$ m/s, Shin *et al.* [84] showed that CHF for the intermediate H/W_n value was lower than for both the higher and lower. On the

other hand, using confined round jet arrays of $D_n=1$ mm, $H=1, 1.5, 3$ mm and $U_n=0.2 - 0.5$ m/s, Hong *et al.* [64] showed that H influenced CHF the other way around; an intermediate H of 1.5 mm yielded the highest CHF. Both the Shin *et al.* and Hong *et al.* studies point to existence of an optimum confinement height for maximum CHF.

Overall, the present authors believe that jet height, by itself, does not affect CHF. Rather, it affects CHF through combination with other measured parameters such as velocity, nozzle size, and heated surface size, as well as other unmeasured parameters such as the wall jet flow area within the confinement region. Further research on this parameter is required until consensus is reached on its effects.

2.8. Effects of Heated Surface Orientation

A general consensus is that orientation of heated surface with respect to gravity does not affect CHF for jets. Almost all studies have focused on use of a single orientation, mostly upward-, downward-, or sideward-facing. But there are a few exceptions. Monde and Katto [26,34] investigated CHF for free-surface single round jets of water and R-113 impinging onto both upward- and downward-facing surfaces. For their geometries ($D_n=2.0$ and 2.5

mm, $H = 0.3$ and 0.5 mm, $D_s = 10 - 21$ mm) and operating conditions ($\Delta T_{sub,in} = 3 - 30^\circ\text{C}$, $U_n = 1 - 30$ m/s), there were no significant differences between the two orientations. In fact, some of the early CHF correlations [26,85–88] have incorporated data from different orientations without a gravity term. Sharan and Lienhard [88] used a Froude number defined as $Fr_{Ds} = U_n / \sqrt{gD_s}$ to assess any influence of gravity in Monde and Katto's [26,34] data, and concluded that CHF for both orientations coincide for $Fr_{Ds} \geq 10$ (which incidentally is an appropriate criteria to neglect gravity effects [88]). Unfortunately, there were no data available to determine if orientation played a role on CHF for lower Fr , i.e., very low jet velocities. Nonn *et al.* [32] experimented with free-surface round jets of FC-72 impinging onto sideward-facing single heaters and arrays of 3 heaters arranged either vertically (3×1) or horizontally (1×3). Crossflow-effects due to gravity in a heat source array affected neither the boiling curve nor CHF.

The present authors anticipate that gravity effects would play a role for very small jet velocities and/or large heated areas. For such configurations, the liquid wall jets might not be strong enough to maintain contact with a downward-facing heated surface with gravity pulling it downwards. For submerged jets, downward-facing surfaces might prompt vapor to get accumulated near the heated surface due to buoyancy if the wall jets are not strong enough to push them away. It is also anticipated that gravity effects would play a lesser role on CHF for confined jets with smaller confinement heights.

2.9. Effects of Dissolved Non-Condensable Gases

Many authors [13,16,17,61,89] specifically stated that the fluid batch used was thoroughly de-aerated (de-gassed) before experiments, while some [69] indicated otherwise. Some [18] used closed loops that had to be vacuumed before charging with pure fluid. And some [73–76] intentionally added non-condensable gases to increase the fluid subcooling. However, many studies have not stated if the liquid was pure or saturated with gases, either assuming that this is implicitly understood or believing the insignificant role of dissolved gases on jet CHF.

Non-condensable gases are capable of being dissolved in most liquids and this is an important consideration for two-phase flows. They could contribute a serious partial pressure and increase the total system pressure. They could also accumulate as gas bubbles near the heated surface. This has been shown to be important for pool boiling CHF by Haramura [90], who reported 25–30% lower CHF for gas-saturated water than degassed water. Monde and his co-workers [74–76] justified their use of nitrogen to pressurize the working fluid and measure CHF at higher subcoolings by stating that, for heat fluxes close to CHF, the dissolved gas would be removed from liquid near the heated surface due to violent nucleate boiling producing massive amounts of vapor.

The effects of dissolved non-condensable gases on jet CHF were inadvertently observed by Browne *et al.* [62] in their experiments of confined circular jet arrays of R-134a. Their experimental setup used a bladder accumulator, which was faulty and leaked nitrogen into the refrigerant. Comparing the faulty data to pure-R-134a data, they observed that they were able to further extend their boiling curves, increasing both CHF and the corresponding wall superheat for similar operating conditions. Their follow-up study [63] involved systematic investigation of the effects of dissolved nitrogen for partial pressures of 0, 103 and 241 kPa. They ended up contradicting their previous hypothesis and showed the boiling curves were not significantly affected by nitrogen content. As shown in Fig. 8, for all inlet subcoolings, their data indicate that CHF does not follow any trend with respect to the partial pressure offered by dissolved non-condensable gas.

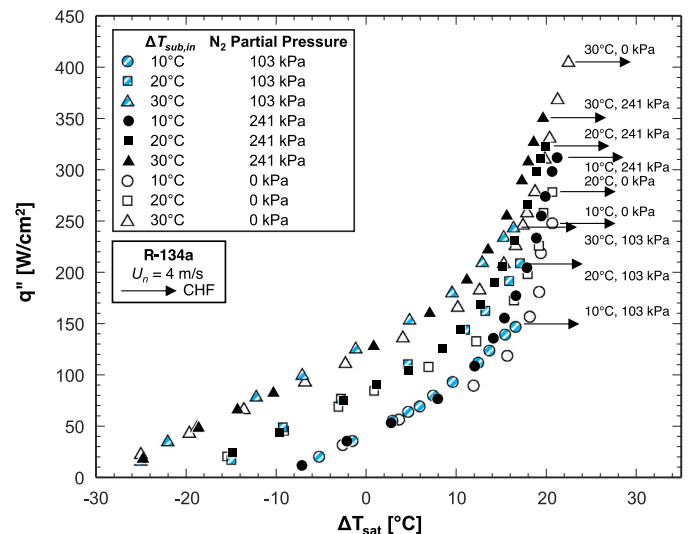


Fig. 8. Jet impingement boiling curves, indicating CHF, for different subcoolings and nitrogen partial pressures. Legend listed in chronological order of experiments. Data adapted from Browne *et al.* [63].

2.10. Effects of Nozzle Shape

Although numerous studies have studied CHF for circular and slot jets in detail, this was done by focusing on either and not both. Since no study systematically investigated CHF for both geometries using the same experimental setup and identical operating parameters, the present authors refrain from commenting on any differences between the two jet geometries.

3. CHF for Special Jet Configurations

CHF for special (unconventional) jet configurations is discussed in this section. This includes jets that impinge at various angles other than normal, such as oblique and wall jets, liquid jets created by techniques other than pump or gravity head, such as using a strong electric field (electrohydrodynamic or ionic jets), and use in a vapor compression cycle.

3.1. Oblique Jets

CHF for confined arrays of round impinging jets impinging at a fixed oblique angle of 45° was investigated by Buchanan and Shedd [30]. Their investigation encompassed various geometrical parameters and operating conditions using R-245fa, culminating in CHF values in the range of $\sim 35 - 110$ W/cm². Like conventional jets, CHF for oblique jet arrays was also strongly influenced by T_{in} and Q_v . But their CHF values were strongly underpredicted by the free-surface jet correlations of both Monde [87] and Katto and Yokoya [85], which could be attributed to differences in confinement effects. So, Buchanan and Shedd developed their own correlation based on pool boiling principles.

3.2. Slot Wall Jets

Jets introduced at an edge of the heated surface are termed wall jets and they are typically planar to cover the entire heated surface with a film of liquid. They are typically introduced parallel to the surface [31,91–96], but researchers have also studied oblique planar wall jets [97]. Planar wall jets parallel to the surface can be viewed as open channel flows, external flows over a flat plate, or forced convective liquid films. These wall jets have somewhat similar flow physics as the wall jets that develop far downstream from the impingement point of normally impinging jets.

Baines *et al.* [92] studied CHF for free-surface planar wall jets of water introduced at the top edge of a heated surface that was inclined at either 45° or 90° to horizontal. CHF was found to increase with increasing jet velocity, but this effect was weaker for velocities greater than 2.5 m/s. But CHF was independent of angle of surface inclination. In a series of studies [93–96], Monde and his co-workers studied CHF for free-surface planar wall jets of water, R-22, and R-113 over upward-facing surfaces. For subcooled jets, prior to CHF, a subcooled region existed for a certain length, after which saturated nucleate boiling took effect. CHF was associated with evaporation of a thin liquid layer near the downstream edge of the heated surface. Katto and Ishii [97] experimented with free-surface planar wall jets of water, R-113, and trichloroethane on downward-facing surfaces with oblique angles of 15° and 60°. Katto and Haramura [91] tested CHF for free-surface planar wall jets of water and R-113 on downward-facing surfaces. Overall, planar free-surface wall jet CHF data for both upward- [93–96] and downward-facing [91,97] surfaces did not show differences, meaning that gravity did not play an important role in the CHF mechanism.

CHF for a submerged planar wall jet introduced from the bottom edge of a sideward-facing surface was studied by Katto and Kurata [31]. Using water and R-113 for different nozzle widths and heated surface lengths, CHF was shown to be independent of nozzle width.

3.3. Electrohydrodynamic (Ionic) Jets

Electrohydrodynamic (ionic) jets are produced by application of large potential difference between two electrodes within a dielectric medium. Ions are injected from an electrode toward the heated surface. This technique voids the need for nozzles or fluid collection plenums. Essentially, it creates an axisymmetric jet of ions within a submerged heated surface similar to that of a conventional submerged round jet. CHF for these jets was first studied by Grassi and Testi [98] for single jets and in-line jet arrays of FC-72 and HFE-7100. The jets of ions were formed at high-voltage (on the order of 10⁴ V) negative DC polarity electrodes made of regular tailor’s steel pins and impinging onto an electrically grounded heated plate. The heated plate itself was 40-μm thick and heated directly with current applied at lower voltage. CHF was augmented using the ionic jets compared to pool boiling, with better augmentation achieved with multiple jets. A follow-up study by Grassi *et al.* [99] used a platinum electrode to produce a single jet of FC-72 that impinged onto a copper surface. Boiling curves for both ionic jets and pool are shown in Fig. 9(a), along with values of the injection current required to produce the jets. Improvement of the entire boiling curve was possible with a small amount of energy. As shown in Fig. 9(b), CHF was enhanced over pool boiling by up to ~40%, with the enhancement ratio proportional to the estimated electrohydrodynamic Reynolds number.

3.4. Vapor Compression Cycle

Jet impingement cooling using fluids such as refrigerants possess the added advantage of being incorporated into the vapor compression cycle. The jet nozzles could be used as expansion devices, making it possible for integration of expansion devices and evaporator into one unit, the jet impingement cooling module. This was studied in detail in a series of articles by de Oliveira and Barbosa [100–102], but the results were presented for the entire system in refrigeration application terms rather than the cooling module alone. Both single and multiple jets were tested for different jet heights, nozzle diameters, compressor piston displacements, and condenser secondary fluid temperatures. CHF decreased with a reduction in jet height for the 75% and 100% compressor strokes but

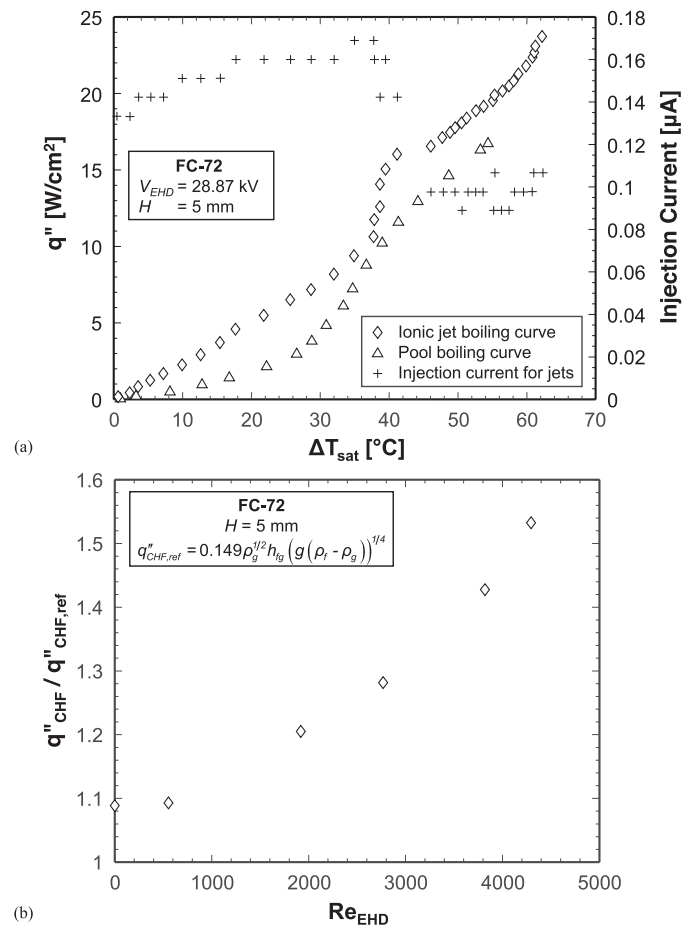


Fig. 9. (a) Boiling curves for ionic jet impingement boiling and pool boiling, along with injection current required to produce the jets, and (b) CHF enhancement using ionic jets for different Re_{EHD} . Data adapted from Grassi *et al.* [99].

remained unaffected for the 50% stroke; this was attributed to visual observations of increased jet splattering and droplet breakup for low jet heights. CHF was higher for the higher condenser secondary fluid temperature. This could be due to increased inlet temperature of the cooling module. Multiple jets enhanced CHF because of a less abrupt transition from a fully wetted to a partially wetted surface.

4. CHF Enhancement Techniques

4.1. Surface Modification

4.1.1. Surface Curvature

Although almost all jet studies have been conducted on flat surfaces, a few researchers have investigated the effects of surface curvature on impinging jet CHF.

With a focus on cooling the divertor surface of magnetic confinement fusion reactors, where local dissipation rates as high as 30 MW/m² are required, Inoue *et al.* [103] proposed using free-surface planar jet impingement boiling on both flat and concave surfaces. Three curvature radii were tested, $R_c = 24.8, 62.1$ mm, and ∞ , and jet velocity was varied from $U_n = 6.3$ to 14.6 m/s. They reported that the centrifugal force of wall jets on concave surfaces augmented CHF by providing better liquid contact near the heated surface edges, especially for $Fr_{Rs} > 100$. The same research group published another study by Furuya *et al.* [104], wherein they considered different nozzle widths and lower velocities of $U_n = 1.3 - 3.2$ m/s for the same three heated surfaces. They noticed that cur-

vature had a small effect on CHF, presumably because of the small velocities tested. With an aim to further enhance CHF for the same application, Inoue *et al.* [105] proposed using confined planar jet impingement boiling on both flat and concave surfaces. CHF always seemed to occur at the outer edges of the heated surface. By comparing their flat surface results to some of their past free-surface jet results [103], they found that having a confinement wall enhanced CHF by $\sim 100\%$ in the downstream wall jet region. On the other hand, surface curvature did not play an important CHF augmentation role because the confinement overshadowed the centrifugal effects in terms of splashing reduction. An improved jet plate design (with a rounded nozzle exit and a linear confinement flow area reduction towards the outlet) prevented abnormal unexpected CHF occurrences and improved local CHF profiles.

Surface curvature was also studied for smaller area ratios. Zhang *et al.* [80] experimentally investigated submerged tube-in-tube round jets of liquid nitrogen impinging onto three different heat transfer surfaces: flat, concave with $R_s = 2.5$ mm, and flat with a 5-mm-tall needle of base diameter 1 mm. CHF was found to increase with increasing jet velocity, and highest values were obtained for the concave surface for similar operating conditions.

4.1.2. Extended Surface Structures

Heat transfer enhancement using extended surfaces (typically fins) is a well-known concept that has shown viability for both single-phase and two-phase heat transfer situations. The principle behind this is simple: extended surface structures increase surface area for heat transfer which in turn augments heat transfer rate.

Wadsworth and Mudawar [14] were amongst the first to investigate the effect of surface micro-structures on impinging jet CHF. They compared impingement of a single slot jet onto three different heat transfer surfaces: bare flat, micro-stud (also called pin-fin), and micro-groove (longitudinal 2D fins producing open micro-channels), the dimensions of which are illustrated in Fig. 10(a). The micro-stud and micro-groove surfaces provided substantial area enhancements of 4.255 and 4.444, respectively, over the flat surface. Figures 10(b) and 10(c) show variations of CHF with jet velocity based, respectively, on planform area and total wetted area. Notice that CHF based on planform area is highest for the micro-grooved surface, followed by the micro-studded and flat surfaces for all velocities. Inlet subcooling produced a strange effect with the micro-grooved surface; CHF decreased with increasing subcooling up to a point, after which it increased in a predictable fashion.

Many other researchers [58,106–109] investigated CHF for round jets impinging onto surfaces with extended structures, and all agree that surface structures augment CHF. Copeland [58,106] studied two nozzle plate configurations and multiple fin thicknesses and heights, and showed pin-finned surfaces to consistently enhance CHF over bare flat surfaces. CHF seemed to have a stronger dependence on pin-fin aspect ratio but independent of pin-fin width for a fixed aspect ratio. Zhang *et al.* [107,108] studied confined jets impinging onto surfaces with two different pin-fin heights and thicknesses and showed that fin height-to-pitch ratio and jet velocity were the main parameters affecting CHF, and larger CHF enhancements with increasing Re were obtained for smaller jet heights.

Recently, Zhang and Chen [110,111] showed that CHF augmentation could be achieved for both free-surface and submerged single round jets by attaching brass bead-packed layers to the heated surface. They suggested that both the number of layers and bead diameter ought to be optimized to obtain the highest CHF enhancement.

4.1.3. Surface Coatings

Surface coatings involve the deposition of certain materials onto the heated surface. These affect boiling heat transfer by modifying

both the solid-fluid contact angle and the distribution of bubble nucleation cavities.

A series of articles by Liu and Qiu [112–114] addressed the effects of coating a copper surface with $\sim 1\text{-}\mu\text{m}$ -thick TiO_2 layer by the dipping method. Some of the coated surfaces were then irradiated with ultraviolet light of wavelength 275 – 315 nm to make them superhydrophilic. Contact angles for the bare copper, TiO_2 coated, and TiO_2 superhydrophilic (irradiated) surfaces were 40–70°, 20–40°, and $\sim 0^\circ$, respectively. CHF for the superhydrophilic surfaces were $\sim 30\text{-}50\%$ higher than for bare copper. The quantitative effects of other parameters such as jet velocity, nozzle diameter, and subcooling were found to be same for all surfaces.

Li *et al.* [115] studied the effects of nano-scale surface modification on free-surface jet CHF. The heat transfer surfaces were made either hydrophilic or hydrophobic by different chemical processes described in their study. The contact angles were $\theta_{CA} = 5^\circ, 60^\circ,$ and 105° for the hydrophilic, bare copper, and hydrophobic surfaces, respectively, and CHF was found to increase with decreasing contact angle. Another study by Wang *et al.* [72] tested 8 surfaces: 1 bare nickel, 3 chemically-treated, and 4 electrochemically treated with nanocone array. The different surfaces had $\theta_{CA} = 5\text{-}90^\circ$, average roughnesses of $R_a = 0.021 - 0.189 \mu\text{m}$, and roughness parameters of $r = 1 - 1.45$. CHF was unaffected by the average nanoscale surface roughness but increased with increasing roughness parameter. In contradiction to their previous study [115], CHF was concluded to “obviously worsen” with decreasing contact angle, although their data suggests the opposite.

4.1.4. Combinations of Enhanced Surface Structures and Coatings

Some researchers attempted to combine the advantages of both enhanced surface structures and surface coatings. Lay and Dhir [116] investigated free-surface jets on nine different surfaces: 1 bare flat, 3 macro-structured (with grooves and ridges), 1 micro-structured (sintered), and 4 surfaces with both macro- and micro-structuring, and found all structured surfaces to augment CHF. The amount of CHF augmentation depended on actual geometry of structuring, with the highest increase of $\sim 125\%$ obtained for a surface with both macro- and micro- structuring, proving combinations of surface enhancement techniques is an effective means to achieving large CHF values. They also noted that a simple oxidation of the bare copper surface augmented CHF by $\sim 5\text{-}10\%$. With a focus towards cooling wide band-gap power semiconductor devices, Joshi and Dede [117] studied the use of confined 5×5 jet arrays impinging onto 4 different microporous-copper-coated copper surfaces and found CHF to increase in the order of flat surface, flat with closed tunnels, flat with open tunnels, and pin-finned.

Overall, all studies discussed in this section promise augmentation of jet impingement CHF by use of extended surface structures or surface coatings, and larger CHF augmentation is made possible by combining both. It is well-known that a major limitation of jet impingement is possible erosion of the surface due to both high impact and shear stresses. But the life of surface coatings has not been assessed for reliable operation of jet-impingement modules. Additionally, available studies concern very specific geometries and coatings, rendering optimal choice of surface condition based on currently available data quite difficult.

4.2. Specialized Spent Fluid Removal

Spent fluid refers to the fluid that has passed over the heated surface and acquired sensible and/or latent heat. The most common spent fluid removal scheme is fluid exiting from the sides of the heated surface, either due to gravity or cooling module design. This might be sufficient for single jets, but for jet arrays, complex jet interactions between the wall jets of neighboring jets point to a

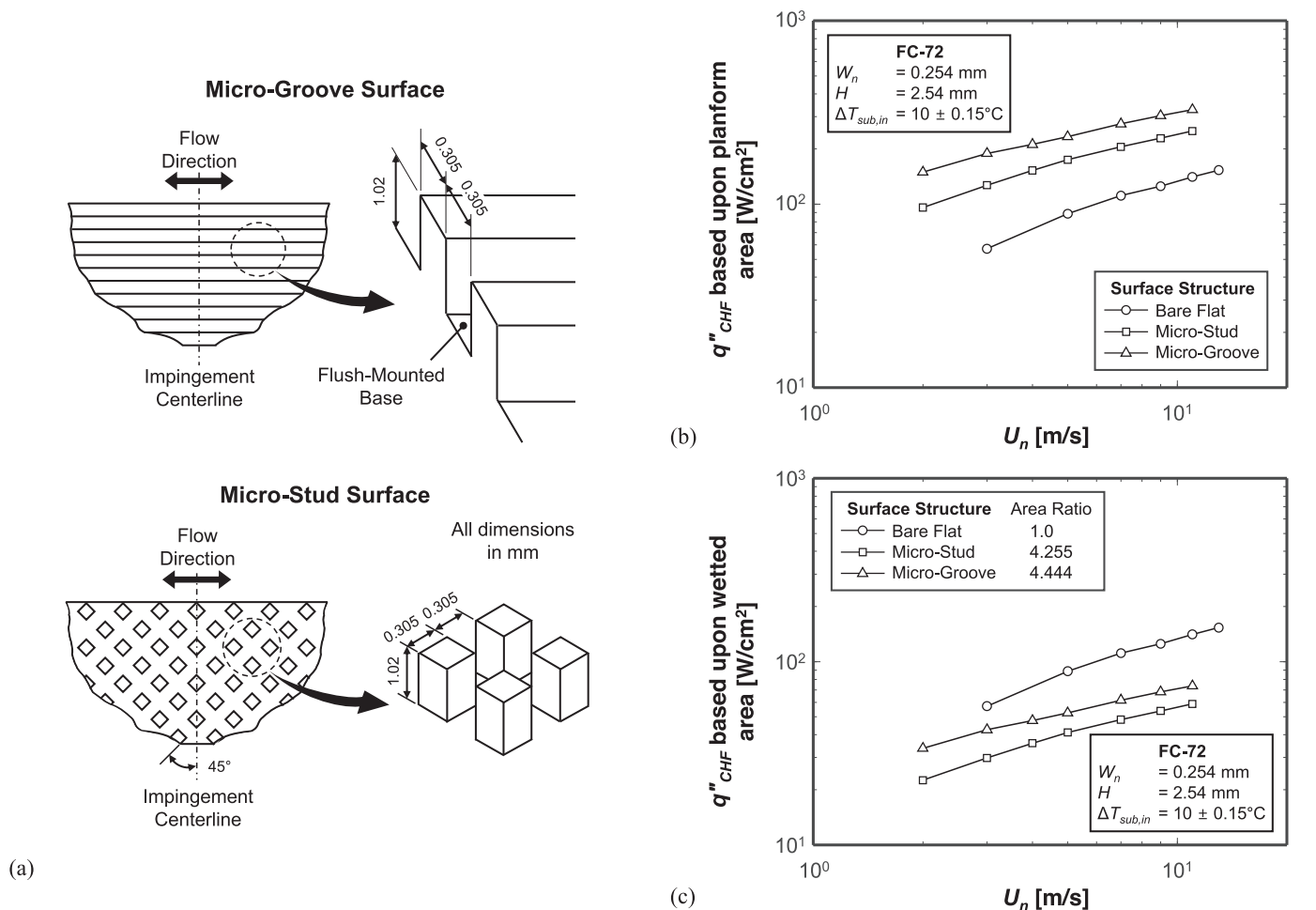


Fig. 10. Surface enhancement techniques: (a) schematics of micro-groove and micro-stud surfaces, and CHF dependence on jet velocity for different surfaces based upon (b) planform area and (c) total wetted area. Adapted from Wadsworth and Mudawar [14].

need for more specialized spent fluid removal schemes in pursuit of higher CHF.

Copeland [106] experimented with arrays of slot jets impinging on different pin-finned surfaces, which were also used in their previous study [58]. Their nozzle manifold housed an assembly of 1-mm-thick plates making alternating inlet and outlet channels 1-mm wide on a 2-mm pitch. They termed this configuration as “multiple slot jet nozzle suction and impingement”, but, unfortunately, no comparisons were made with conventional slot jet arrays. CHF showed a rather weak dependence on flow rate, a stronger dependence on pin-fin aspect ratio and an independence of pin-fin width.

Meyer *et al.* [17] designed a specialized slot jet array nozzle plate that had provisions for both impinging jet nozzles and spent fluid return paths, as shown in Fig. 11(a). An array of 3 slot jets of FC-72 or ethanol impinged onto a heated surface at the centers of equally divided jet cells. Slots in larger width at the geometric centers between neighboring nozzles collected the spent fluid, which was then returned to the flow loop. Return slots were also available at both ends of the array. The main concept here is that the wall jets, after colliding, would rise upwards and pass through the return slots without recirculating over the heated surface. Recirculation of spent fluid could bring the hotter fluid close to the surface, which would reduce cooling effectiveness. Immediate removal of produced vapor might augment CHF by not allowing large vapor masses to accumulate in the lower velocity regions above the heated surface. Furthermore, this nozzle plate served as a confine-

ment wall, parallel to the heated surface, helping to reduce splashing during boiling. Photos of different jet plates fabricated for their study are included in Fig. 11(b). Typical trends of CHF were observed: CHF increased with increases in jet velocity, nozzle width, and inlet subcooling. But, for a fixed flow rate, CHF decreased with increasing nozzle width, proving jet velocity has a stronger influence on CHF than flow rate. They showed that their configuration helped maintain surface temperature uniformity, with variations of less than 2.6°C.

Sarkar *et al.* [118] designed a specialized 4 × 4 jet array nozzle plate that has provisions for both circular jet nozzles of diameter $D_n = 1.6$ mm and circular spent fluid return holes of diameter $D = 1.32$ mm. The return holes were machined at the four corners of each jet cell, making it a 5 × 5 circular hole array. As seen in most experiments, higher CHF was obtained with higher flow rates and higher inlet subcoolings. Upon testing different confinement heights of $H = 0.254, 0.381,$ and 0.635 mm, highest CHF was achieved with the intermediate confinement height. Their jet plate geometry also made it possible to reverse flow direction quite easily; but no significant differences were seen in boiling curves and more importantly, CHF, for similar flow rates. A similar concept was tested by Cui *et al.* [109], who showed that a distributed jet plate with spent fluid removal holes at the four corners of each jet cell augmented CHF compared to a jet plate without the fluid removal holes due to improved flow uniformity in each cell.

It is clear that utilizing these novel nozzle plate designs does help cool very large surfaces using large jet arrays, by providing

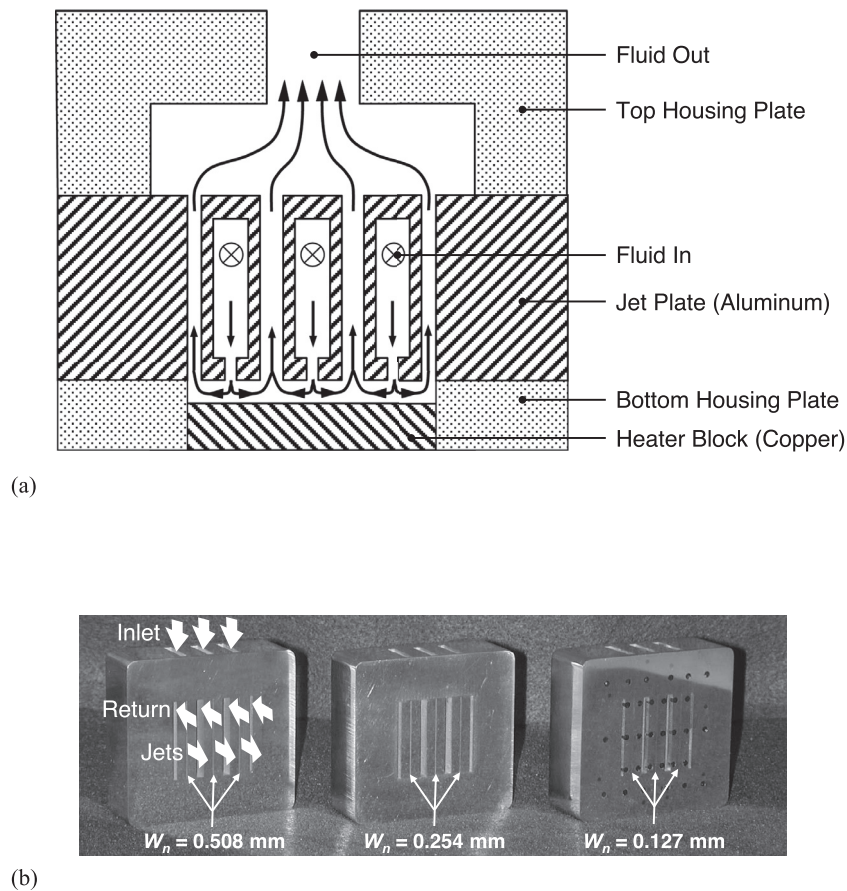


Fig. 11. Spent fluid removal scheme for slot jet arrays. (a) Coolant path inside cooling module. (b) Photos of underside of jet plates. Adapted from Meyer *et al.* [17].

both improved CHF and a more uniform surface temperature. But, some foreseeable drawbacks of these nozzle plates are increases in total cooling module size and weight.

4.3. Nanofluid Jet Impingement

Nanofluids are specialized fluids with nanoparticles such as Al_2O_3 , TiO_2 , or CuO (of typical size 1 – 100 nm) suspended in a base liquid such as water or glycol. While numerous studies have been published on usage of nanofluids for enhancing heat transfer in single-phase jet impingement and a few in jet impingement boiling, only one study addressed the CHF aspects of nanofluids (to the best of the authors' knowledge). Liu and Qiu [119] investigated impinging jet boiling and CHF on a large surface using both CuO /water nanofluids and pure water. As shown in Fig. 12, CHF gradually increased with increasing nanoparticle concentration up to 1% wt., above which it became unaffected by concentration. CHF increased by a maximum of $\sim 25\%$ for nanofluids over water. They attributed this enhancement to surface sorption layer effect, which enhances liquid trapping near the surface and decreases both active nucleation and contact angle, and in turn decreases ability of vapor bubbles to coalesce together into a vapor blanket along the surface. Increasing nanoparticle concentration increased the thickness of this sorption layer, and hence the CHF. But the sorption layer thickness remained unaffected after a certain concentration. It was also noted that the stability of nanofluids was poor and sedimentation occurred after “a long time” for concentrations higher than 1% wt. This last statement is an important hinderance for deploying nanofluids in thermal management systems. Further practical concerns of using nanofluids are detailed in a review article by Liang and Mudawar [120].

4.4. Other Techniques Proven Inefficacious

4.4.1. Rotating Nozzle Plate

With a motivation to improve surface cooling by wetting the surface with a thin liquid film of continuously replenished coolant, Pais *et al.* [121] experimented with rotating circular nozzle plates of nozzle diameters $D_n = 127 - 368 \mu\text{m}$. The free-surface jet nozzle plate was mounted atop the heating surface such that its axis of rotation was aligned in a way to uniformly traverse all jets over the circular heated surface. A motor with a variable speed drive was connected to the jet plate by a timing belt. Arrays of both 4 and 9 jets were tested, with the 4 jets aligned in-line along a radius of the jet plate, and 9 jets aligned both in-line along a radius, and in a ‘+’ fashion, as shown in Fig. 13. Their idea proved inefficacious as no significant change in CHF was observed with jet velocity, number of jets, or speed of rotation for a fixed flow rate. This was attributed to the circumferential component of liquid film velocity inducing a radially-outward-moving swirling flow and a reduced residence time of coolant on the surface. They proposed that fabricating jet plates with micro-jets of diameters $D_n < 25 \mu\text{m}$ might help maintain a very thin evaporative film ($< 3 \mu\text{m}$ thickness) on the heated surface and therefore enhance CHF. However, as seen in most other studies, higher CHF was indeed obtained for higher flow rates and higher inlet subcoolings.

4.4.2. Heating Element Protrusion

Almost all studies on CHF are from a surface that is flush with its housing, with the main exceptions being Copeland [23] who did not insulate the sides of the heater block, and Lay and Dhir [116] whose heater protruded outside the housing by $\sim 0.5 \text{ mm}$.

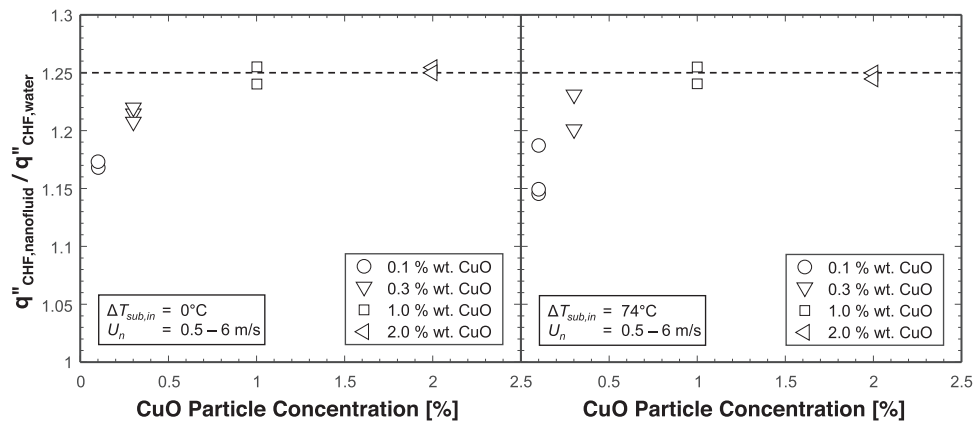


Fig. 12. Enhancement of CHF by addition of nanoparticles to water at different subcoolings (reference dashed lines indicate 25% enhancement). Data adapted from Liu and Qiu [119].

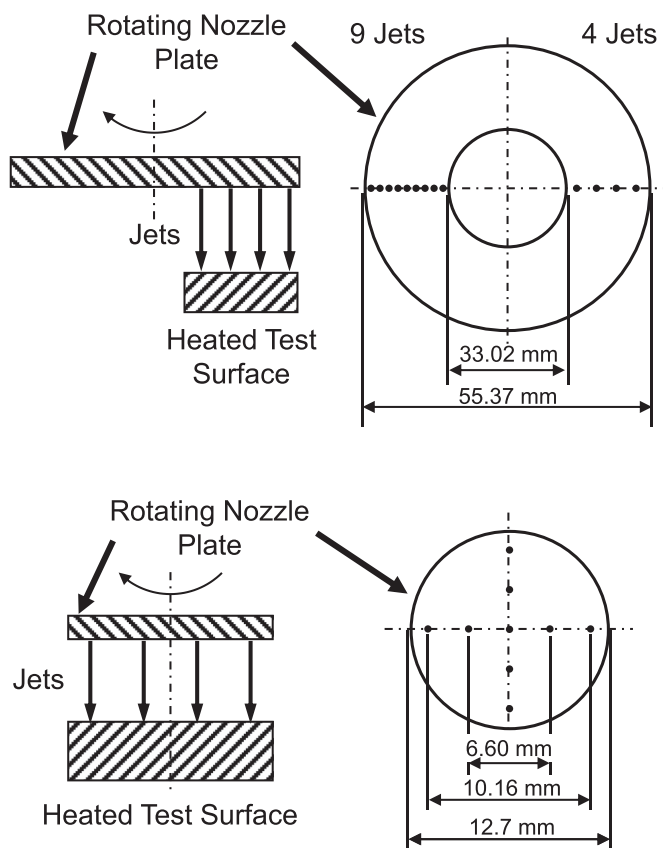


Fig. 13. Rotating nozzle plate configurations over a circular heated surface. Redrawn based on Pais et al. [121].

But, in cooling systems for devices and electronic chips, the heated surface need not be fully flush with the coolant flow path and could slightly protrude outward. With an idea to reduce the effective heat flux by heating surface protrusion, McGillis and Carey [122] studied this aspect using confined single jets of R-113 with $6.4 \times 6.4 \text{ mm}^2$ heating elements that were either flush or protruding outwards by 0.8 mm. For similar operating conditions, neither boiling curve nor CHF were noticeably different for the two configurations. It is noted that heat flux for the protruding elements was based on total surface area exposed to the flow.

4.4.3. Jet Suction

In addition to jet impingement, McGillis and Carey [122] tested jet suction as a means to enhance pool boiling CHF of R-113. This was done using the same test setup as jet impingement by reversing flow direction; the jet nozzle was essentially used to suck the spent two-phase mixture. For comparable operating conditions, CHF values for both jet impingement and jet suction were in good agreement, although results were limited to a small heated surface area of $6.4 \times 6.4 \text{ mm}^2$. Jet suction performed on a par with impingement by virtue of its own advantage of better removal of produced vapor from the middle of the heated surface, where the fluid is hottest and has the highest velocity.

The present authors anticipate that jet suction would yield lower CHF than impinging jets for larger surfaces, as liquid flow in suction could not enable liquid to pierce the vapor film but rather act as channel flow. However, more data is needed to reach a definite conclusion.

5. Jet CHF Prediction Techniques

Many experimental studies on jet impingement CHF have yielded design correlations for CHF prediction. Table 4 gives a summary of available correlations for CHF in jet impingement boiling, along with the rationale behind their development and some remarks on their applicability. Most were developed by dimensional analysis, trial-and-error procedures, or modifying previous correlations to fit newer experimental data. Some were developed based on the underlying CHF mechanisms and further reduced based on a variety of assumptions and approximations. Some examples are discussed here.

For very low flow rates, a very simple CHF mechanism was proposed: CHF is the outcome of deficiency of liquid supply. By assuming that all the liquid is vaporized (without any splashing), and that jet velocity is high enough to neglect both surface tension and gravity effects, Katto and Shimizu [42] proposed that CHF can be predicted via an energy balance as

$$\frac{q''_{CHF}}{\rho_g h_{fg} U_n} = C \frac{\rho_f}{\rho_g} \left(\frac{D_n}{D_s}\right)^2, \tag{1}$$

where C is the fraction of liquid that is evaporated, therefore $C = 1$ at CHF. Many later studies were successful in predicting this kind of CHF in their own experiments by merely modifying the value of C to account for splashing effects. Katsuta and Kurose [123] used $C = 0.04$ for single round jets of R-11 impinging onto upward-facing surfaces, while Monde and Okuma [43] proposed a function to determine C for both water and R-113 jets impinging onto downward-facing surfaces, which was based on parameters that

Table 4
Summary of correlations for CHF in jet impingement boiling.

Author(s)	Correlation(s)	Rationale	Applicability and Remarks ^c
Katto & Monde (1974) [35]	$q''_{CHF} = 3.4 \times 10^6 U_n^{0.39}$; q''_{CHF} in W/m ² and U_n in m/s	Exponential fit of data	Refer to Table 2
Monde & Katto (1977, 1978) [26,196]	$\frac{q''_{CHF}}{\rho_b h_{fg} U_n} = 0.0745 \left(\frac{\rho_l}{\rho_g}\right)^{0.725} \left(\frac{\sigma}{\rho_l U_n^2 D_s}\right)^{1/3} (1 + \varepsilon_{sub})$; $\varepsilon_{sub} = 2.7 \left(\frac{\rho_l}{\rho_g}\right)^{0.5} \left(\frac{c_{p,l}(T_{sat} - T_{in})}{h_{fg}}\right)^2$	Dimensional analysis of numerous physical parameters assumed/known to influence CHF	Refer to Table 2
Katto & Ishii (1978) [97]	$\frac{q''_{CHF}}{\rho_b h_{fg} U_n} = 0.0164 \left(\frac{\rho_l}{\rho_g}\right)^{0.867} \left(\frac{\sigma}{\rho_l U_n^2 L_s}\right)^{1/3}$	Similar to Monde and Katto [26]	Refer to Table 3
Katto & Shimizu (1979) [42]	V-regime (R-12 at $P_{sat} = 6.0 - 17.7$ bar, water, R-113): $\frac{q''_{CHF}}{\rho_b h_{fg} U_n} = 0.188 \left(\frac{\rho_l}{\rho_g}\right)^{0.614} \left(\frac{\sigma}{\rho_l U_n^2 D_s}\right)^{1/3}$ I-regime (R-12 at $P_{sat} = 17.7 - 27.9$ bar): $\frac{q''_{CHF}}{\rho_b h_{fg} U_n} = 1.18 \left(\frac{\rho_l}{\rho_g}\right)^{0.614} \left(\frac{\sigma}{\rho_l U_n^2 D_s}\right)^{1/2}, \frac{\rho_l}{\rho_g} > 6$ D-regime (very low velocities): $\frac{q''_{CHF}}{\rho_b h_{fg} U_n} = \frac{\rho_l}{\rho_g} \left(\frac{D_n}{D_s}\right)^2$ Boundary between D- and V- regimes: $\frac{\sigma}{\rho_l U_n^2 D_s} = 150 \left(\frac{\rho_l}{\rho_g}\right)^{1.16} \left(\frac{D_n}{D_s}\right)^6$ Boundary between V- and I-regimes: $\frac{\sigma}{\rho_l U_n^2 D_s} = 1.64 \times 10^{-5}$	Similar to Monde and Katto [26]; D-regime: heat balance; boundaries between regimes determined by equating respective q''_{CHF} correlations	Refer to Table 2
Lienhard & Eichhorn (1979) [125]	$\frac{q''_{CHF}}{\rho_b h_{fg} U_n} = C_1 \left(\frac{D_n}{D_s}\right) \left(\left(\frac{D_s}{D_n}\right)^3 \frac{\sigma}{\rho_l U_n^2 D_s}\right)^{C_2}$; $C_1 = \left(\frac{\rho_l}{\rho_g}\right)^{0.725}$; $C_2 = \{3/8, 1/3, 1/4\}$	Mechanical Energy Stability Criterion previously proposed by same authors [197] applied to jet impingement	Empirical fitting of C_1 and C_2 based on experimental data from [26,97] given in Table 2
Lienhard & Hasan (1979) [198]	$\frac{q''_{CHF}}{\rho_b h_{fg} U_n} = C_1 \left(\frac{D_n}{D_s}\right) \left(\left(\frac{D_s}{D_n}\right)^3 \frac{\sigma}{\rho_l U_n^2 D_s}\right)^{C_2}$; $C_1 = (0.744 + 0.0084 \frac{\rho_l}{\rho_g})$ $C_2 = 0.4346 + 0.1027 \ln\left(\frac{\rho_l}{\rho_g}\right) - 0.0474 \left[\ln\left(\frac{\rho_l}{\rho_g}\right)\right]^2 + 0.00426 \left[\ln\left(\frac{\rho_l}{\rho_g}\right)\right]^3$	Same overall formulation as Lienhard and Eichhorn [125]	Expressions of C_1 and C_2 based on experimental data from [26,35,42] in Table 2; $n=250$
Miyasaka et al. (1980) [70]	$\frac{q''_{CHF,jet}}{q''_{CHF,pool}} = 1 + 0.86 U_n^{0.38}$; U_n in m/s	Fit of experimental data	Refer to Table 3; good predictions of data from [165,196]; $n=3$
Monde (1980) [167]	$\frac{q''_{CHF}}{\rho_b h_{fg} U_n} = 0.0601 \left(\frac{\rho_l}{\rho_g}\right)^{0.725} \left(\frac{2\sigma}{\rho_l U_n^2 D_s}\right)^{1/3} (1 + 0.00113 \left(\frac{D_s}{D_n}\right)^2)^{-1}$ for jets at center	Dimensional analysis of numerous physical parameters, similar to Monde and Katto [26]	Refer to Table 2; for eccentrically impinging jets, $D_s/2$ replaced by L_{char} , distance from jet center to farthest point of heated surface
Monde et al. (1980) [66]	$\frac{q''_{CHF}}{\rho_b h_{fg} U_n} = C \left(\frac{\rho_l}{\rho_g}\right)^{0.615} \left(\frac{\sigma}{\rho_l U_n^2 L_{char}}\right)^{1/3} \left(1 + 0.00113 \left(\frac{2L_{char}}{D_n}\right)^2\right)^{-1}$ $C=0.150$ for cases where burnout is observed at edge of heated surface, and $C=0.114$ for burnout at surface center; L_{char} is characteristic length for CHF, distance from jet center to farthest point of jet cell	Modification to Monde [167]	Refer to Table 2
Katto & Kurata (1980) [31]	$\frac{q''_{CHF}}{G h_{fg}} = 0.186 \left(\frac{\rho_g}{\rho_l}\right)^{0.559} \left(\frac{\sigma \rho_l}{G^2 L_s}\right)^{0.264}$ (or) $\frac{q''_{CHF}}{\rho_b h_{fg} U_n} = 0.186 \left(\frac{\rho_l}{\rho_g}\right)^{0.441} \left(\frac{\sigma}{\rho_l U_n^2 L_s}\right)^{0.264}$	Similar to Monde and Katto [26]	Refer to Table 3
Miyasaka et al. (1980) [70]	$\frac{q''_{CHF,sc}}{q''_{CHF,sc,pool}} = 1 + 0.86 U_n^{0.38}$; $\frac{q''_{CHF,sc,pool}}{q''_{CHF,sat,pool}} = 1 + 0.112 \left(\frac{\rho_l}{\rho_g}\right)^{0.8} \left(\frac{c_{p,l} \Delta T_{sub}}{h_{fg}}\right)^{1.13}$ $q''_{CHF,sat,pool} = 0.16 h_{fg} \rho_g \left(\frac{\sigma g(\rho_l - \rho_g)}{\rho_g^2}\right)^{1/4}$; q''_{CHF} in kcal/m ² .hr and U_n in m/s	Both jet CHF and subcooled pool boiling CHF are basic fits of experimental data, the latter being similar to Kutateladze's [172] relation; saturated pool boiling CHF given by Kutateladze's [172] correlation	Refer to Table 3
Katsuta & Kurose (1981) [123]	$\frac{q''_{CHF}}{\rho_b h_{fg} U_n} = 0.160 \left(\frac{\rho_l}{\rho_g}\right)^{0.7} \left(\frac{\sigma}{\rho_l U_n^2 D_s}\right)^{1/4} \left(\frac{D_n}{D_s}\right)^{3/4}$ Low mass flow rate cases for R-11 well correlated by the simple relation $\frac{q''_{CHF}}{\rho_l h_{fg} U_n} = 0.04 \left(\frac{\rho_l}{\rho_g}\right) \left(\frac{D_n}{D_s}\right)^2$	Dimensional analysis similar to Monde and Katto [26]; low mass flow rate CHF derived from energy balance	Refer to Table 2
Haramura & Katto (1983) [126,127]	$\frac{q''_{CHF}}{G h_{fg}} = 0.175 \left(\frac{\rho_g}{\rho_l}\right)^{0.467} \left(1 + \frac{\rho_g}{\rho_l}\right)^{1/3} \left(\frac{\sigma \rho_l}{G^2 L_s}\right)^{1/3}$ (or) $\frac{q''_{CHF}}{\rho_b h_{fg} U_n} = 0.175 \left(\frac{\rho_l}{\rho_g}\right)^{0.533} \left(1 + \frac{\rho_g}{\rho_l}\right)^{1/3} \left(\frac{\sigma}{\rho_l U_n^2 L_s}\right)^{1/3}$	Helmholtz instability theory applied to CHF conditions to develop new hydrodynamic CHF model, which is adopted for submerged plane wall jets	Same geometry as Katto and Kurata's [31]; provides decent predictions of their own data
Monde (1984, 1985) [86,87]	$\frac{q''_{CHF}}{\rho_b h_{fg} U_n} = 0.221 \left(\frac{\rho_l}{\rho_g}\right)^{0.645} \left(\frac{2\sigma}{\rho_l U_n^2 (D_s - D_n)}\right)^{0.343} \left(1 + \frac{D_n}{D_s}\right)^{-0.364}$	Based on Haramura and Katto's [126] hydrodynamic CHF model and dimensional analysis	V-regime (velocity dependent, low pressure, large density ratio); water, R-12, R-113; $D_s = 10.0 - 60.1$ mm; $D_s/D_n = 5.0 - 57.1$; $\rho_l/\rho_g = 5.3 - 1603$; $U_n = 0.21 - 60.0$; based on data from [26,29,35,42,166,167,199,200] as well as unpublished data

(continued on next page)

Table 4 (continued)

Author(s)	Correlation(s)	Rationale	Applicability and Remarks ^c
Monde & Okuma (1985) [43]	L-regime: $\frac{q''_{CHF}}{\rho_g h_{fg} U_n} = C \left(\frac{\rho_l}{\rho_g} \right) \left(\frac{D_n}{D_s} \right)^2$; $\frac{1}{C} = 0.0389 \left(\frac{\rho_l}{\rho_g} \right)^{0.674} \left(\frac{D_n}{\lambda_c} \right)^{1.24}$ Boundary between V- and L-regimes: $\frac{D_n}{D_s} = 18.4 \left(\frac{\rho_l}{\rho_g} \right)^{0.194} \left(\frac{D_n}{\lambda_c} \right)^{-0.76} \left(\frac{2\sigma}{\rho_l U_n^2 (D_s - D_n)} \right)^{-0.209}$	Heat balance for overall form; C determined empirically by assuming dependence on two dimensionless parameters that govern Taylor instability of liquid film; boundary relation determined by equating CHF correlations for V- and L-regimes	Refer to Table 2
Sharan & Lienhard (1985) [88]	$\frac{q''_{CHF}}{\rho_g h_{fg} U_n} = C_1 \left(\frac{D_n}{D_s} \right)^{1/3} \left(\frac{1000\sigma}{\rho_l U_n^2 D_s} \right)^{C_2}$; $C_1 = \left(0.21 + 0.00171 \frac{\rho_l}{\rho_g} \right)$ $C_2 = 0.486 + 0.06052 \ln \left(\frac{\rho_l}{\rho_g} \right) - 0.0378 \left[\ln \left(\frac{\rho_l}{\rho_g} \right) \right]^2 + 0.00362 \left[\ln \left(\frac{\rho_l}{\rho_g} \right) \right]^3$	Modified form of Lienhard and Hasan [198]	Free-surface round single jets; water, R-12, R-113; C_1 and C_2 refitted based on [26,35,42,167] in Table 2; highest accuracy achieved for $\frac{D_n}{D_s} \left(\frac{\rho_l U_n D_n}{\mu_f} \right)^{-1/3} < 0.40$. $Fr_{D_s} = U_n / \sqrt{g D_s} \geq 8$
Monde (1987) [44], Monde et al. (1986) [45]	$\frac{q''_{CHF}}{\rho_g h_{fg} U_n} = C_1 \left(\frac{\rho_l}{\rho_g} \right)^{C_2} \left(\frac{2\sigma}{\rho_l U_n^2 (D_s - D_n)} \right)^{C_3} \left(1 + \frac{D_n}{D_s} \right)^{C_4}$ V-regime C_1 0.221, C_2 0.645, C_3 0.343, C_4 -0.364 l-regime 0.691, 0.466, 0.421, -0.303 HP-regime 0.172, 1.27, 0.28, -1.01	Same correlation form as Monde [87]; same coefficients for V-regime; new empirically fitted coefficients for l- and HP-regimes	Refer to Table 2; $n_{HP-regime} = 24$; $n_{l-regime} = 117$
Katto & Yokoya (1988) [85]	$\frac{q''_{CHF}}{G h_{fg}} = C_1 \left[\frac{\sigma \rho_f}{G^2 (D_s - D_n)} \right]^{-1} \left(1 + \frac{D_n}{D_s} \right)^{C_2}$; $C_1 = 0.0166 + 7 \left(\frac{\rho_l}{\rho_g} \right)^{-1.12}$ $C_2 = \begin{cases} 0.374 \left(\frac{\rho_g}{\rho_l} \right)^{0.0155}, & \frac{\rho_g}{\rho_l} \leq 0.00403 \\ 0.532 \left(\frac{\rho_g}{\rho_l} \right)^{0.0794}, & \frac{\rho_g}{\rho_l} \geq 0.00403 \end{cases}$	Based on Haramura and Katto's [126] hydrodynamic CHF model applied to jet disk system and analysis of consolidated database	Water, R-12, R-113; $\rho_g/\rho_f = 0.000624 - 0.189$; $D_s/D_n = 3.9 - 53.9$; $U_n = 0.3 - 60.0$ m/s; $D_s = 10.0 - 60.1$ mm; $D_n = 0.7 - 4.1$ mm; based on data from [26,29,35,42-44,166,167,200]; $n = 564$
Nonn et al. (1988) [32]	$\frac{q''_{CHF}}{\rho_g h_{fg} U_n} = 0.0745 \left(\frac{\rho_l}{\rho_g} \right)^{0.725} \left(\frac{\sqrt{2}\sigma}{\rho_l U_n^2 L_s} \right)^{1/3} (1 + \varepsilon_{sub})$; $\varepsilon_{sub} = 0.456 \left(\frac{\rho_l}{\rho_g} \right)^{0.5} \left(\frac{c_{p,f}(T_{sat} - T_{in})}{h_{fg}} \right)^2$	Same correlation form as Monde and Katto [26]; only differences are characteristic heated length and empirical constant for ε_{sub}	Refer to Table 2; single jets only
Cho & Wu (1988) [171] Kandula (1990) [128]	$q''_{CHF} = 1.354 \left(\frac{\rho_l U_n^2 D_s}{\sigma} \right)^{0.319}$; q''_{CHF} in W/cm ² Transition criteria: $We_{f,trans}^{1/3} = 0.456 \frac{D_n}{D_s} \left(\frac{\eta \mu_l}{\sigma} \right) \left(\frac{\rho_l}{\rho_g} \right)^{0.772}$ σ -regime ($We_f \leq We_{f,trans}$): $\frac{q''_{CHF}}{\rho_g h_{fg} U_n} = 0.188 \left(\frac{\rho_l}{\rho_g} \right)^{0.614} We_f^{-1/3}$; $We_f = \frac{\rho_l U_n^2 D_s}{\sigma}$ μ -regime ($We_f \geq We_{f,trans}$): $\frac{q''_{CHF}}{\rho_g h_{fg} U_n} = 0.127 \frac{\rho_l}{\rho_g} \sqrt{\frac{\eta \nu_f}{D_n U_n^2}}$; $\eta = \sqrt{\frac{\omega R_g R T_{crit}}{M}}$ ω is Pitzer's acentric factor, g_c Newton constant, R universal gas constant, T_{crit} critical temperature in K, and M molecular weight	Empirical relation Physical model based on postulate CHF mechanism governed by relative liquid-vapor velocity; two CHF regimes identified; surface tension dominant regime reverted back to Katto and Shimizu's [42] correlation due to complexity in determining droplet splash rate; transition criteria determined by eliminating q''_{CHF} from both correlations	Refer to Table 2 Free-surface circular single jet impinging on heated disk
Skema & Slanciauskas (1990) [57]	$\frac{q''_{CHF,sc}}{q''_{CHF,sc,pool}} = 1 + 0.92 U_n^{0.44}$; $\frac{q''_{CHF,sc,pool}}{q''_{CHF,sat,pool}} = 1 + 0.112 \left(\frac{\rho_l}{\rho_g} \right)^{0.8} \left(\frac{c_{p,f} \Delta T_{sub}}{h_{fg}} \right)^{1.13}$ $q''_{CHF,sat,pool} = 0.16 h_{fg} \rho_g \left(\frac{\sigma g (\rho_l - \rho_g)}{\rho_g^2} \right)^{1/4}$; q''_{CHF} in W/m ² and U_n m/s	Basic fit of experimental data; saturated pool boiling CHF by Kutateladze's [172] correlation; subcooled pool boiling CHF by Miyasaka et al. [70]	Refer to Table 2
Maceika & Skema (1990) [56]	$\frac{P_{sat} - P_{amb}}{\rho_l U_n^{1/2}} = \exp \left[- (0.75 \left(\frac{H}{D_n} \right)^{-0.1} \left(\frac{D_n}{D_s} \right) \right]^2$	Appears same as Skema and Slanciauskas [57], except for different saturation pressure relation	Refer to Table 2
Monde & Inoue (1991) [68]	Same correlation as Monde [87]	Confirms accuracy of prior correlations by same authors	Multiple free-surface round jets impinging on heated disk; $N = 2 - 4$; $D_n = 2.0, 2.1$ mm; $L_{char} = 9.1 - 24.6$ mm; $U_n = 2.34 - 16.8$ m/s; based on Monde et al.'s [66] data in Table 2 and additional unpublished data

(continued on next page)

Table 4 (continued)

Author(s)	Correlation(s)	Rationale	Applicability and Remarks ^c																												
Mudawar & Wadsworth (1991) [13]	$\frac{q''_{CHF}}{\rho_b h_{fg} U_n} = \frac{C_1 \left(\frac{\sigma}{\rho_l U_n^2 (L_s - W_n)} \right)^{C_2}}{\left(\frac{\rho_l}{\rho_g} \right)^{2/3} \left(1 + \frac{C_{p,f} \Delta T_{sub,in}}{h_{fg}} \right)^{1/3} \left(1 + C_{sub} \frac{\rho_l C_{p,f} \Delta T_{sub,in}}{\rho_g h_{fg}} \right)^{2/3} \left(\frac{W_n}{L_s - W_n} \right)^{C_3}}$ $C_{sub} = 0.058; C_1 = 0.0786; C_2 = 0.149; C_3 = 0.396$	Correlation formulated by combination of energy balance of liquid sublayer and Helmholtz criterion; model further adjusted by physical reasoning and fitted empirically	Refer to Table 3; medium velocity regime; $n = 137$																												
Pais et al. (1993) [121]	$\frac{q''_{CHF}}{G_{h,fg}} = C_1 \left[\frac{\sigma (\rho_l - \rho_g)}{G^2 (D_s - D_n)} \right]^{-1} \left(1 + \frac{D_s}{D_n} \right)^{-1} C_2 (1 + \epsilon_{sub}); \epsilon_{sub} = C_{sub} \left(\frac{\rho_l}{\rho_g} \right)^{C_3} \left(\frac{C_{p,f} \Delta T_{sub,in}}{h_{fg}} \right)^{C_4}$ $C_1 = 0.0169; C_2 = 0.334; C_{sub} = 0.578; C_3 = 0.232; C_4 = 2.0$	Modified form of Katto and Yokoya's [85] saturated CHF correlation for water at 1 atm with a subcooling effectiveness factor	Refer to Table 2																												
Monde et al. (1994) [75,76]	$\frac{q''_{CHF,sc}}{q''_{CHF,sat}} = \frac{1 + \sqrt{1 + 4C_1 J_a}}{2}; J_a = \frac{\rho_l C_{p,f} \Delta T_{sub,in}}{\rho_g h_{fg}}; C = \frac{0.95 (D_n/L_s)^2 (1 + L_s/D_n)^{0.364}}{(\rho_l/\rho_g)^{0.43} (2\sigma/\rho_l U_n^2 (L_s - D_n))^{0.343}}$ $\frac{q''_{CHF,sat}}{\rho_b h_{fg} U_n} = 0.221 \left(\frac{\rho_l}{\rho_g} \right)^{0.645} \left(\frac{2\sigma}{\rho_l U_n^2 (L_s - D_n)} \right)^{0.343} \left(1 + \frac{L_s}{D_n} \right)^{-0.364}$	Subcooled CHF based on previous subcooled jet boiling model by same authors; saturated CHF same as Monde [87], but adapted for rectangular heated surface	Refer to Table 2; $n_{sc} = 224; n_{sat} = 47$																												
Estes & Mudawar (1995) [11]	$\frac{q''_{CHF}}{\rho_b h_{fg} U_n} = 0.221 \left(\frac{\rho_l}{\rho_g} \right)^{0.645} \left(\frac{2\sigma}{\rho_l U_n^2 (L - D_n)} \right)^{0.343} \left(1 + \frac{L}{D_n} \right)^{-0.364} (1 + \epsilon_{sub})$ $\epsilon_{sub} = 1.17 \left(\frac{\rho_l}{\rho_g} \right)^{0.5} \left(\frac{C_{p,f} \Delta T_{sub,in}}{h_{fg}} \right)^2; L = \sqrt{2} L_s$	Monde and Inoue's [68] saturated CHF correlation adjusted for effect of subcooling; subcooling effectiveness similar to Monde and Katto [26] but with smaller subcooling coefficient	Refer to Table 2																												
Furuya et al. (1995) [104]	Simple CHF correlation: $\frac{q''_{CHF}}{\rho_b h_{fg} U_n} = 7.67 \left(\frac{2\sigma}{\rho_l U_n^2 z} \right)^{0.327} (1 + \epsilon_{sub}); \epsilon_{sub} = 21.5 \frac{C_{p,f} \Delta T_{sub,in}}{h_{fg}}$ CHF model-based correlation: $\frac{q''_{CHF}}{\rho_b h_{fg} U_n} = 0.0458 \left(\frac{\rho_l}{\rho_g} \right)^{2/3} \left(\frac{\sigma}{\rho_l U_n^2 (z - W_n/2)} \right)^{1/3} \left(1 + \frac{C_{p,f} \Delta T_{sub,in}}{h_{fg}} \right)^{1/3} \left(1 + 0.0289 \frac{\rho_l C_{p,f} \Delta T_{sub,in}}{\rho_g h_{fg}} \right)^{2/3}$ z is local downstream from jet center	CHF correlation obtained by fitting data with two dimensionless parameters; CHF model-based correlation based on refs. [13,124,126] and fitted empirically with data	Refer to Table 3																												
Inoue et al. (1995) [103]	$\frac{q''_{CHF}}{\rho_b h_{fg} U_n} = 2.34 \left(\frac{\sigma}{\rho_l U_n^2 z} \right)^{0.49} \left(1 + 209 \left(\frac{C_{p,f} \Delta T_{sub,in}}{h_{fg}} \right)^{0.74} \right) \left(1 + 0.026 \left(\frac{U_n^2}{g R_s} \right)^{0.27} \left(\frac{z}{W_n} \right)^{0.64} \right)$ z is local downstream from jet center	Correlation form adapted from refs. [36,44,124] and fitted with data	Refer to Table 3																												
Copeland (1995) [106]	Pin-fin arrays: $\frac{q''_{CHF}}{\rho_b h_{fg} U_n} = C_1 (1 + \epsilon_{sub}) \left(\frac{\rho_l}{\rho_g} \right)^{2/3} \left(\frac{\sigma}{\rho_l U_n^2 W_{pin-fin}} \right)^{C_2}$ <table border="1"> <thead> <tr> <th>$W_{pin-fin}$ (mm)</th> <th>$H_{pin-fin}$ (mm)</th> <th>C_1</th> <th>C_2</th> </tr> </thead> <tbody> <tr> <td>0.1</td> <td>0.1</td> <td>0.0061</td> <td>-0.28</td> </tr> <tr> <td>0.1</td> <td>0.225</td> <td>0.0070</td> <td>-0.27</td> </tr> <tr> <td>0.1</td> <td>0.5</td> <td>0.0096</td> <td>-0.26</td> </tr> <tr> <td>0.2</td> <td>0.2</td> <td>0.0063</td> <td>-0.22</td> </tr> <tr> <td>0.2</td> <td>0.45</td> <td>0.0078</td> <td>-0.24</td> </tr> <tr> <td>0.2</td> <td>1.0</td> <td>0.0082</td> <td>-0.25</td> </tr> </tbody> </table>	$W_{pin-fin}$ (mm)	$H_{pin-fin}$ (mm)	C_1	C_2	0.1	0.1	0.0061	-0.28	0.1	0.225	0.0070	-0.27	0.1	0.5	0.0096	-0.26	0.2	0.2	0.0063	-0.22	0.2	0.45	0.0078	-0.24	0.2	1.0	0.0082	-0.25	Correlation form inspired from Mudawar and Wadsworth [13]	Refer to Table 3; $\epsilon_{sub} = 2.3$ for $\Delta T_{sub,in} = 40^\circ\text{C}$
$W_{pin-fin}$ (mm)	$H_{pin-fin}$ (mm)	C_1	C_2																												
0.1	0.1	0.0061	-0.28																												
0.1	0.225	0.0070	-0.27																												
0.1	0.5	0.0096	-0.26																												
0.2	0.2	0.0063	-0.22																												
0.2	0.45	0.0078	-0.24																												
0.2	1.0	0.0082	-0.25																												
Copeland (1996) [58]	Smooth surface: $\frac{q''_{CHF}}{\rho_b h_{fg} U_n} = 0.28 (1 + \epsilon_{sub}) \left(\frac{\rho_l}{\rho_g} \right)^{2/3} \left(\frac{\rho_l U_n^2 L}{\sigma} \right)^{-0.19} \left(\frac{A_n}{A_c} \right)^{0.23} N^{-0.03}; L = \frac{\sqrt{2} L_c}{2}$ Surface with pin fin arrays: $\frac{q''_{CHF}}{\rho_b h_{fg} U_n} = 0.28 (1 + \epsilon_{sub}) \left(\frac{\rho_l}{\rho_g} \right)^{2/3} \left(\frac{\rho_l U_n^2 L}{\sigma} \right)^{-0.19} \left(\frac{A_n}{A_c} \right)^{0.23} N^{-0.03} \left(1 + \frac{H_{pin-fin}}{W_{pin-fin}} \right)^{0.39}; L = \frac{\sqrt{2} L_c}{2}$	Same correlation form as Copeland [59]; another dimensionless term included to address pin fin effects	Refer to Table 2; $\epsilon_{sub} = 2.3$ for $\Delta T_{sub,in} = 40^\circ\text{C}$																												
Johns & Mudawar (1996) [16]	$\frac{q''_{CHF}}{\rho_b h_{fg} U_n} = \frac{C_1 \left(\frac{\sigma}{\rho_l U_n^2 (L_s - D_n)} \right)^{0.611} \left(1 + 0.028 \frac{\rho_l C_{p,f} \Delta T_{sub,in}}{\rho_g h_{fg}} \right)^{2/3} \left(\frac{C_{p,f} \Delta T_{sub,in}}{h_{fg}} \right)^{1/3}}{\left(\frac{\rho_l}{\rho_g} \right)^{2/3} \left(\frac{D_n}{L_s - D_n} \right)^{0.611}}$	Mudawar and Wadsworth's [13] correlation for rectangular jets adapted for round jets using different coefficients	Refer to Table 2; $n = 68$																												
Wang & Monde (1997) [93], Monde et al. (1998) [94]	$\frac{q''_{CHF}}{\rho_b h_{fg} U_n} = 0.193 \left(\frac{\rho_l}{\rho_g} \right)^{0.533} \left(\frac{\sigma}{\rho_l U_n^2 L_s} \right)^{1/3} (1 + \epsilon_{sub}); \epsilon_{sub} = 0.35 \left(\frac{\rho_g}{\rho_l} \right)^{0.46} \left(\frac{\rho_l C_{p,f} \Delta T_{sub,in}}{\rho_g h_{fg}} \right)$	Dimensionless groups selected based on experimental data; saturated CHF similar to Haramura and Katto [126]	Refer to Table 3																												

(continued on next page)

Table 4 (continued)

Author(s)	Correlation(s)	Rationale	Applicability and Remarks ^c
Copeland (1998) [59]	$\frac{q''_{CHF}}{\rho_b h_{fg} U_n} = 0.084(1 + \varepsilon_{sub}) \left(\frac{\rho_l}{\rho_g}\right)^{2/3} \left(\frac{\rho_l U_n^2 L}{\sigma}\right)^{0.25} \left(\frac{A_n}{A_c}\right)^{0.18} N^{0.07}; L = \frac{\sqrt{2}z}{2}$	No information provided on correlation form, except that subcooling effectiveness is based on Mudawar and Wadsworth [13]	Refer to Table 2; $\varepsilon_{sub} = 1.8$ for $\Delta T_{sub,in} = 32^\circ\text{C}$
Inoue et al. (2000) [105]	$\frac{q''_{CHF}}{\rho_b h_{fg} U_n} = 0.0241 \left(\frac{\rho_l}{\rho_g}\right)^{2/3} \left(\frac{\sigma}{\rho_l U_n^2 z}\right)^{1/3} \left(1 + \frac{c_{p,f} \Delta T_{sub,in}}{h_{fg}}\right)^{1/3} (1 + 0.036 \frac{\rho_l}{\rho_g} \frac{c_{p,f} \Delta T_{sub,in}}{h_{fg}})^{2/3} \left(1 + \frac{U_n^2}{g R_c}\right)^{0.122}$ z is local downstream from jet center	Same correlation form as Furuya et al. [104], but with different empirical constants and inclusion of Froude number term	Refer to Table 3; local CHF values based on local velocities
Monde & Wang (2000) [95]	$\frac{q''_{CHF}}{\rho_b h_{fg} U_n} = 0.25(1 + 0.0012 \left(\frac{\rho_l}{\rho_g}\right)) \left(\frac{\rho_l}{\rho_g}\right)^{0.35} \left(\frac{\sigma}{\rho_l U_n^2 L_s}\right)^{1/3}$	Dimensionless groups selected based on experimental data and fitted empirically	Free surface plane wall jet; water, R-22, R-113; $\rho_l/\rho_g = 6.6 - 1603$; based on data from [91,93,97] and their own data in Table 3; n = 339
Cheng et al. (2001) [49]	$q''_{CHF,sub} = \frac{C_2 + \sqrt{C_2^2 - 4C_3}}{2}; C_2 = \frac{C_1 \rho_f U_n c_{p,f} \Delta T_{sub,in}}{(D_s/D_n)^2 - 1} + q''_{CHF} \left(1 + \frac{c_{p,f} \Delta T_{sub,in}}{h_{fg}}\right) + h \Delta T_{sub,in}$ $C_3 = h \Delta T_{sub,in} \frac{C_1 \rho_f U_n c_{p,f} \Delta T_{sub,in}}{(D_s/D_n)^2 - 1}; \frac{q''_{CHF}}{\rho_b h_{fg}} = 0.21 \left(\frac{\rho_l}{\rho_g}\right)^{2/3} \left(\frac{\sigma}{\rho_l U_n^2 (D_s - D_n)}\right)^{1/3} \left(\frac{D_n}{D_s + D_n}\right)^{1/3}$	Correlation based on heat and hydrodynamic analysis, and effect of subcooling on sensible heat transfer and vapor blanket coverage area; no information given about h and C ₁	Good agreement with both Estes and Mudawar's [11] data and their own data in Table 2
Liu & Zhu (2002) [129]	$\frac{q''_{CHF}}{G h_{fg}} = C(1 + \frac{\rho_k}{\rho_f})^{1/3} \left(\frac{\sigma \rho_l}{G^2 D_n}\right)^{1/3} \left(\frac{\rho_k}{\rho_f}\right)^{1.4/3}; C = 0.132$	Correlation form based on Helmholtz instability model of maximum liquid subfilm layer; C determined empirically	Saturated free-surface round water jet; C based on Kumagai et al.'s [201] data as well as their data in Table 2; n = 21 (based on plots)
Liu et al. (2004) [52]	$\frac{q''_{CHF,sc}}{q''_{CHF,sat}} = 1 + C_{sub} \left(\frac{c_{p,f} \Delta T_{sub,in}}{h_{fg}}\right) C; \frac{q''_{CHF,sat}}{G h_{fg}} = 0.132(1 + \frac{\rho_k}{\rho_f})^{1/3} \left(\frac{\sigma \rho_l}{G^2 D_n}\right)^{1/3} \left(\frac{\rho_k}{\rho_f}\right)^{1.4/3}$ C _{sub} = 11.82; C = 1	Saturated CHF from Liu and Zhu [129]; subcooled CHF relation based on studies like [92,124] with C _{sub} and C determined empirically	Refer to Table 2; subcooled free surface round water jet
Qiu & Liu (2005) [53]	$\frac{q''_{CHF,sc}}{q''_{CHF,sat}} = 1 + C_{sub} \left(\frac{c_{p,f} \Delta T_{sub,in}}{h_{fg}}\right); \frac{q''_{CHF,sat}}{G h_{fg}} = C(1 + \frac{\rho_k}{\rho_f})^{1/3} \left(\frac{\sigma \rho_l}{G^2 D_n}\right)^{1/3} \left(\frac{\rho_k}{\rho_f}\right)^{1.4/3}$ C _{sub} = 22.46; C = 0.130	Same correlation form as Liu and Zhu [129] and Liu et al. [52], but with different empirical constants	Refer to Table 2; n _{sc} = 36; n _{sat} = 21
Qiu & Liu (2005) [54]	Same saturated correlation as Qiu and Liu [53]	Same correlation form as Liu and Zhu [129]	Refer to Table 2; n _{water} = 25; n _{ethanol} = 20; n _{R-11} = 16; n _{R-113} = 21; n = 82
Qiu & Liu (2005) [55]	$\frac{q''_{CHF,sc}}{q''_{CHF,sat}} = 1 + C_{sub} \Delta T_{sub,in}; \frac{q''_{CHF,sat}}{G h_{fg}} = C \left(\frac{\sigma \rho_l}{G^2 D_n}\right)^{1/3} \left(\frac{\rho_k}{\rho_f}\right)^{1.4/3}; C = 0.130; \Delta T_{sub,in}$ in K C _{sub} = 0.0224 (water), 0.0275 (ethanol), 0.153 (R-113)	Saturated CHF from Liu and Zhu [129], but with a different empirical constant; simple subcooled CHF relation by fitting experimental data	Refer to Table 2; n _{sat} = 82
Meyer et al. (2006) [17]	$\frac{q''_{CHF}}{\rho_b h_{fg} U_n} = \frac{\left(\frac{\rho_l}{\rho_g}\right)^{2/3} \left(1 + \frac{c_{p,f} \Delta T_{sub,in}}{h_{fg}}\right)^{1/3}}{\left(1 + 0.034 \frac{\rho_l c_{p,f} \Delta T_{sub,in}}{\rho_g h_{fg}}\right)^{2/3} \left(\frac{W_n}{L_c - W_n}\right)^{0.331}} = 0.0919 \left(\frac{\sigma}{\rho_l U_n^2 (L_c - W_n)}\right)^{0.157}$	Same correlation form as Mudawar and Wadsworth [13], but with different empirical coefficients	Refer to Table 3; n _{FC-72} = 30; n _{ethanol} = 7
Qiu & Liu (2008) [114]	Saturated CHF: $\frac{q''_{CHF}}{\rho_b h_{fg}} = 0.0985 \left(\frac{\rho_k}{\rho_f}\right)^{0.275} \left(\frac{\sigma \rho_l}{G^2 D_n}\right)^{1/3} \left(1 + 0.00113 \left(\frac{D_n}{D_s}\right)^2\right)^{-1}$ Subcooled CHF: same as Monde et al. [75,76] with L _s replaced by D _s	Saturated CHF correlation form same as Monde [167], except for different empirical coefficients and definition of Weber number based on D _n	Refer to Table 2; superhydrophilic surfaces irradiated with ultraviolet light
Shin et al. (2009) [84]	$q''_{CHF} = 17.47(\log G)^2 + 8.5831(\log(10H/W_n))^2 + 11.7931 \log G \log(10H/W_n) - 83.7 \log G - 50.251 \log(10H/W_n) + 138.1$ G in kg/m ² s, q'' _{CHF} in W/cm ² Lowest CHF criterion: $H/D_n _{lowest-CHF} = 1.4016(\log G)^2 - 9.4548 \log G + 16.493$	Second order function of H/W _n and G fitted empirically	Refer to Table 3; n = 9
Qiu & Liu (2010) [130]	$q''_{CHF} = \frac{2h_{fg} \rho_l \delta U_n}{3D_n}; \delta$ is average sub-film thickness $q''_{CHF} = 360000(1.49 - 0.009\theta_{CA}) \left(\frac{U_n}{D_n}\right)^{1/3};$ q'' _{CHF} , U _n , D _n , and θ _{CA} are, respectively, in W/m ² , m/s, m, and degrees	Theoretical model based on Long-wave instability for prediction of CHF in stagnation zone Dimensional correlation that considers solid-liquid contact angle	Good prediction of data from [113,129]

(continued on next page)

Table 4 (continued)

Author(s)	Correlation(s)	Rationale	Applicability and Remarks ^c
Zhang <i>et al.</i> (2011) [80]	$\frac{q''_{CHF}}{Gh_{fg}} = 0.16 \left(\frac{\rho_k}{\rho_f}\right)^{0.399} \left(\frac{2\sigma}{\rho_f U_n^2 D_n}\right)^{0.267} \left(1 + \frac{H}{D_s}\right)^{-0.44}$	Three dimensionless parameters employed based on past correlations [54,75,202], with constants fitted empirically	Refer to Table 2; hemispherical surface
Cong <i>et al.</i> (2011) [133]	$\frac{q''_{CHF}}{\rho_k h_{fg} U_n} = 0.0966 \left(\frac{\rho_f}{\rho_k}\right)^{0.6877} \left[\frac{2\sigma}{\rho_f U_n^2 (L_{char} - D_n)}\right]^{0.2926} \left(1 + \frac{L_{char}}{D_n}\right)^{-0.5592} (1 + 0.6107N^{-1.7828})$ L_{char} is twice distance from jet center to farthest point on heated surface	Statistical formulation using Artificial Neural Network and Genetic Algorithm tools	Round jets; water, R-12, R-113; $P_{sat} = 1 - 27.8$ bar, $N = 1 - 4$, $D_n = 1 - 4.14$ mm; $L_{char} = 9.1 - 60.6$ mm; $U_n = 0.15 - 26.6$ m/s; based on data from [43,44,68,74,87]; $n = 710$ (single), 369 ($N = 2-4$)
Li & Liu (2012) [131]	$\frac{q''_{CHF}}{Gh_{fg}} = 0.13 \left(\frac{\sigma \rho_f}{G^2 D_n}\right)^{1/3} \left(\frac{\rho_k}{\rho_f}\right)^{1.4/3} + 1.97 \left(\frac{k_f}{c_{p,f} G D_n}\right)^{0.5} \left(\frac{c_{p,f} \Delta T_{sub,in}}{h_{fg}}\right)$	Theoretical formulation based on combination of Helmholtz instability theory of microlayer and bubble induced turbulent heat transfer, with constants fitted empirically	Empirical coefficients based on data from [52,54,55]
Mahmoudi <i>et al.</i> (2012) [77]	$\frac{q''_{CHF}}{\rho_k h_{fg} U_n} = C_1 \left(\frac{\Gamma D_n}{D_s}\right)^{1/3} \left(\frac{1000\sigma}{\rho_f U_n^2 D_s} \frac{\rho_k}{\rho_f}\right) C_2$; $C_1 = (0.21 + 0.00171 \frac{\rho_f}{\rho_k})$ $C_2 = 0.486 + 0.06052 \ln\left(\frac{\rho_f}{\rho_k}\right) - 0.0378 \left[\ln\left(\frac{\rho_f}{\rho_k}\right)\right]^2 + 0.00362 \left[\ln\left(\frac{\rho_f}{\rho_k}\right)\right]^3$ $\Gamma = \frac{D_n}{D_s} = \left(\frac{U_n}{U_{th}}\right)^{1/2} = \left[1 + \frac{2}{Fr} \frac{H}{D_n/2} + \frac{2}{We} \left(1 - \frac{D_n}{D_s}\right)\right]^{-1/4}$; $Fr = \frac{U_n^2}{g D_n/2}$; $We = \frac{\rho_f U_n^2 D_n}{2\sigma}$ Γ is jet radius reduction coefficient, subscript H indicates value of parameter near impinging zone	Modification of Sharan and Lienhard's [88] correlation with jet radius reduction coefficient; We of original correlation multiplied by density ratio	Refer to Table 2; for higher velocity jets, $\Gamma \sim 1$ and correlation becomes identical to Sharan and Lienhard's [88]
Cardenas & Narayanan (2012) [37]	For $0 \leq Re_{Ds} < 4000$: $\frac{q''_{CHF,sat}}{q''_{CHF,sat,pool}} = 1 + C_2 Re_{Ds}$; $q''_{CHF,sat,pool} = C_1 h_{fg} \rho_k \left(\frac{\sigma g (\rho_f - \rho_k)}{\rho_k^2}\right)^{1/4}$ For $4000 \leq Re_{Ds} < 14000$: $\left(\frac{q''_{CHF,sat}}{\rho_f U_n h_{fg}} \frac{A_k}{A_n}\right)^{-1} \left(\frac{\rho_f}{\rho_k}\right)^{-2/3} = C_3 Re_{Ds}^{1/2}$ $R_a = 123$ nm $R_a = 33$ nm C_1 0.1556 0.1379 C_2 7.5347×10^{-5} 4.4585×10^{-5} C_3 3.3328×10^{-4} 3.9994×10^{-4}	CHF for saturated inlet at lower Re correlated as linear function of Re and Kutateladze's pool boiling CHF correlation [203]; CHF for saturated inlet at higher Re based on best fit to the data; CHF for subcooled inlet correlated using Inoue <i>et al.</i> 's [204] relation with a modified coefficient of $C_{sub} = 2.528$ instead of 3.318	Refer to Table 2; subcooled CHF correlation only for lowest pressure and based on one subcooling value
Cardenas & Narayanan (2012) [205]	$\frac{q''_{CHF,sub}}{q''_{CHF,sat}} = 1 + C_{sub} \left(\frac{\rho_f}{\rho_k}\right)^{-0.156} Pe^{-0.385} Ja$; $C_{sub} = 2.528$; $Pe = \frac{\sigma^{3/4}}{\alpha \rho_k^{1/2} (g(\rho_f - \rho_k))^{1/4}}$; $Ja = \frac{\rho_f c_{p,f} \Delta T_{sub}}{\rho_k h_{fg}}$ $\frac{q''_{CHF,sat}}{q''_{CHF,sat,pool}} = (1 + K)^{5/16}$; $K = 1.2592 \times 10^{-5} \left(\frac{\rho_f U_n D_n}{\mu_f}\right)^{1.599} \left(\frac{\rho_f}{\rho_k} \frac{\sigma}{g(\rho_f - \rho_k) D_n^2}\right)^{0.234} R_a^{0.252}$ $\frac{q''_{CHF,sub}}{q''_{CHF,sat}} = 1 + C_{sub} \left(\frac{\rho_f}{\rho_k}\right)^{-0.156} Pe^{-0.385} Ja$; $C_{sub} = 2.528$; $Pe = \frac{\sigma^{3/4}}{\alpha \rho_k^{1/2} (g(\rho_f - \rho_k))^{1/4}}$; $Ja = \frac{\rho_f c_{p,f} \Delta T_{sub}}{\rho_k h_{fg}}$	Based on hydrodynamic stability CHF model by Haramura and Katto [126]; statistically significant non-dimensional parameters chosen for best statistical fit; subcooled inlet CHF based on Inoue <i>et al.</i> 's [204] relation with a modified coefficient of $C_{sub} = 2.528$ instead of 3.318	Submerged jet; single round jet on flat circular surface; $Re_{Dn} = 0 - 14000$, $D_s/D_n = 6 - 25$, $P_{sat} = 0.2 - 1$ bar, $R_a = 33, 123$ nm, $\Delta T_{sub,in} = 0, 17^\circ\text{C}$; correlation based on data from [37,185].
Buchanan & Shedd (2013) [30]	$q''_{CHF} = 0.013 Re_{Dn}^{1/2} [55 P_R^{0.12 - 0.4343 \ln(P_R)} (-0.4343 \ln(P_R))]^{-0.55} M^{-0.5} \Delta T_{CHF}]^3$ $\Delta T_{CHF} = \begin{cases} 32.5^\circ\text{C}, & T_{in} = 10^\circ\text{C} \\ 30.0^\circ\text{C}, & T_{in} = 20^\circ\text{C} \\ 27.5^\circ\text{C}, & T_{in} = 30^\circ\text{C} \end{cases}$ R_p is roughness parameter, M molar mass	Analysis of the data shows heat transfer behavior closely follows that of pool boiling until CHF; CHF is a weak function of Re	Refer to Table 2
Li <i>et al.</i> (2013) [115]	$\frac{q''_{CHF,sat}}{Gh_{fg}} = (0.191 - 0.055 \theta_{CA}) \left(\frac{\sigma \rho_f}{G^2 D_n}\right)^{1/3} \left(\frac{\rho_k}{\rho_f}\right)^{1.4/3}$ $\frac{q''_{CHF,sub}}{q''_{CHF,sat}} = 1 + 15.15 \left(\frac{\rho_f}{\rho_k}\right)^{1.4/3} \left(\frac{k_f}{c_{p,f} G D_n}\right)^{1/2} \left(\frac{G^2 D_n}{\sigma \rho_f}\right)^{1/3} \left(\frac{c_{p,f} \Delta T_{sub,in}}{h_{fg}}\right)$	Saturated CHF correlation form similar to Liu and Zhu [129], but with leading empirical coefficient replaced with linear function of θ_{CA} ; subcooled CHF correlation based on Li and Liu [131]	Refer to Table 2
Li <i>et al.</i> (2014) [48]	$\frac{q''_{CHF,sat}}{Gh_{fg}} = 0.160 \left(\frac{\sigma \rho_f}{G^2 D_n}\right)^{1/3} \left(\frac{\rho_k}{\rho_f}\right)^{1.4/3}$; $\frac{q''_{CHF,sub}}{q''_{CHF,sat}} = 1 + 0.26 \left(\frac{\rho_k}{\rho_f}\right)^{-0.55} \left(\frac{c_{p,f} \Delta T_{sub,in}}{h_{fg}}\right)^{0.64}$	Saturated CHF correlation form similar to Liu and Zhu [129], but with modified leading empirical coefficient; subcooled CHF correlation based on [92,124] but modified with new empirical constants	Refer to Table 2

(continued on next page)

Table 4 (continued)

Author(s)	Correlation(s)	Rationale	Applicability and Remarks ^c																								
Cardenas & Narayanan (2014) [206]	$\frac{q''_{CHF}}{q''_{CHF,pool}} = (1 + K)^{5/16}; K = 2185.06 \left(\frac{\rho_f U_n D_n}{\mu_f} \right)^{1.5935} \left(\frac{D_n}{\lambda_c} \frac{\rho_f g (\rho_f - \rho_g) D_n^2}{\mu_f^2} \right)^{-0.6638} \left(\frac{\rho_f}{\rho_g} \left(\frac{D_n}{\lambda_c} \right)^3 \right)^{-0.8745}$	Based on hydrodynamic stability CHF model by Haramura and Katto [126]; Statistically significant non-dimensional parameters chosen for best statistical fit	Both submerged and free surface jets; single round jet on flat circular surface; saturated water, FC-72, R-113; $Re_{Dn} = 0 - 60000$, $D_n/\lambda_c = 0.44 - 5.50$, $D_s/\lambda_c = 4.47 - 38.42$, $\rho_f/\rho_g = 119 - 8502$; correlation based on data from [26,37,185]																								
Chen et al. (2015) [71]	$q''_{CHF,slot} = (1 + e^{-L_s/6}) q''_{CHF,round}; L'_s = \frac{L_s}{\lambda_c}$ $q''_{CHF,round} = (0.191 - 0.055\theta_{CA}) [h_{fg} (\sigma \rho_f^2)^{1/3} \left(\frac{\rho_g}{\rho_f} \right)^{1.4/3} \left(\frac{U_n}{D_n} \right)^{1/3} + 15.15 (k_f \rho_f c_{p,f})^{1/2} \left(\frac{U_n}{D_n} \right)^{1/2} \Delta T_{sub,in}]$ <p>D_n replaced by W_s for slot jet impinging on rectangular surface</p> $q''_{CHF} = Ch_{fg} \rho_g^{1/2} (\sigma g (\rho_f - \rho_g))^{1/4}$	CHF for slot jets predicted using round jet correlation modified with a theoretical correction factor; q''_{CHF} of round jets taken from Li et al. [115]	Refer to Table 2																								
Wang et al. (2016) [72]	$C = (1 + e^{-L_s/6}) \left(\frac{1 + \cos\theta_{CA}}{16} \right) \left(\frac{2}{\pi} (1 - \sqrt{\phi_s})^{-1/2} \frac{r + \cos\theta_{CA}}{1 + \cos\theta_{CA}} + \frac{\pi}{4} (1 - \sqrt{\phi_s})^{1/2} (1 + \cos\theta_{CA}) \right)^{1/2}$ <p>ϕ_s is solid fraction (fraction of solid surface area wetted by liquid, $\phi_s = 0$ for smooth surface), and r surface roughness factor (ratio of actual solid area over projected area; $r = 1$ for smooth surface)</p>	CHF correlation of Quan et al. [207] multiplied by the same correction factor as Chen et al. [71]	Refer to Table 3																								
Zhang et al. (2018) [108]	$\frac{q''_{CHF}}{Ch_{fg}} = C_1 \left(\frac{\rho_g}{\rho_f} \right)^{C_2} \left(\frac{\sigma \rho_f}{G^2 D_{n,e}} \right)^{C_3} \left(1 + \frac{c_{p,f} \Delta T_{sub,in}}{h_{fg}} \right)^{C_4} \left(\frac{H}{D_{n,e}} \right)^{C_5} \left(\frac{D_{s,e}}{D_{n,e}} \right)^{C_6} \dots$ $(1.123 + 0.041 \frac{A_{s,fin}}{A_s} + 0.721 \frac{h_{fg} L_{fin-ppf}}{L_s/4} \frac{(H_{fin} + L_{fin-ppf})}{L_s/4})^{C_7}$ $D_{n,e} = \sqrt{ND_n}; D_{s,e} = \sqrt{4A_s/\pi}$ <p>A_s is actual heated surface area and $A_{s,fin}$ total heated area of finned surface</p> <table border="1"> <thead> <tr> <th>Surfaces</th> <th>C_1</th> <th>C_2</th> <th>C_3</th> <th>C_4</th> <th>C_5</th> <th>C_6</th> <th>C_7</th> </tr> </thead> <tbody> <tr> <td>Bare</td> <td>0.221</td> <td>0.529</td> <td>0.209</td> <td>3.246</td> <td>-0.316</td> <td>-0.086</td> <td>0</td> </tr> <tr> <td>Pin-finned</td> <td>1.0</td> <td>0.941</td> <td>0.248</td> <td>3.246</td> <td>-0.170</td> <td>-0.086</td> <td>0.975</td> </tr> </tbody> </table>	Surfaces	C_1	C_2	C_3	C_4	C_5	C_6	C_7	Bare	0.221	0.529	0.209	3.246	-0.316	-0.086	0	Pin-finned	1.0	0.941	0.248	3.246	-0.170	-0.086	0.975	Dimensionless groups chosen to consider effects of all parameters tested; C_4 determined from data of refs. [17,208]; other constants based on their own data	Refer to Table 2; good prediction of data from [17,80,208]
Surfaces	C_1	C_2	C_3	C_4	C_5	C_6	C_7																				
Bare	0.221	0.529	0.209	3.246	-0.316	-0.086	0																				
Pin-finned	1.0	0.941	0.248	3.246	-0.170	-0.086	0.975																				
Grassi & Testi (2019) [132]	<p>Velocity-dependent regime (atmospheric FC-72 and R-113):</p> $\frac{q''_{CHF}}{q''_{CHF,pool}} = 1.0084 \left(\frac{2}{2 + Fr_{\lambda_c}^2} \right)^{-0.1887} \left(4.20 \left(\frac{D_n - D_n}{\lambda_c} \right)^{-0.415} \right); Fr_{\lambda_c} = Fr_{\lambda_c} \sqrt{\frac{\rho_g}{\rho_f}}; Fr_{\lambda_c} = \frac{U_n}{\sqrt{g \lambda_c}}$ <p>Gravity-dependent regime (sub-atmospheric water), $Fr_{\lambda_c} / \sqrt{2\rho_f/\rho_g} \ll 1$:</p> $\frac{q''_{CHF}}{q''_{CHF,pool}} = 0.01 Fr_{\lambda_c}^2 + 0.0382 Fr_{\lambda_c} + 1.0196$	Relationship based on hydrodynamic instability model of liquid-vapor interfaces, empirically fitted using power or second-order polynomial functions	Submerged saturated (including ionic) round jets of water, FC-72, and R-113; $P_{slot} = 0.176 - 1.013$ bar, $D_s = 2.5 - 27.7$ mm, $D_n = 1.01 - 3$ mm, $U_n = 0 - 13.7$ m/s; based on data from [37,99,182,185]																								
Devahdhanush & Mudawar (2020) [18]	$\left(\frac{q''_{CHF}}{\rho_g h_{fg} U_n} \right) = 0.270 \left(\frac{\sigma}{\rho_f U_n^2 (\sqrt{2} L_c - D_n)} \right)^{0.277} \left(\frac{\rho_f}{\rho_g} \right)^{2/3} \left(\frac{NA_n}{A_s} \right)^{0.259} \dots$ $\left(1 + 0.034 \frac{\rho_f}{\rho_g} \frac{c_{p,f} \Delta T_{sub,in}}{h_{fg}} \right)^{2/3} \left(1 + \frac{c_{p,f} \Delta T_{sub,in}}{h_{fg}} \right)^{1/3} N^{-0.109}$	'Statistical inference' techniques applied to large database, accounting for physics of two-phase flow and heat transfer	Based on their own data and data from [15,16] in Table 2; $n_{R-134a} = 152$; $n_{FC-72} = 168$																								

^c Reference to Tables 2 (round) and 3 (slot) indicates correlation is applicable for corresponding experimental parameter ranges listed in that respective table; applicable to entire experimental ranges unless noted otherwise

govern the Taylor instability for liquid films. It was noted that this function might not hold well for other surface orientations since splashing at low flow rates is gravity dependent.

Using energy balance over a liquid film and Helmholtz instability criterion, Mudawar and Wadsworth [13] proposed a correlation for predicting CHF for confined single slot jets. At CHF, the rate of energy required to completely vaporize a liquid surface sublayer residing beneath a coalescent vapor layer can be expressed as

$$q''_{CHF} \left(\frac{L_s - W_n}{2} \right) = \rho_f U_n \delta (h_{fg} + c_{p,f} \Delta T_{sub}), \quad (2)$$

where δ is upstream thickness of the liquid sublayer, which can be determined from the Helmholtz instability criterion as

$$\delta = \psi \left[\frac{\sigma}{\rho_g (q''_{CHF} / \rho_g h_{fg})^2} \right] \left[1 + C_{sub} \frac{\rho_f c_{p,f} \Delta T_{sub}}{\rho_g h_{fg}} \right]^2, \quad (3)$$

where ψ is an empirical constant that considers the surface area fraction occupied by vapor [124]. Further simplifications were made to arrive at their final correlation form and empirical constants were found from experimental data. The same correlation form was later modified for confined single round jets [16] and confined slot jet arrays [17] and gave good predictions. It is noteworthy that a recently proposed correlation by the present authors [18] based on a larger database including both confined round single jets and jet arrays of both R-134a (refrigerant) and FC-72 (dielectric fluid) by statistical inference techniques ended up with a form similar to that of Mudawar and Wadsworth [13]. This indicates the CHF mechanism for confined jets could be well modelled using the same assumptions. Many other researchers [125–132] have derived mechanism-based correlations based on different proposed mechanisms and/or assumptions.

Another distinct approach is employing artificial neural network and genetic algorithm tools to experimental CHF databases. Cong *et al.* [133] showed the viability of this approach for predicting datapoints collected from the literature.

At this point, the authors direct the reader to Table 4, which is a thorough list of published jet CHF correlations. To the authors' best knowledge, there are no studies that utilize computational methods (numerical simulations) to predict jet impingement CHF. Also, there are no fully theoretical models that capture the true fluid flow and heat transfer physics surrounding CHF.

6. CHF for Hybrid Cooling Schemes

Several researchers have utilized the advantages of impinging jets to improve the heat transfer performance of various other two-phase thermal management schemes, especially micro- and macro-channel flow boiling. These *hybrid* cooling schemes have been shown to augment both heat transfer performance and CHF by taking advantage of the flow characteristics of both underlying schemes. Liquid could enter the cooling module only through the jet nozzles or through both jet nozzles and channels, the latter is termed 'crossflow configuration'. Table 5 provides a summary of CHF investigations utilizing hybrid cooling schemes.

6.1. Liquid Entry only through Jet Nozzles

When liquid enters the cooling module through only a single jet nozzle in a hybrid impinging jet/channel flow configuration, flow can be described as conventional confined jet impingement configuration with long wall jets. The confined jet studies of Wadsworth and Mudawar [12–14] provided an early concept of combining impinging jets and channel flow.

A borderline study between confined impinging jets and hybrid impinging jet/channel flow was performed by Nakayama *et*

al. [134], who experimentally analyzed the impingement of a single slot jet onto an in-line array of five heating elements, with the jet facing the middle heater. The middle heater experienced confined jet impingement, whereas the other four heaters experienced channel flow created by the wall jets as the fluid moved toward the cooling module's outlet. However, CHF measurements were made by supplying power to only the middle heater. CHF was found to increase with increasing velocity up to a point, after which it began to decrease. Higher CHF values were obtained by increasing the inlet subcooling. Heat transfer measurements by powering all five heaters showed large variations in heat transfer coefficient between the different heaters, but values approached that of the middle heater with increasing jet velocity.

Sung and Mudawar [135] developed a hybrid slot jet/microchannel cooling module and explored parametric trends of CHF using dielectric fluid PF-5052. Fluid entered the cooling module through slot jet nozzles, with one nozzle feeding each micro-channel as shown in Fig. 14(a). The micro-channels were formed within the jet nozzle plate with a gap between the jet plate and heated surface allowing fluid interactions between neighboring cells. CHF was noticed to occur first at the downstream edge of the heated surface. Parametric trends of CHF were found to be similar to those of conventional jet impingement schemes discussed in previous sections: CHF increased with increasing flow rate and/or inlet subcooling. Their CHF data followed $q''_{CHF} \propto U_n^{0.45}$; the velocity exponent being in-between those of channel flow ($q''_{CHF} \propto U_n^{0.30}$) [6] and confined slot jet impingement ($q''_{CHF} \propto U_n^{0.70}$) [13]. When the predictive performances of previous correlations were examined, confined impinging jet correlations [13,17] were found to provide better predictions than those of channel flow [6], proving the flow characteristics were dominated more by impinging jets than channel flow. To achieve more accurate CHF predictions for this hybrid flow geometry, a simple superpositioning scheme, based on an area-weighted average of CHF values predicted by impinging jet and channel flow CHF correlations, was proposed,

$$q''_{CHF, hybrid} A_{s, tot} = q''_{CHF, jet} A_{s, jet} + q''_{CHF, ch} (A_{s, tot} - A_{s, jet}), \quad (4)$$

where $A_{s, tot}$, and $A_{s, jet}$ are the total heated surface area, and the portion dominated by jets (equal to nozzle area). CHF for impinging jets and channel flow were determined, respectively, using the correlations of Mudawar and Wadsworth [13] and Mudawar and Maddox [6], the latter given by

$$\frac{q''_{CHF}}{\rho_g h_{fg} U_{ch}} \left(\frac{\rho_f}{\rho_g} \right)^{15/23} \left(\frac{L_{ch}}{D_{ch}} \right)^{7/23} \left(1 + 0.021 \frac{\rho_f c_{p,f} \Delta T_{sub, in}}{\rho_g h_{fg}} \right)^{16/23} \left(1 + \frac{c_{p,f} \Delta T_{sub, in}}{h_{fg}} \right)^{7/23} = 0.161 \left(\frac{\sigma}{\rho_f U_{ch}^2 L_{ch}} \right)^{8/23} \quad (5)$$

Later, Sung and Mudawar [136] investigated another hybrid cooling scheme that combined arrays of circular jets with micro-channel flow, as shown in Fig. 14(b). This differed from their previous hybrid geometry [135] in three main ways: (i) micro-channels were formed within the heated surface itself, (ii) fluid interaction between neighboring channels was prohibited, and (iii) an in-line array of 14 circular jets replaced a single slot jet. Using HFE-7100, the trends of CHF increasing with increases in flow rate and/or subcooling followed those of conventional impinging jets. CHF values as high as 1080 W/cm² were achieved for $U_n = 5.70$ m/s and $T_{in} = -20^\circ\text{C}$. Figure 15(a) illustrates the complex interactions between micro-channel flow and impinging jets in this hybrid configuration, which lead to unusual spatial variations of both quality and void fraction. Void fraction continuously increases along the flow direction in conventional micro-channel flows, but the vapor growth is interrupted and greatly diminished by the impinging jet

Table 5
Summary of experimental studies on CHF for hybrid cooling schemes.

Author(s)	Fluid(s)	Jet Geometry	Heated Surface Geometry ^d	Operating Conditions	Remarks and Major Conclusions
Nakayama <i>et al.</i> (2000) [134]	FX-3250	Hybrid jet impingement/channel flow Slot: $N = 1$, $A_n = 1 \times 35 \text{ mm}^2$, $H = 2 \text{ mm}$	► Constantan 1×5 array of $35 \times 4 \text{ mm}^2$ 10- μm -thick foil heaters with middle heater below jet nozzle; 1-mm gap between heaters	$U_n = 0.53, 3.2, 5.3 \text{ m/s}$ $P_{sat} = 1 \text{ atm}$; $T_{sat} = 56^\circ\text{C}$ $T_{in} = 36, 46, 54^\circ\text{C}$ $\Delta T_{sub,in} = 2, 10, 20^\circ\text{C}$	CHF data measured by applying heat input only to middle foil heater; CHF first increases then decreases with increasing U_n ; CHF increases with increasing $\Delta T_{sub,in}$
Sung & Mudawar (2006) [135]	PF-5052	Hybrid jet impingement/micro-channel flow Slot: $N = 5 \times 1$, $A_n = 0.48 \times 12.7 \text{ mm}^2$, $L_n = 0.76 \text{ mm}$ Each jet has 1.59-mm wide and 1.02-mm deep channel as part of jet plate, which is 0.76 mm above heated surface	▲ Oxygen-free copper $20 \times 10 \text{ mm}^2$ flat surface with flow along longer dimension	$Q_v = (1.69 - 6.60) \times 10^{-5} \text{ m}^3/\text{s}$ $\Delta T_{sub,in} = 13.1 - 35.1^\circ\text{C}$	CHF first occurs at edges of heated surface; CHF increases with increases in Q_v and $\Delta T_{sub,in}$; cooling performance of hybrid configuration is contributed more by jets than by micro-channel flow
Sung & Mudawar (2009) [136]	HFE-7100	Hybrid jet impingement/micro-channel flow Circular: $N = 5 \times 14$, $D_n = 0.39 \text{ mm}$, $L_n = 1.65 \text{ mm}$, jet pitch = 1.43 mm 1×14 jets per channel; no clearance between jet plate and heater block	▲ Oxygen-free copper $20 \times 10 \text{ mm}^2$ surface with flow along longer dimension; 5 channels of 1-mm width and 3-mm depth; fin width = 0.84 mm	$U_n = 1.05 - 6.50 \text{ m/s}$ $T_{in} = -40 - 20^\circ\text{C}$ $\Delta T_{sub,in} = 51.8 - 111.6^\circ\text{C}$	CHF increases with increases in Q_v and $\Delta T_{sub,in}$; hybrid configuration involves complex interactions between jets and channel flow resulting in unusual spatial variations in quality and void fraction; $n = 15$
Sung & Mudawar (2009) [140]	HFE-7100	Hybrid jet impingement/micro-channel flow Circular: $N = 5 \times 14$, $D_n = 0.30 - 0.60 \text{ mm}$ 1×14 jets per channel in 3 configurations: equal size, decreasing size, and increasing size from middle	▲ Oxygen-free copper $20 \times 10 \text{ mm}^2$ surface with flow along longer dimension; 5 channels of 1-mm width and 3-mm depth; fin width = 0.84 mm	$U_n = 0.48 - 7.35 \text{ m/s}$ $P_{sat} = 1.31 - 1.67 \text{ bar}$ $T_{in} = -40 - 20^\circ\text{C}$	Max. $q''_{CHF} = 1080 \text{ W/cm}^2$; CHF is highest for decreasing-jet-size pattern due to its highest outlet subcooling
Sung & Mudawar (2009) [141]	HFE-7100	Hybrid jet impingement/micro-channel flow Circular: $N = 5 \times 14$, $D_n = 0.39 \text{ mm}$ Slot: $N = 5 \times 1$, $A_n = 0.60 \times 2.94 \text{ mm}^2$ 1×14 circular jets or 1 slot jet per channel	▲ Oxygen-free copper $A_s = 20 \times 10 \text{ mm}^2$ with flow along longer dimension; 5 channels of 1-mm width and 3-mm depth; fin width = 0.84 mm	$Q_v = (6.82 - 45.5) \times 10^{-6} \text{ m}^3/\text{s}$ $P_{sat} = 1.31 - 1.67 \text{ bar}$ $T_{in} = -40 - 20^\circ\text{C}$	Max. $q''_{CHF} = 1080 \text{ W/cm}^2$; heat transfer performance of circular jet arrays is better than single slot jets
Guo <i>et al.</i> (2011) [142]	FC-72	Hybrid jet impingement/channel crossflow $A_{ch} = 30 \times 5 \text{ mm}^2$ cross-section Circular: 300 mm downstream from inlet, $N = 1$, $H = 5 \text{ mm}$	▲ 0.5-mm-thick P-doped N-type silicon chips $A_s = 10 \times 10 \text{ mm}^2$; centered below jet nozzle; bare flat and 4 micro-pin-finned surfaces; pin-fin thickness \times height = 30×60 , 30×120 , 50×60 , $50 \times 120 \mu\text{m}^2$	$U_{ch} = 0.5, 1, 1.5 \text{ m/s}$ $U_n = 0, 1, 2 \text{ m/s}$ $P_{sat} = 1 \text{ atm}$ $T_{sat} = 56^\circ\text{C}$ $\Delta T_{sub,in} = 25, 35^\circ\text{C}$	Max. $q''_{CHF} = 167 \text{ W/cm}^2$ (for $U_{ch} = 1.5 \text{ m/s}$, $U_n = 2 \text{ m/s}$, $\Delta T_{sub,in} = 35^\circ\text{C}$, and largest pin-fins); CHF increases with increases in U_n and $\Delta T_{sub,in}$ for all surfaces but the increase is more pronounced for pin-finned surfaces
Choi <i>et al.</i> (2014) [143]	FC-72	Hybrid jet impingement/channel crossflow $A_{ch} = 8 \times 8 \text{ mm}^2$ cross-section, $L_{ch} = 375 \text{ mm}$ Circular: 230 mm downstream from inlet, $N = 1$, $D_n = 3 \text{ mm}$, $L_n = 30 \text{ mm}$	▲ Indium tin oxide heater $A_s = 5 \times 10 \text{ mm}^2$ centered below jet nozzle	$Re_{ch} = 6000$ $U_n/U_{ch} = 0 - 10$ $P_{sat} = 1 \text{ atm}$; $T_{sat} = 56^\circ\text{C}$ $\Delta T_{sub,in} \approx 0^\circ\text{C}$	CHF increases quasi-linearly with increasing jet-to-channel velocity ratio, U_n/U_{ch} ; $n = 4$
Werneke (2015) [65]	HFE-7000	Hybrid jet impingement/micro-channel crossflow $L_{ch} = 8 \text{ mm}$, $W_{ch} = 2 \text{ mm}$, $N = 9 - 23$, $D_n = 98 \mu\text{m}$, $H = 192 \mu\text{m}$, jet spacing = $230 - 360 \mu\text{m}$	▲ Thin-film titanium heater $A_s = 1 \times 1 \text{ mm}^2$ ($A_r = 0.065 - 0.164$)	$U_n = 2.6 - 7.5 \text{ m/s}$ $G_r \approx 0.015 - 2.06$ $T_{sat} \approx 58.2^\circ\text{C}$ $\Delta T_{sub,in} = 17 - 35^\circ\text{C}$	Higher CHF than typical jet impingement without crossflow only for $U_n = 2.6 \text{ m/s}$ and G_r (crossflow-to-jet mass velocity ratio) > 1.25 ; higher CHF than for micro-channel flow boiling

^d ▲: upward-facing surface, ▼: downward-facing surface, ►: sideward-facing surface; A_s denotes base (planform) area for non-flat surfaces

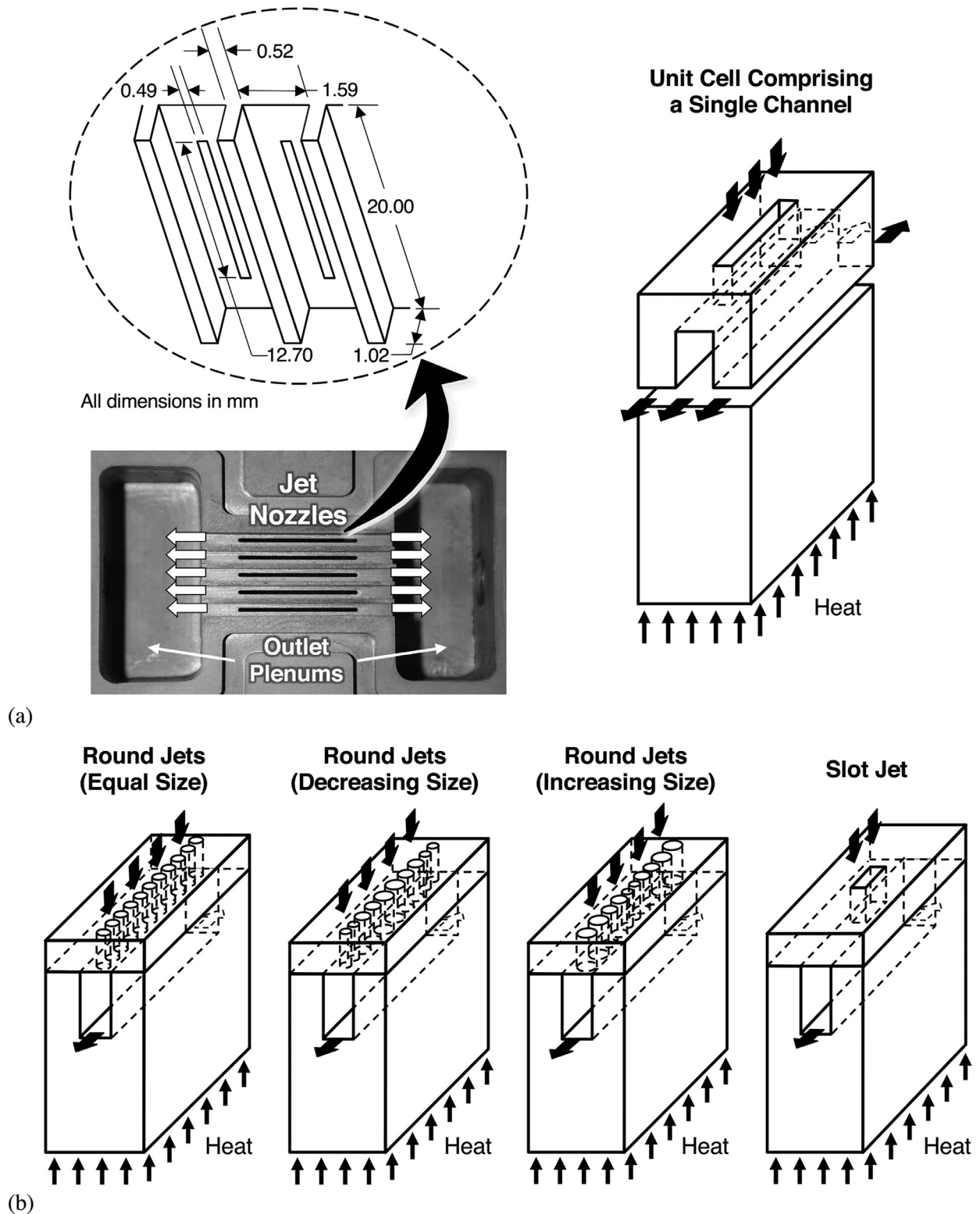


Fig. 14. Schematics of hybrid jet impingement/micro-channel cooling schemes: (a) micro-channels formed within jet plate (earliest design) and unit cell comprising a single channel, (b) unit cells of later designs (micro-channels part of heated surface). Adapted from works of Sung and Mudawar [135,136,140,141].

array in hybrid schemes. The void fraction repeatedly increases between jets but decreases sharply near the jet center due to strong condensation effects of incoming fluid. This prevents the vapor entities from coalescing together to form large structures that occupy a significant portion of the channel, and thereby leads to a smaller void fraction at the outlets. Adapting the Developing Homogeneous

Layer Model (DHLM) (which was developed for subcooled two-phase flow in conventional micro-channels by Lee and Mudawar [137]) to this hybrid flow geometry, an accurate determination of the complex velocity variation along the channel was made possible. A simple superpositioning scheme for determining CHF, based on an area-weighted average of CHF values for jet impingement

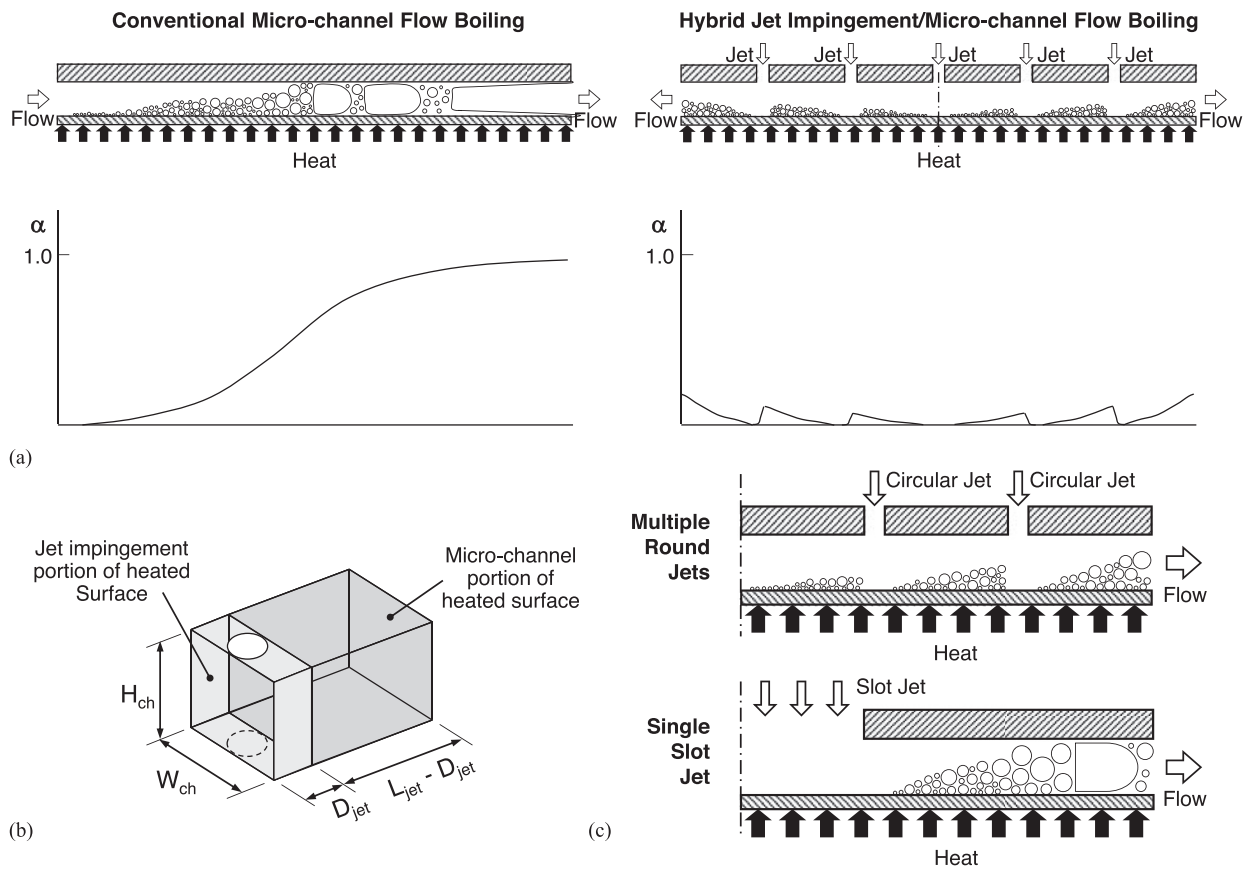


Fig. 15. (a) Schematic representation of vapor growth and void fraction variation along conventional micro-channels and hybrid jet impingement/micro-channel flow boiling. (b) Partitioning of one segment of heated micro-channel wall. (c) Vapor growth in hybrid schemes utilizing multiple round jets and single slot jet. Adapted from works of Sung and Mudawar [136,140,141].

and channel flow, was proposed,

$$(W_{ch} + 2W_w)L_{jet}q''_{CHF,hybrid} = 2(W_{ch} + H_{ch})(L_{jet} - D_{jet})\frac{1}{N} \sum q''_{CHF,ch} + \left[2(W_{ch} + H_{ch})D_{jet} - \frac{\pi D_{jet}^2}{4} \right] q''_{CHF,jet}, \quad (6)$$

where W_w is the half-width of microchannel walls (sometimes called fins) and the other geometrical parameters are as per Fig. 15(b). In Eq. (6), $q''_{CHF,jet}$ was based on a correlation by Monde *et al.* [75], which was modified by replacing L_s with $2\sqrt{(W_{ch}/2)^2 + H_{ch}^2}$, twice the distance from the jet center to farthest point on the micro-channel wall. And $q''_{CHF,ch}$ was based on a correlation by Hall and Mudawar [138] for small channels. Note that Sung and Mudawar initially recommended using Bowers and Mudawar's [139] channel flow correlation with U_{ch} in each flow cell determined using DHLM, but better results were later realized using Hall and Mudawar's [138] correlation.

A follow-up study by Sung and Mudawar [140] explored two additional jet patterns, decreasing-jet-size and increasing-jet-size, Fig. 14(b), for their previous hybrid geometry with equal jet size [136], with the sum of the flow areas through all three nozzle plates maintained constant. CHF was found to be highest for the decreasing-size jet pattern due to its highest outlet subcooling. And CHF mechanism in these hybrid schemes was postulated to resemble the Departure from Nucleate Boiling (DNB) encountered in short channel flow with high flow rate and high subcooling.

Another follow-up study by Sung and Mudawar [141] compared their previous hybrid configurations with an in-line array of circular jets [136] to that with a single slot jet per micro-channel, which is also shown in Fig. 14(b). The heat transfer performance

of the circular jet array proved better than for a single slot jet because of drastic differences in vapor production between the two geometries as illustrated in Fig. 15(c). The circular jet array provided repeated bubble growth and condensation along the channel and took better advantage of the subcooled bulk fluid. At a similar inlet subcooling of $\Delta T_{sub,in} \approx 68.2^\circ\text{C}$, representative CHF values for the circular jet arrays at $Q_v = 8.77 \times 10^{-6} \text{ m}^3/\text{s}$ and single slot jets at $Q_v = 7.15 \times 10^{-6} \text{ m}^3/\text{s}$ are 305 and 243 W/cm^2 , respectively.

6.2. Liquid Entry through both Jet Nozzles and Channels (Crossflow Configuration)

Guo *et al.* [142] attempted to enhance subcooled flow boiling heat transfer of FC-72 on micro-pin-finned surfaces using jet impingement. A $10 \times 10 \text{ mm}^2$ silicon chip was placed at the bottom of a rectangular channel of $30 \times 5 \text{ mm}^2$ cross-section. A circular jet nozzle was formed in the channel's top wall facing the chip center 300-mm downstream from the channel inlet. Flow velocities at the channel inlet and jet nozzle were varied from $U_{ch} = 0.5$ to 1.5 m/s and $U_n = 0$ to 2 m/s, respectively. Five different surfaces were tested: bare flat surface and 4 different micro-pin-finned surfaces. CHF was found to be higher for higher velocities and inlet subcoolings for all surfaces, but this effect was more pronounced with the pin-finned surfaces. The highest CHF was 167 W/cm^2 , which was achieved at $U_{ch} = 1.5 \text{ m/s}$ and $U_n = 2 \text{ m/s}$ using the largest pin-fins. Guo *et al.* concluded that the crossflow effect of impinging jets is more significant for faster jets.

Choi *et al.* [143] investigated a similar crossflow configuration in a 375-mm-long, $8 \times 8\text{-mm}^2$ rectangular channel with a single circular jet placed 230 mm downstream from the inlet. The heated

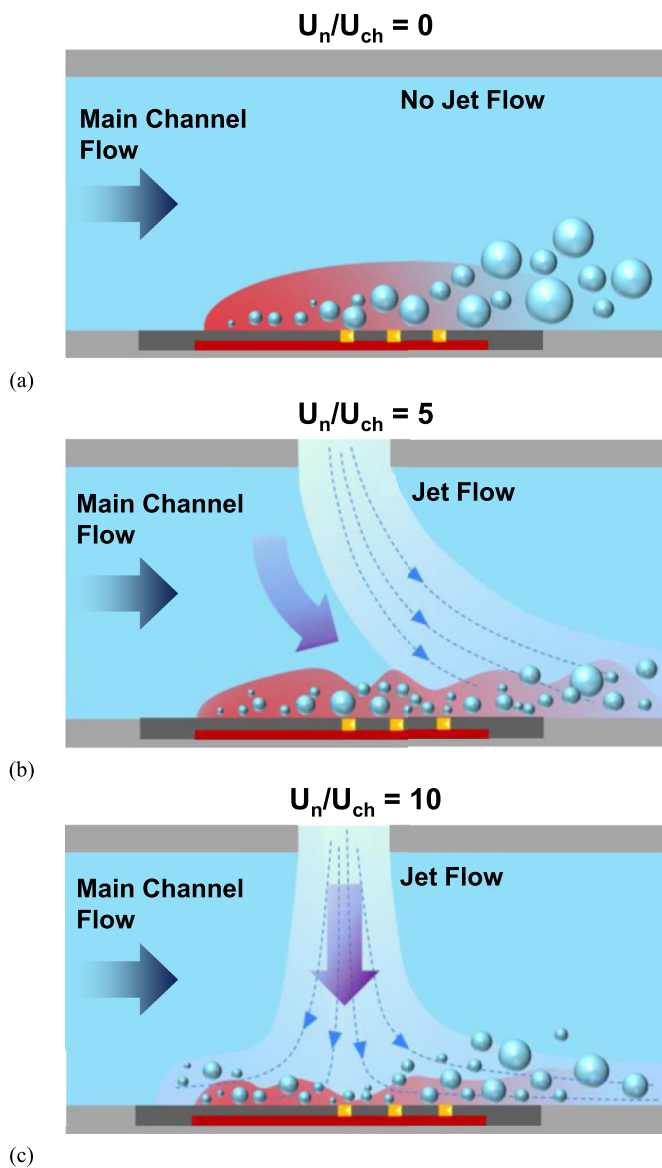


Fig. 16. Illustration of boiling behavior for crossflow jet impingement/channel flow cooling scheme with jet-to-channel velocity ratios of (a) $U_n/U_{ch} = 0$, (b) $U_n/U_{ch} = 5$, and (c) $U_n/U_{ch} = 10$. Adapted from Choi *et al.* [143].

surface was similarly placed in the channel bottom wall centered around the jet. The channel flow velocity was maintained constant with $Re_{ch} = 6000$, but the jet-to-channel velocity ratio, U_n/U_{ch} was varied from 0 to 10. CHF was found to vary quasi-linearly with velocity ratio for the four cases tested. Based on flow visualizations of the area above the heated surface, they illustrated the effect of impinging jet on channel flow boiling, as shown in Fig. 16. It is obvious that very low jet velocities have negligible impact on boiling behavior at the surface due to the stronger channel flow dissipating momentum of the jet within the bulk fluid flow. But as U_n/U_{ch} was brought close to 5, the jet began to impinge downstream from the center of the heated surface and was able to remove larger coalesced bubbles. The full effect of the jet was observed at $U_n/U_{ch} = 10$, where much larger momentum of the jet allowed it to impinge almost symmetrically while also reducing the amount and size of vapor bubbles at the surface. This naturally leads to a larger enhancement in CHF, but a remarkable increase in ONB heat flux was also noticed. They suggested that $U_n/U_{ch} = 5$ be

used for best overall heat transfer performance, based on a compromise between CHF enhancement and ONB deferral.

Using a similar experimental configuration with $1 \times 1 \text{ mm}^2$ heater, Werneke [65] compared CHF for conventional round jet array, micro-channel flow boiling, and hybrid jet array impingement/micro-channel crossflow by allowing liquid to enter through the jet nozzles, one channel end, or both nozzles and one channel end together. CHF for both conventional jet impingement and hybrid scheme were higher than for micro-channel flow boiling. And hybrid scheme CHF was higher than jet impingement CHF only at low jet velocity ($U_n = 2.6 \text{ m/s}$) and with a crossflow-to-jet mass velocity ratio of $G_r > 1.25$, which are representative of weak jet impingement effects.

Overall, hybrid cooling schemes utilizing jet impingement show a lot of potential in enhancing CHF and overall heat transfer performance, along with other advantages such as low two-phase pressure drop, suppression of flow instabilities, and diminution of temperature overshoot at ONB. Unfortunately, most hybrid cooling studies have been focused on single-phase cooling. With only a handful of CHF datapoints for a specific hybrid cooling configuration, future work needs to address expanding investigation to more configurations as well broader ranges of geometrical parameters and operating conditions. It should be noted that the only CHF prediction technique available for hybrid schemes is the simple area-weighted averaging of values predicted using jet impingement and channel flow correlations; no equivalent techniques are available for crossflow schemes.

7. Remarks on Experimental CHF Measurement

A recent experimental study on jet impingement CHF by the present authors [18], coupled with careful assessment of jet-impingement data from the literature prompted a closer look into conflicting methods to both measuring and interpreting jet CHF.

It is general knowledge among two-phase investigators that CHF marks the upper limit for the nucleate boiling regime. When conducting experiments, CHF is typically marked as the heat flux that leads to temperature excursion towards film boiling. During the present authors' recent experiments [18], CHF was detected by an unsteady and uncontrollable increase in surface temperature. A representative boiling curve from the study is shown in Fig. 17(a), which includes the different heat transfer regimes and points of transition between them. For very low heat fluxes, the curve is linear and has a small slope, which represents single-phase liquid convection. The slope changes at ONB, where bubbles begin to form on the heated surface. Following ONB, the slope increases appreciably to a higher value and becomes almost constant; this represents the lower part of the nucleate boiling regime. Operation in this regime yields the desired cooling advantages of both large heat transfer coefficients and ability to dissipate a broad range of heat fluxes corresponding to only modest change in surface temperature. However, the upper portion of nucleate boiling shows appreciable heat transfer degradation evidenced by a pronounced decline in slope. Denoting the point at which the degradation begins as Onset of Nucleate Boiling Degradation (ONBD), the authors pointed out the importance of distinguishing ONBD from true CHF due to large differences in both heat flux and surface superheat between the two. The authors believe that the region between ONBD and CHF is an important characteristic of impinging jets, albeit with apparent degradation, presumably the outcome of increased bubble coalescence and formation of discrete, localized vapor layers upon the surface. Interestingly, ONBD lies very close to CHF in pool boiling and many flow boiling situations, but, as shown in Fig. 17(a), not jet impingement boiling. It is noted that some micro-channel flow boiling studies denote ONBD as point of *dryout incipience* [144].

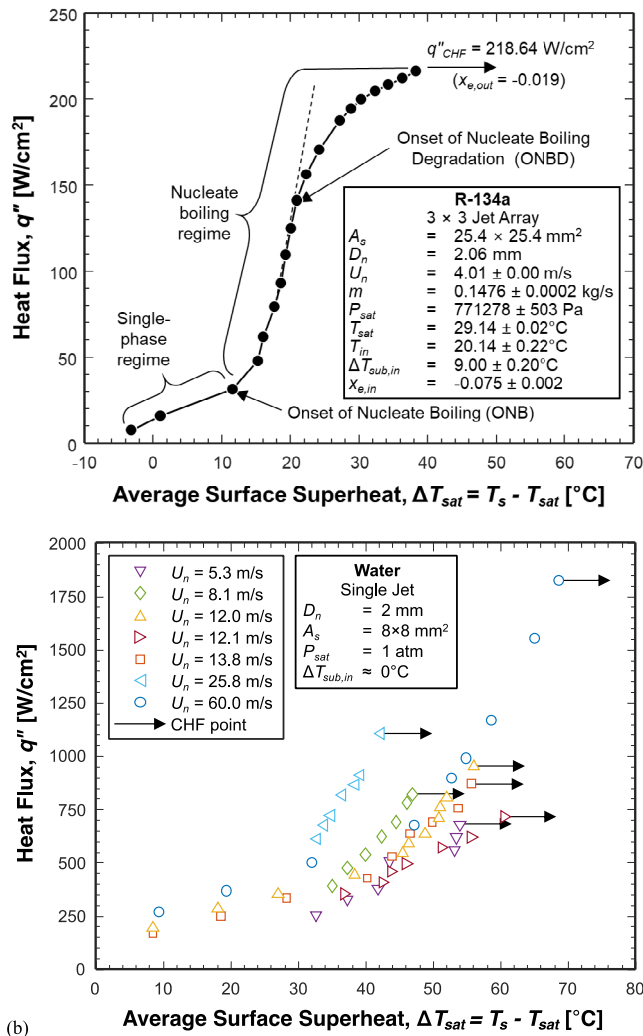


Fig. 17. (a) Representative jet impingement boiling curve indicating broad heat transfer degradation region preceding CHF (adapted from Devahdhanush and Mudawar [18]). (b) Representative boiling curves that do not show heat transfer degradation prior to CHF (data adapted from Katto and Monde [36]).

Most studies have included some boiling curves or heat transfer coefficient plots along with CHF results. This enabled the present authors to categorize the jet CHF studies into two: (a) those that clearly show distinct ONBD and CHF points with a large heat transfer coefficient degradation region in between, and (b) others that seem to not show the degradation region or a distinct ONBD point. Examples of boiling curves that do and do not show the degradation portion of the nucleate boiling regime are shown in Figs. 17(a) and 17(b), respectively. Possible reasons for the latter group of studies are: (i) while conducting experiments, researchers opted to identify ONBD itself as CHF, (ii) investigators could have prematurely defined CHF based on relatively minor temperature excursions (the present authors observed such excursions to subside after some time in their own experiments [18]), perhaps to protect their heaters from physical burnout, (iii) fluid flow and heat transfer mechanism triggering CHF could have been different from cases involving a broad degradation region, (iv) large heat flux increases close to CHF might have prematurely triggered CHF or missed the ONBD point (this was pointed out by Estes and Mudawar [11] who demonstrated premature dryout occurrence when heater power was increased too quickly), and (v) in case of directly heated thin metal foils, burnout failure could have occurred be-

cause of localized overheating following ONBD, coupled with an inability of the thin foil to conduct the heat away to more adequately cooled surface regions (Mitsutake and Monde [74] experimentally showed that heater thickness within certain limits does significantly affect CHF results). For instance, while not always explicitly stated in publications, Katto and co-workers often identified the heat flux corresponding to ONBD as CHF (this is based on a private communication between I. Mudawar and Y. Katto in 1995). It is noted that CHF in jet impingement is influenced by effects of non-isothermal surface and uneven heat transfer coefficient, making heat conduction effects and surface/heater thickness play an important role in experimentally determining the value of CHF; investigating this problem systematically and proposing criteria for selecting appropriate (minimum) heater/surface thickness could alleviate one of the concerns mentioned here.

Overall, the present authors urge the two-phase heat transfer community to be scrupulous when measuring CHF and to explicitly state details regarding the measurements in their publications, however rudimentary they may seem. The present authors also feel that a 'standard' for measuring jet impingement CHF might be of the essence to ensure that measured values are indeed accurate. The discussion in this section might also be applicable to CHF with other cooling schemes, but systematically analyzing those is beyond the scope of this review.

8. Concluding Remarks

This article presented a systematized review of articles addressing CHF for different jet impingement schemes. A very comprehensive search for studies on jet CHF was conducted, which included articles published over a span of five decades and jets of various fluids, operating conditions, and geometrical configurations. Also discussed were hybrid cooling schemes of which jet impingement is an integral part. Key conclusions and recommendations based on this review are as follows:

- (1) The majority of jet impingement CHF literature is experimental, and concerns mostly conventional jet configurations, including both round and slot jets impinging normally onto a flat heated surface. These include free-surface, submerged, and confined jets, as well as single and multiple jets, produced by a pressure differential via either a pump or large gravitational head. Overall, there is consensus regarding effects of most parameters on CHF, but some parameters are still not well understood.
- (i) CHF for confined jets is generally higher than for free-surface jets. Also, CHF for submerged jets is higher than for pool boiling, and also typically higher than for free-surface jets. However, some researchers have shown localized stagnation line CHF to be smaller for submerged jets compared to free-surface jets.
- (ii) Augmentation of CHF is typically achieved by increasing jet velocity within certain limits, outside which CHF becomes invariant with velocity or even deteriorates with increasing velocity. However, these limits are not well understood and cannot be universally predicted using available data.
- (iii) For most nozzle and heater size combinations, CHF is higher for smaller heated surfaces, larger nozzles for fixed jet velocity, and smaller nozzles for fixed flow rate. However, for single nozzles which are of the same size as surfaces, CHF decreases with increasing size. Some studies have shown that CHF increases as heater size increases until a certain limit, after which it monotonically decreases.
- (iv) Jet arrays yield higher CHF and more uniform surface temperatures than single jets. CHF increases with increasing number of jets for fixed velocity and decreases for fixed flow rate. Although earlier studies have shown that single jet correlations

could be adapted to predict CHF for multiple jets, recent studies have incorporated the effects of wall jet interactions into their multiple jet correlations. There are mixed results on influence of array patterns on CHF.

- (v) Choices of working fluid and saturation pressure affect CHF by virtue of different thermophysical properties. This has manifested in CHF results as different trends with increasing saturation pressure for different fluids and operating conditions. Most studies have estimated thermophysical properties at saturation pressure, while others on stagnation pressure to incorporate effects of faster jets.
- (vi) There is consensus that increasing fluid subcooling ameliorates CHF, however exact trends are different for different studies as evident from different forms of subcooling terms in their correlations. Different techniques for increasing the subcooling, including decreasing inlet fluid temperature, increasing saturation pressure, or both, have been utilized.
- (vii) Jet height is one parameter where literature shows most contradictory results on CHF for different geometrical parameters and operating conditions. The present authors believe that jet height, by itself, does not affect CHF. But rather, it affects CHF in combination with other parameters. Further research is needed until a consensus is reached.
- (viii) For typical operating conditions and geometries, orientation of heated surface does not affect CHF. However, the present authors anticipate gravity to influence CHF for very small jet velocities or large heated surfaces.
- (ix) Presence of non-condensable gases in the fluids does not seem to affect jet CHF.
- (2) Researchers have studied CHF for certain special jet configurations such as oblique and wall jets, and liquid jets created by techniques such as application of strong electric field or use as part of a vapor compression cycle.
- (3) Various techniques for enhancing jet impingement CHF, including surface modification (like surface curvature, extended surface structures, surface coatings, or combinations thereof), specialized spent fluid removal, and nanofluids, have shown promise. However, the life and repeatability of some techniques, especially coatings and nanofluids, are doubtful. Some other techniques, such as rotating nozzle plates, heating element protrusion, and jet suction, proved to be inefficient.
- (4) Almost all prediction techniques for jet impingement CHF are either semi-theoretical or fully empirical correlations. An exhaustive list of correlations that were developed from different CHF databases, along with their underlying rationale was provided. Most were developed by dimensional analysis, trial-and-error procedures, or modifying prior correlations to fit newer experimental data. Some were developed based on underlying CHF mechanisms and further modified using a variety of assumptions and approximations, while a few have been constructed using statistical techniques or machine learning tools. No studies have utilized computational methods (numerical simulations) to predict CHF in jet impingement boiling, nor are there fully theoretical models based on true fluid flow and heat transfer characteristics at CHF.
- (5) Hybrid cooling schemes combining flow features of both jet impingement and channel flow show potential for enhancing both heat transfer performance and CHF by combining advantages of the individual schemes. With only a handful of CHF data-points available for a specific hybrid cooling configuration, future work needs to address expanding investigation to more configurations as well broader ranges of geometrical parameters and operating conditions. It should be noted that the only CHF prediction technique available for hybrid schemes is the simple area-weighted averaging of values predicted using jet impinge-

ment and channel flow correlations; no equivalent techniques are available for crossflow schemes.

- (6) Finally, some remarks on measurement of CHF in jet impingement boiling experiments are provided based on systematic observation of all studies incorporated in this review. Some studies show distinct ONBD points preceding CHF with an intermediary heat transfer degradation region, while some do not. Researchers experimentally measuring CHF are urged to be scrupulous and to explicitly state details of their measurements in publications, however rudimentary they might seem. It might be about time a 'standard' for measuring jet impingement CHF is proposed by the heat transfer community to ensure accuracy of measured values and uniformity amongst experimental studies.

Declaration of Competing Interest

None. The authors declare that they have no known competing financial interests or personal relationships that could have appeared to influence the work reported in this paper.

Acknowledgement

The authors are appreciative for the support of the Center for Integrated Thermal Management for Aerospace Vehicles (CITMAV) under grant No. 40001302. The authors are also grateful to the Purdue University Libraries and School of Information Studies for their assistance in procuring numerous hard-to-access articles from around the world.

References

- [1] I. Mudawar, Assessment of high-heat-flux thermal management schemes, *IEEE Trans. Compon. Packag. Technol.* 24 (2) (2001) 122–141, doi:[10.1109/6144.926375](https://doi.org/10.1109/6144.926375).
- [2] J. Lee, I. Mudawar, Critical heat flux for subcooled flow boiling in micro-channel heat sinks, *Int. J. Heat Mass Transfer* 52 (13–14) (2009) 3341–3352, doi:[10.1016/j.ijheatmasstransfer.2008.12.019](https://doi.org/10.1016/j.ijheatmasstransfer.2008.12.019).
- [3] T.J. LaClair, I. Mudawar, Thermal transients in a capillary evaporator prior to the initiation of boiling, *Int. J. Heat Mass Transfer* 43 (21) (2000) 3937–3952, doi:[10.1016/S0017-9310\(00\)00042-9](https://doi.org/10.1016/S0017-9310(00)00042-9).
- [4] I. Mudawar, T.M. Anderson, Parametric investigation into the effects of pressure, subcooling, surface augmentation and choice of coolant on pool boiling in the design of cooling systems for high-power-density electronic chips, *J. Electron. Packag.* 112 (4) (1990) 375–382, doi:[10.1115/1.2904392](https://doi.org/10.1115/1.2904392).
- [5] I. Mudawar, R.A. Houpt, Mass and momentum transport in smooth falling liquid films laminarized at relatively high Reynolds numbers, *Int. J. Heat Mass Transfer* 36 (14) (1993) 3437–3448, doi:[10.1016/0017-9310\(93\)90162-Y](https://doi.org/10.1016/0017-9310(93)90162-Y).
- [6] I. Mudawar, D.E. Maddox, Critical heat flux in subcooled flow boiling of fluorocarbon liquid on a simulated electronic chip in a vertical rectangular channel, *Int. J. Heat Mass Transfer* 32 (2) (1989) 379–394, doi:[10.1016/0017-9310\(89\)90184-1](https://doi.org/10.1016/0017-9310(89)90184-1).
- [7] S. Mukherjee, I. Mudawar, Pumpless loop for narrow channel and micro-channel boiling, *J. Electron. Packag.* 125 (3) (2003) 431–441, doi:[10.1115/1.1602708](https://doi.org/10.1115/1.1602708).
- [8] S. Lee, V.S. Devahdhanush, I. Mudawar, Pressure drop characteristics of large length-to-diameter two-phase micro-channel heat sinks, *Int. J. Heat Mass Transfer* 115 (2017) 1258–1275, doi:[10.1016/j.ijheatmasstransfer.2017.08.104](https://doi.org/10.1016/j.ijheatmasstransfer.2017.08.104).
- [9] W.P. Klingning, J.C. Rozzi, I. Mudawar, Film and transition boiling correlations for quenching of hot surfaces with water sprays, *J. Heat Treat.* 9 (2) (1992) 91–103, doi:[10.1007/BF02833145](https://doi.org/10.1007/BF02833145).
- [10] G. Liang, I. Mudawar, Review of spray cooling – Part 2: High temperature boiling regimes and quenching applications, *Int. J. Heat Mass Transfer* 115 (2017) 1206–1222, doi:[10.1016/j.ijheatmasstransfer.2017.06.022](https://doi.org/10.1016/j.ijheatmasstransfer.2017.06.022).
- [11] K.A. Estes, I. Mudawar, Comparison of two-phase electronic cooling using free jets and sprays, *J. Electron. Packag.* 117 (4) (1995) 323–332, doi:[10.1115/1.2792112](https://doi.org/10.1115/1.2792112).
- [12] D.C. Wadsworth, I. Mudawar, Cooling of a multichip electronic module by means of confined two-dimensional jets of dielectric liquid, *J. Heat Transfer* 112 (4) (1990) 891–898, doi:[10.1115/1.2910496](https://doi.org/10.1115/1.2910496).
- [13] I. Mudawar, D.C. Wadsworth, Critical heat flux from a simulated chip to a confined rectangular impinging jet of dielectric liquid, *Int. J. Heat Mass Transfer* 34 (6) (1991) 1465–1479, doi:[10.1016/0017-9310\(91\)90289-Q](https://doi.org/10.1016/0017-9310(91)90289-Q).
- [14] D.C. Wadsworth, I. Mudawar, Enhancement of single-phase heat transfer and critical heat flux from an ultra-high-flux simulated microelectronic heat source to a rectangular impinging jet of dielectric liquid, *J. Heat Transfer* 114 (3) (1992) 764–768, doi:[10.1115/1.2911348](https://doi.org/10.1115/1.2911348).

- [15] M.E. Johns, Application of jet impingement boiling in an ultra-high power avionic clamshell module, M.S. Thesis, Purdue University, West Lafayette, IN, USA, 1994.
- [16] M.E. Johns, I. Mudawar, An ultra-high power two-phase jet-impingement avionic clamshell module, *J. Electron. Packag.* 118 (4) (1996) 264–270, doi:10.1115/1.2792162.
- [17] M.T. Meyer, I. Mudawar, C.E. Boyack, C.A. Hale, Single-phase and two-phase cooling with an array of rectangular jets, *Int. J. Heat Mass Transfer* 49 (1–2) (2006) 17–29, doi:10.1016/j.ijheatmasstransfer.2005.07.039.
- [18] V.S. Devahdhanush, I. Mudawar, Critical heat flux of confined round single jet and jet array impingement boiling, *Int. J. Heat Mass Transfer* 169 (2021) 120857, doi:10.1016/j.ijheatmasstransfer.2020.120857.
- [19] I. Mudawar, Recent advances in high-flux, two-phase thermal management, *J. Therm. Sci. Eng. Appl.* 5 (2) (2013) 021012, doi:10.1115/1.4023599.
- [20] S. Lee, V.S. Devahdhanush, I. Mudawar, Frequency analysis of pressure oscillations in large length-to-diameter two-phase micro-channel heat sinks, *Int. J. Heat Mass Transfer* 116 (2018) 273–291, doi:10.1016/j.ijheatmasstransfer.2017.08.107.
- [21] M. Visaria, I. Mudawar, Application of two-phase spray cooling for thermal management of electronic devices, *IEEE Trans. Compon. Packag. Technol.* 32 (4) (2009) 784–793, doi:10.1109/TCPAPT.2008.2010405.
- [22] A.M. Huber, R. Viskanta, Effect of jet-jet spacing on convective heat transfer to confined, impinging arrays of axisymmetric air jets, *Int. J. Heat Mass Transfer* 37 (18) (1994) 2859–2869, doi:10.1016/0017-9310(94)90340-9.
- [23] R.J. Copeland, Boiling heat transfer to a water jet impinging on a flat surface, Ph.D. Thesis, Southern Methodist University, Dallas, TX, USA, 1970.
- [24] H. Zhang, I. Mudawar, M.M. Hasan, Experimental and theoretical study of orientation effects on flow boiling CHF, *Int. J. Heat Mass Transfer* 45 (22) (2002) 4463–4477, doi:10.1016/S0017-9310(02)00152-7.
- [25] C. Konishi, I. Mudawar, Review of flow boiling and critical heat flux in microgravity, *Int. J. Heat Mass Transfer* 80 (2015) 469–493, doi:10.1016/j.ijheatmasstransfer.2014.09.017.
- [26] M. Monde, Y. Katto, Burnout in a high heat-flux boiling system with an impinging jet, *Int. J. Heat Mass Transfer* 21 (3) (1978) 295–305, doi:10.1016/0017-9310(78)90122-9.
- [27] R. Cardenas, V. Narayanan, Submerged jet impingement boiling of water under subatmospheric conditions, *J. Heat Transfer* 134 (2) (2012) 020909, doi:10.1115/1.4005064.
- [28] L.E. O'Neill, I. Park, C.R. Kharangate, V.S. Devahdhanush, V. Ganesan, I. Mudawar, Assessment of body force effects in flow condensation, part II: Criteria for negating influence of gravity, *Int. J. Heat Mass Transfer* 106 (2017) 313–328, doi:10.1016/j.ijheatmasstransfer.2016.07.019.
- [29] Y. Katto, M. Kunihiro, Study of the mechanism of burn-out in boiling system of high burn-out heat flux, *Bull. JSME* 16 (99) (1973) 1357–1366, doi:10.1299/jsme1958.16.1357.
- [30] R.A. Buchanan, T.A. Shedd, Extensive parametric study of heat transfer to arrays of oblique impinging jets with phase change, *J. Heat Transfer* 135 (11) (2013) 111017, doi:10.1115/1.4024625.
- [31] Y. Katto, C. Kurata, Critical heat flux of saturated convective boiling on uniformly heated plates in a parallel flow, *Int. J. Multiphase Flow* 6 (6) (1980) 575–582, doi:10.1016/0301-9322(80)90052-X.
- [32] T. Nonn, Z. Dagan, L.M. Jiji, Boiling jet impingement cooling of simulated microelectronic heat sources, *ASME Paper No. 88-WA/EEP-3* (1988).
- [33] W. Qu, I. Mudawar, Measurement and correlation of critical heat flux in two-phase micro-channel heat sinks, *Int. J. Heat Mass Transfer* 47 (10–11) (2004) 2045–2059, doi:10.1016/j.ijheatmasstransfer.2003.12.006.
- [34] M. Monde, Y. Katto, Study of burn-out in a high heat-flux boiling system with an impinging jet: Part 1. Behavior of the vapour-liquid flow, *Trans. Jpn. Soc. Mech. Eng.* 43 (373) (1977) 3399–3407, doi:10.1299/kikai1938.43.3399.
- [35] Y. Katto, M. Monde, Study of mechanism of burn-out in a high heat-flux boiling system with an impinging jet, in: *Proc. Int. Heat Transfer Conf. 5*, Begell House Inc., Tokyo, Japan, 1974, pp. 245–249, doi:10.1615/IHTC5.570.
- [36] Y. Katto, M. Monde, Mechanism of burn-out in a high heat-flux boiling system with an impinging jet, *Trans. Jpn. Soc. Mech. Eng.* 41 (341) (1975) 306–314, doi:10.1299/kikai1938.41.306.
- [37] R. Cardenas, V. Narayanan, Critical heat flux in submerged jet impingement boiling of water under subatmospheric conditions, *J. Heat Transfer* 134 (8) (2012) 081502, doi:10.1115/1.4006206.
- [38] R. Cardenas, V. Narayanan, Comparison of deionized water and FC-72 in pool and jet impingement boiling thermal management, *IEEE Trans. Compon. Packag. Manuf. Technol.* 2 (11) (2012) 1811–1823, doi:10.1109/TCPMT.2012.2210717.
- [39] M. Monde, Y. Furukawa, Critical heat flux in saturated forced convective boiling with an impinging jet: Coexistence of pool and forced convective boilings, *Trans. Jpn. Soc. Mech. Eng. Ser. B* 53 (485) (1987) 199–203, doi:10.1299/kikaib.53.199.
- [40] M. Monde, Y. Furukawa, Critical heat flux in saturated forced convective boiling with an impinging jet coexistence of pool and forced convective boilings, *Heat Transfer - Jpn. Res.* 17 (5) (1988) 81–91.
- [41] H. Robidou, H. Auracher, P. Gardin, M. Lebouché, Controlled cooling of a hot plate with a water jet, *Exp. Therm. Fluid Sci.* 26 (2–4) (2002) 123–129, doi:10.1016/S0894-1777(02)00118-8.
- [42] Y. Katto, M. Shimizu, Upper limit of CHF in the saturated forced convection boiling on a heated disk with a small impinging jet, *J. Heat Transfer* 101 (2) (1979) 265–269, doi:10.1115/1.3450958.
- [43] M. Monde, Y. Okuma, Critical heat flux in saturated forced convective boiling on a heated disk with an impinging jet—CHF in L-regime, *Int. J. Heat Mass Transfer* 28 (3) (1985) 547–552, doi:10.1016/0017-9310(85)90177-2.
- [44] M. Monde, Critical heat flux in saturated forced convection boiling on a heated disk with an impinging jet, *J. Heat Transfer* 109 (4) (1987) 991–996, doi:10.1115/1.3248215.
- [45] M. Monde, O. Nagae, Y. Ishibashi, Critical heat flux in a saturated forced convective boiling on a heated disk with an impinging jet: In a high pressure region, *Trans. Jpn. Soc. Mech. Eng. Ser. B* 52 (476) (1986) 1799–1804, doi:10.1299/kikaib.52.1799.
- [46] M. Monde, O. Nagae, Y. Ishibashi, Critical heat flux in saturated forced convective boiling on a heated disk with an impinging jet, *Heat Transfer - Jpn. Res.* 16 (5) (1987) 70–82.
- [47] M. Monde, Critical heat flux in saturated forced convective boiling on a heated disk with one or multiple impinging jets, *Trends Heat, Mass Momentum Transfer* 1 (1991) 33–44.
- [48] Y.Y. Li, Z.H. Liu, Q. Wang, Experimental study on critical heat flux of steady boiling for high-velocity slot jet impinging on the stagnation zone, *Int. J. Heat Mass Transfer* 70 (2014) 1–9, doi:10.1016/j.ijheatmasstransfer.2013.10.058.
- [49] Y. Cheng, A.A.O. Tay, X. Hong, An experimental study of liquid jet impingement cooling of electronic components with and without boiling, *Adv. Electron. Mater. Packag.* (1979) 369–375 2001, doi:10.1109/EMAP.2001.984012.
- [50] F.J. Hong, C.Y. Zhang, W. He, P. Cheng, G. Chen, The local and average heat transfer characteristic of confined jet array impingement boiling of aqueous ethylene glycol solutions, in: *Proc. ASME 2013 4th Int. Conf. Micro/Nanoscale Heat Mass Transfer*, ASME, Hong Kong, China, 2013, <https://doi.org/10.1115/MNHMT2013-22260>, V001T11A013.
- [51] A.M.T. Omar, M.S. Hamed, M. Shoukri, Nucleate boiling heat transfer under liquid jet impingement, in: *Proc. ASME/JSME 2007 Therm. Eng. Heat Transfer Summer Conf.*, ASME, Vancouver, British Columbia, Canada, 2007, pp. 723–729, doi:10.1115/HT2007-32020.
- [52] Z.H. Liu, T.F. Tong, Y.H. Qiu, Critical heat flux of steady boiling for subcooled water jet impingement on the flat stagnation zone, *J. Heat Transfer* 126 (2) (2004) 179–183, doi:10.1115/1.1668054.
- [53] Y.H. Qiu, Z.H. Liu, Critical heat flux in saturated and subcooled boiling for R-113 jet impingement on the stagnation zone, *Appl. Therm. Eng.* 25 (14–15) (2005) 2367–2378, doi:10.1016/j.applthermaleng.2004.12.004.
- [54] Y.H. Qiu, Z.H. Liu, Critical heat flux of steady boiling for saturated liquids jet impinging on the stagnation zone, *Int. J. Heat Mass Transfer* 48 (21–22) (2005) 4590–4597, doi:10.1016/j.ijheatmasstransfer.2005.06.002.
- [55] Y.H. Qiu, Z.H. Liu, Predicting of critical heat flux of steady boiling for subcooled liquids jet impingement on the flat stagnation zone, in: L. Guo, X. Chen, Z. Lin (Eds.), *Proc. 5th Int. Symp. Multiphase Flow, Heat Mass Transfer Energy Convers.*, Xi'an Jiantong University Press, Xi'an, China, 2005, pp. 212–218.
- [56] A.A. Maceika, R.K. Skema, Boiling crisis burnout in the zone of interaction of a circular submerged water jet with a flat wall, *Heat Transfer - Sov. Res.* 22 (5) (1990) 587–594.
- [57] R.K. Skema, A.A. Slanciauskas, Critical heat fluxes at jet-cooled flat surfaces, *Heat Transf. Electron. Microelectron. Equip.* (1990) 621–626.
- [58] D. Copeland, Single-phase and boiling cooling of small pin fin arrays by multiple nozzle jet impingement, *J. Electron. Packag.* 118 (1) (1996) 21–26, doi:10.1115/1.2792122.
- [59] D. Copeland, Single-phase and boiling cooling of a small heat source by multiple nozzle jet impingement, *Int. J. Microelectron. Packag.* 1 (1998) 105–113.
- [60] D. Copeland, Single-phase and boiling cooling of a small heat source by multiple nozzle jet impingement, *ASME Paper No. 92-WA/EEP-4* (1992).
- [61] T. Nonn, Z. Dagan, L.M. Jiji, Jet impingement flow boiling of a mixture of FC-72 and FC-87 liquids on a simulated electronic chip, *Heat Transfer in Electronics*, in: *Proc. 1989 Natl. Heat Transfer Conf. - Heat Transfer Electron.*, ASME, Philadelphia, PA, 1989, pp. 121–128.
- [62] E.A. Browne, G.J. Michna, M.K. Jensen, Y. Peles, Microjet array single-phase and flow boiling heat transfer with R134a, *Int. J. Heat Mass Transfer* 53 (23–24) (2010) 5027–5034, doi:10.1016/j.ijheatmasstransfer.2010.07.062.
- [63] E.A. Browne, M.K. Jensen, Y. Peles, Microjet array flow boiling with R134a and the effect of dissolved nitrogen, *Int. J. Heat Mass Transfer* 55 (4) (2012) 825–833, doi:10.1016/j.ijheatmasstransfer.2011.10.025.
- [64] F.J. Hong, C.Y. Zhang, W. He, P. Cheng, G. Chen, Confined jet array impingement boiling of subcooled aqueous ethylene glycol solution, *Int. Commun. Heat Mass Transfer* 56 (2014) 165–173, doi:10.1016/j.icheatmasstransfer.2014.06.013.
- [65] B.M. Werneke, Microjet array impingement heat transfer crossflow effects in single-phase and flow boiling, Ph.D. Thesis, Rensselaer Polytechnic Institute, Troy, NY, USA, 2015.
- [66] M. Monde, H. Kusuda, H. Uehara, Burnout heat flux in saturated forced convection boiling with two or more impinging jets, *Heat Transfer - Jpn. Res.* 9 (3) (1980) 18–31.
- [67] M. Monde, H. Kusuda, H. Uehara, Burnout in a high heat-flux boiling system with more than two jets: 4th Report, Liquid is fed to the heated surface through more than two jets, *Trans. Jpn. Soc. Mech. Eng. Ser. B* 46 (409) (1980) 1834–1843, doi:10.1299/kikaib.46.1834.
- [68] M. Monde, T. Inoue, Critical heat flux in saturated forced convective boiling on a heated disk with multiple impinging jets, *J. Heat Transfer* 113 (3) (1991) 722–727, doi:10.1115/1.2910623.

- [69] Y. Miyasaka, S. Inada, The effect of pure forced convection on the boiling heat transfer between a two-dimensional subcooled water jet and a heated surface, *J. Chem. Eng. Jpn.* 13 (1) (1980) 22–28, doi:10.1252/jcej.13.22.
- [70] Y. Miyasaka, S. Inada, Y. Owase, Critical heat flux and subcooled nucleate boiling in transient region between a two-dimensional water jet and a heated surface, *J. Chem. Eng. Jpn.* 13 (1) (1980) 29–35, doi:10.1252/jcej.13.29.
- [71] Y.J. Chen, Y.Y. Li, Z.H. Liu, Experimental study on the stagnation line heat transfer characteristics with high-velocity free slot jet impingement boiling, *Int. J. Heat Mass Transfer* 91 (2015) 282–292, doi:10.1016/j.ijheatmasstransfer.2015.07.114.
- [72] X.J. Wang, Z.H. Liu, Y.Y. Li, Experimental study of heat transfer characteristics of high-velocity small slot jet impingement boiling on nanoscale modification surfaces, *Int. J. Heat Mass Transfer* 103 (2016) 1042–1052, doi:10.1016/j.ijheatmasstransfer.2016.07.110.
- [73] D.T. Vader, G.M. Chrysler, R.C. Chu, R.E. Simons, Experimental investigation of subcooled liquid nitrogen impingement cooling of a silicon chip, *IEEE Trans. Compon. Packag. Manuf. Technol. Part A* 18 (4) (1995) 788–794, doi:10.1109/95.477465.
- [74] Y. Mitsutake, M. Monde, Ultra high critical heat flux during forced flow boiling heat transfer with an impinging jet, *J. Heat Transfer* 125 (6) (2003) 1038–1045, doi:10.1115/1.1621899.
- [75] M. Monde, K. Kitajima, T. Inoue, Y. Mitsutake, Critical heat flux in a forced convective subcooled boiling with an impinging jet, in: *Proc. Int. Heat Transfer Conf. 10*, Begell House Inc., Brighton, UK, 1994, pp. 515–520, doi:10.1615/IHTC10.1380.
- [76] M. Monde, K. Kitajima, T. Inoue, Y. Mitsutake, Critical heat flux in forced convective subcooled boiling with impinging jet: Effect of subcooling, *Trans. Jpn. Soc. Mech. Eng. Ser. B* 60 (571) (1994) 932–939, doi:10.1299/kikaib.60.932.
- [77] S.R. Mahmoudi, K. Adamiak, G.S.P. Castle, Two-phase cooling characteristics of a saturated free falling circular jet of HFE7100 on a heated disk: Effect of jet length, *Int. J. Heat Mass Transfer* 55 (21–22) (2012) 6181–6190, doi:10.1016/j.ijheatmasstransfer.2012.06.039.
- [78] T. Aihara, K. Suzuki, J.-K. Kim, K. Kasahara, Boiling heat transfer of a LN2 micro-jet in a very slender cryoprobe, *Trans. Jpn. Soc. Mech. Eng. Ser. B* 57 (538) (1991) 2112–2117, doi:10.1299/kikaib.57.2112.
- [79] T. Aihara, J.K. Kim, K. Suzuki, K. Kasahara, Boiling heat transfer of a micro-impinging jet of liquid nitrogen in a very slender cryoprobe, *Int. J. Heat Mass Transfer* 36 (1) (1993) 169–175, doi:10.1016/0017-9310(93)80076-7.
- [80] P. Zhang, G.H. Xu, X. Fu, C.R. Li, Confined jet impingement of liquid nitrogen onto different heat transfer surfaces, *Cryogenics* 51 (6) (2011) 300–308, doi:10.1016/j.cryogenics.2010.06.018.
- [81] D.G. Andrews, P.K.M. Rao, Peak heat fluxes on thin horizontal ribbons in submerged water jets, *Can. J. Chem. Eng.* 52 (3) (1974) 323–330, doi:10.1002/cjce.5450520305.
- [82] T. Kamata, S. Kumagai, T. Takeyama, Boiling heat transfer to an impinging jet spurted into a narrow space (part I, space with an open end), *Heat Transfer - Jpn. Res.* 17 (5) (1988) 71–80.
- [83] T. Kamata, S. Kumagai, T. Takeyama, Boiling Heat Transfer to an Impinging Jet Spurted into a Narrow Space: 1st Report, Space with an Open End, *Trans. Jpn. Soc. Mech. Eng. Ser. B* 53 (485) (1987) 183–187, doi:10.1299/kikaib.53.183.
- [84] C.H. Shin, K.M. Kim, S.H. Lim, H.H. Cho, Influences of nozzle-plate spacing on boiling heat transfer of confined planar dielectric liquid impinging jet, *Int. J. Heat Mass Transfer* 52 (23–24) (2009) 5293–5301, doi:10.1016/j.ijheatmasstransfer.2009.08.002.
- [85] Y. Katto, S. Yokoya, Critical heat flux on a disk heater cooled by a circular jet of saturated liquid impinging at the center, *Int. J. Heat Mass Transfer* 31 (2) (1988) 219–227, doi:10.1016/0017-9310(88)90003-8.
- [86] M. Monde, Critical heat flux in a saturated forced convective boiling with an impinging jet: Applicable limit of a generalized correlation, *Trans. Jpn. Soc. Mech. Eng. Ser. B* 50 (453) (1984) 1392–1396, doi:10.1299/kikaib.50.1392.
- [87] M. Monde, Critical heat flux in saturated forced convective boiling on a heated disk with an impinging jet, *Wärme- Und Stoffübertragung* 19 (1985) 205–209, doi:10.1007/BF01403758.
- [88] A. Sharan, J.H. Lienhard, On predicting burnout in the jet-disk configuration, *J. Heat Transfer* 107 (2) (1985) 398–401, doi:10.1115/1.3247428.
- [89] C.F. Ma, A.E. Bergles, Boiling jet impingement cooling of simulated micro-electronic chips, in: S. Oktay, A. Bar-Cohen (Eds.), *Heat Transfer in Electronic Equipment*, HTD-Vol. 28, ASME, Boston, MA, USA, 1983, pp. 5–12.
- [90] Y. Haramura, Non-condensable gas effect on critical heat flux of subcooled pool boiling of water, in: *Proc. 6th ASME-JSME Therm. Eng. Jt. Conf.*, JSME, Kohala Coast, Hawaii, USA, 2003, p. 278.
- [91] Y. Katto, Y. Haramura, Effect of velocity (Weber number) on CHF for boiling on heated plates cooled by a plane jet, in: *Proc. 18th Natl. Heat Transf. Symp. Japan*, 1981, pp. 382–384.
- [92] R.P. Baines, M.A. El Masri, W.M. Rohsenow, Critical heat flux in flowing liquid films, *Int. J. Heat Mass Transfer* 27 (9) (1984) 1623–1629, doi:10.1016/0017-9310(84)90274-6.
- [93] X. Wang, M. Monde, Critical heat flux in forced convective subcooled boiling with a plane wall jet (effect of subcooling on CHF), *Heat Mass Transfer* 33 (1–2) (1997) 167–175, doi:10.1007/s002310050175.
- [94] M. Monde, Y. Mitsutake, X. Wang, J.Z. Zhu, Critical heat flux in forced convective boiling with a plane jet: Effect of subcooling on CHF, *Trans. Jpn. Soc. Mech. Eng. Ser. B* 64 (617) (1998) 167–173, doi:10.1299/kikaib.64.167.
- [95] M. Monde, X. Wang, Critical heat flux in forced convective boiling with a plane jet (Revised correlation for saturated condition), *Heat Mass Transfer* 36 (2) (2000) 97–101, doi:10.1007/s002310050370.
- [96] M. Monde, X. Wang, Y. Mitsutake, Critical heat flux in saturated forced boiling with a plane jet, *Trans. Jpn. Soc. Mech. Eng. Ser. B* 66 (645) (2000) 1436–1439, doi:10.1299/kikaib.66.1436.
- [97] Y. Katto, K. Ishii, Burnout in a high heat flux boiling system with a forced supply of liquid through a plane jet, *Trans. Jpn. Soc. Mech. Eng.* 44 (384) (1978) 2817–2823, doi:10.1299/kikai1938.44.2817.
- [98] W. Grassi, D. Testi, Effects of ionic jets on nucleate boiling and CHF on a horizontal plate, *Int. J. Transp. Phenom.* 12 (3–4) (2011) 245–258.
- [99] W. Grassi, D. Testi, L. Urbanucci, D. Della Vista, Enhanced nucleate boiling and CHF on a small horizontal plate under ionic jet impingement, *Int. Commun. Heat Mass Transfer* 79 (2016) 67–73, doi:10.1016/j.icheatmasstransfer.2016.10.005.
- [100] P.A. de Oliveira, J.R. Barbosa, Two-phase jet impingement heat sink integrated with a compact vapor compression system for electronics cooling, in: *Proc. 15th Intersoc. Conf. Therm. Thermomech. Phenom. Electron. Syst.*, IEEE, Las Vegas, NV, USA, 2016, pp. 976–986, doi:10.1109/ITHERM.2016.7517652.
- [101] P.A. de Oliveira, J.R. Barbosa, Effect of jet length and ambient temperature on the performance of a two-phase jet impingement heat sink refrigeration system, *Int. J. Refrig.* 75 (2017) 331–342, doi:10.1016/j.ijrefrig.2017.01.001.
- [102] P.A. de Oliveira, J.R. Barbosa, Performance assessment of single and multiple jet impingement configurations in a refrigeration-based compact heat sink for electronics cooling, *J. Electron. Packag.* 139 (3) (2017) 51–53, doi:10.1115/1.4036817.
- [103] A. Inoue, T. Tanno, M. Takahashi, Y. Yamasaki, Two-dimensional impinging jet cooling of high heat flux surfaces in magnetic confinement fusion reactors, *Fusion Eng. Des.* 28 (C) (1995) 81–89, doi:10.1016/0920-3796(95)90024-1.
- [104] M. Furuya, A. Inoue, R. Tanno, Critical heat flux and convective heat transfer with a two-dimensional liquid jet impinging on flat and concave surfaces, *Trans. Jpn. Soc. Mech. Eng. Ser. B* 61 (591) (1995) 4094–4100, doi:10.1299/kikaib.61.4094.
- [105] A. Inoue, A. Ui, Y. Yamazaki, S. Lee, Studies on cooling by two-dimensional confined jet flow of high heat flux surface in fusion reactor, *Nucl. Eng. Des.* 200 (1) (2000) 317–329, doi:10.1016/S0029-5493(99)00329-5.
- [106] D. Copeland, Single-phase and boiling cooling of small pin fin arrays by multiple slot nozzle suction and impingement, *IEEE Trans. Compon. Packag. Manuf. Technol. Part A* 18 (3) (1995) 510–516, doi:10.1109/95.465145.
- [107] Y. Zhang, J. Wei, X. Kong, L. Guo, Confined submerged jet impingement boiling of subcooled FC-72 over micro-pin-finned surfaces, *Heat Transfer Eng.* 37 (3–4) (2016) 269–278, doi:10.1080/01457632.2015.1052661.
- [108] Y. Zhang, B. Liu, J. Wei, B. Sundén, Z. Wu, Heat transfer correlations for jet impingement boiling over micro-pin-finned surface, *Int. J. Heat Mass Transfer* 126 (2018) 401–413, doi:10.1016/j.ijheatmasstransfer.2018.04.167.
- [109] F.L. Cui, F.J. Hong, P. Cheng, Comparison of normal and distributed jet array impingement boiling of HFE-7000 on smooth and pin-fin surfaces, *Int. J. Heat Mass Transfer* 126 (2018) 1287–1298, doi:10.1016/j.ijheatmasstransfer.2018.06.058.
- [110] Y. Zhang, W. Chen, Boiling heat transfer of a brass beads-packed porous layer subjected to submerged jet impingement, *Heat Transfer Res* 50 (15) (2019) 1457–1476, doi:10.1615/HeatTransRes.2019027922.
- [111] Y. Zhang, W. Chen, Experimental study on jet impingement boiling heat transfer in brass beads packed porous layer, *J. Therm. Sci.* 29 (2020) 718–729, doi:10.1007/s11630-019-1148-y.
- [112] Z. Liu, Y. Qiu, Nucleate boiling on the superhydrophilic surface with a small water impingement jet, in: *Proc. Int. Heat Transfer Conf. 13: Jets*, Begell House Inc., Sydney, Australia, 2006, doi:10.1615/IHTC13.p16.150.
- [113] Z.H. Liu, Y.H. Qiu, Critical heat flux of steady boiling for water jet impingement in flat stagnation zone on superhydrophilic surface, *J. Heat Transfer* 128 (7) (2006) 726–729, doi:10.1115/1.2194045.
- [114] Y.H. Qiu, Z.H. Liu, Nucleate boiling on the superhydrophilic surface with a small water impingement jet, *Int. J. Heat Mass Transfer* 51 (7–8) (2008) 1683–1690, doi:10.1016/j.ijheatmasstransfer.2007.07.049.
- [115] Y.Y. Li, Z.H. Liu, G.S. Wang, L. Pang, Experimental study on critical heat flux of high-velocity circular jet impingement boiling on the nano-characteristic stagnation zone, *Int. J. Heat Mass Transfer* 67 (2013) 560–568, doi:10.1016/j.ijheatmasstransfer.2013.08.058.
- [116] J.H. Lay, V.K. Dhir, Nucleate boiling heat flux enhancement on macro/micro-structured surfaces cooled by an impinging jet, *J. Enhanced Heat Transfer* 2 (3) (1995) 177–188, doi:10.1615/JEnhHeatTransf.v2.i3.10.
- [117] S.N. Joshi, E.M. Dede, Two-phase jet impingement cooling for high heat flux wide band-gap devices using multi-scale porous surfaces, *Appl. Therm. Eng.* 110 (2017) 10–17, doi:10.1016/j.applthermaleng.2016.08.146.
- [118] M. Sarkar, R.P. Selvam, M. Kuss, J.C. Balda, Efficient multiphase cooling system for large area using multiple jet/spray, in: *Proc. ASME 2009 Heat Transfer Summer Conf.*, ASME, San Francisco, CA, USA, 2009, pp. 335–343, doi:10.1115/HT2009-88314.
- [119] Z.H. Liu, Y.H. Qiu, Boiling heat transfer characteristics of nanofluids jet impingement on a plate surface, *Heat Mass Transfer* 43 (7) (2007) 699–706, doi:10.1007/s00231-006-0159-x.
- [120] G. Liang, I. Mudawar, Review of pool boiling enhancement with additives and nanofluids, *Int. J. Heat Mass Transfer* 124 (2018) 423–453, doi:10.1016/j.ijheatmasstransfer.2018.03.046.
- [121] M.R. Pais, L.C. Chow, E.T. Mahefkey, Multiple jet impingement cooling, *J. Thermophys. Heat Transfer* 7 (3) (1993) 435–440, doi:10.2514/3.437.
- [122] W.R. McGillis, V.P. Carey, Immersion cooling of an array of heat dissipating elements. An assessment of different flow boiling methodologies, *Cryog. Immersion Cool. Opt. Electron. Equip.* (1990) 37–44.

- [123] M. Katsuta, T. Kurose, A study on boiling heat transfer in thin liquid film: 2nd report, As for the critical heat flux of nucleate boiling, *Trans. Jpn. Soc. Mech. Eng. Ser. B* 47 (421) (1981) 1849–1860, doi:10.1299/kikaib.47.1849.
- [124] I.A. Mudawwar, T.A. Incropera, F.P. Incropera, Boiling heat transfer and critical heat flux in liquid films falling on vertically-mounted heat sources, *Int. J. Heat Mass Transfer* 30 (10) (1987) 2083–2095, doi:10.1016/0017-9310(87)90088-3.
- [125] J.H. Lienhard, R. Eichhorn, On predicting boiling burnout for heaters cooled by liquid jets, *Int. J. Heat Mass Transfer* 22 (5) (1979) 774–776, doi:10.1016/0017-9310(79)90125-X.
- [126] Y. Haramura, Y. Katto, A new hydrodynamic model of critical heat flux, applicable widely to both pool and forced convection boiling on submerged bodies in saturated liquids, *Int. J. Heat Mass Transfer* 26 (3) (1983) 389–399, doi:10.1016/0017-9310(83)90043-1.
- [127] Y. Haramura, Y. Katto, A new hydrodynamic model of critical heat flux: Mechanism of critical heat flux for pool boiling and forced convection boiling on submerged bodies in saturated liquid, *Trans. Jpn. Soc. Mech. Eng. Ser. B* 49 (445) (1983) 1919–1927, doi:10.1299/kikaib.49.1919.
- [128] M. Kandula, Mechanisms and predictions of burnout in flow boiling over heated surfaces with an impinging jet, *Int. J. Heat Mass Transfer* 33 (9) (1990) 1795–1803, doi:10.1016/0017-9310(90)90213-E.
- [129] Z.H. Liu, Q.Z. Zhu, Prediction of critical heat flux for convective boiling of saturated water jet impinging on the stagnation zone, *J. Heat Transfer* 124 (6) (2002) 1125–1130, doi:10.1115/1.1518497.
- [130] Y.H. Qiu, Z.H. Liu, The theoretical simulation of the effect of solid-liquid contact angle on the critical heat flux of saturated water jet boiling on stagnation zone, *Int. J. Heat Mass Transfer* 53 (9–10) (2010) 1921–1926, doi:10.1016/j.ijheatmasstransfer.2009.12.064.
- [131] Y.Y. Li, Z.H. Liu, Theoretical research of critical heat flux in subcooled impingement boiling on the stagnation zone, *Int. J. Heat Mass Transfer* 55 (25–26) (2012) 7544–7551, doi:10.1016/j.ijheatmasstransfer.2012.07.043.
- [132] W. Grassi, D. Testi, A new hydrodynamic approach for jet impingement boiling CHF, *Int. Commun. Heat Mass Transfer* 104 (2019) 83–88, doi:10.1016/j.icheatmasstransfer.2019.02.014.
- [133] T. Cong, R. Chen, G. Su, S. Qiu, W. Tian, Analysis of CHF in saturated forced convective boiling on a heated surface with impinging jets using artificial neural network and genetic algorithm, *Nucl. Eng. Des.* 241 (9) (2011) 3945–3951, doi:10.1016/j.nucengdes.2011.07.029.
- [134] W. Nakayama, M. Behnia, H. Mishima, Impinging jet boiling of a fluorinated liquid on a foil heater array, *J. Electron. Packag.* 122 (2) (2000) 132–137, doi:10.1115/1.483145.
- [135] M.K. Sung, I. Mudawar, Correlation of critical heat flux in hybrid jet impingement/micro-channel cooling scheme, *Int. J. Heat Mass Transfer* 49 (15–16) (2006) 2663–2672, doi:10.1016/j.ijheatmasstransfer.2006.01.008.
- [136] M.K. Sung, I. Mudawar, CHF determination for high-heat flux phase change cooling system incorporating both micro-channel flow and jet impingement, *Int. J. Heat Mass Transfer* 52 (3–4) (2009) 610–619, doi:10.1016/j.ijheatmasstransfer.2008.07.035.
- [137] J. Lee, I. Mudawar, Experimental investigation and theoretical model for subcooled flow boiling pressure drop in microchannel heat sinks, *J. Electron. Packag.* 131 (3) (2009) 031008, doi:10.1115/1.3144146.
- [138] D.D. Hall, I. Mudawar, Ultra-high critical heat flux (CHF) for subcooled water flow boiling-II: High-CHF database and design equations, *Int. J. Heat Mass Transfer* 42 (8) (1999) 1429–1456, doi:10.1016/S0017-9310(98)00242-7.
- [139] M.B. Bowers, I. Mudawar, Parametric study of ultra-high CHF in highly subcooled water flow inside small diameter tubes, in: J.C. Chen, Y. Fujita, F. Mayinger, R.A. Nelson (Eds.), *Convective Flow Boiling*, Taylor & Francis, Washington, DC, USA, 1996, pp. 117–122.
- [140] M.K. Sung, I. Mudawar, Effects of jet pattern on two-phase performance of hybrid micro-channel/micro-circular-jet-impingement thermal management scheme, *Int. J. Heat Mass Transfer* 52 (13–14) (2009) 3364–3372, doi:10.1016/j.ijheatmasstransfer.2008.06.046.
- [141] M.K. Sung, I. Mudawar, Single-Phase and two-phase hybrid cooling schemes for high-heat-flux thermal management of defense electronics, *J. Electron. Packag.* 131 (2) (2009) 021013, doi:10.1115/1.3111253.
- [142] D. Guo, J.J. Wei, Y.H. Zhang, Enhanced flow boiling heat transfer with jet impingement on micro-pin-finned surfaces, *Appl. Therm. Eng.* 31 (11–12) (2011) 2042–2051, doi:10.1016/j.applthermaleng.2011.03.017.
- [143] G. Choi, B.S. Kim, H. Lee, S. Shin, H.H. Cho, Jet impingement in a crossflow configuration: Convective boiling and local heat transfer characteristics, *Int. J. Heat Fluid Flow* 50 (2014) 378–385, doi:10.1016/j.ijheatfluidflow.2014.09.010.
- [144] S.M. Kim, I. Mudawar, Universal approach to predicting saturated flow boiling heat transfer in mini/micro-channels – Part I. Dryout incipience quality, *Int. J. Heat Mass Transfer* 64 (2013) 1226–1238, doi:10.1016/j.ijheatmasstransfer.2013.04.016.
- [145] H. Martin, Heat and Mass Transfer between Impinging Gas Jets and Solid Surfaces, *Adv. Heat Transfer* 13 (C) (1977) 1–60, doi:10.1016/S0065-2717(08)70221-1.
- [146] S. Polat, B. Huang, A.S. Mujumdar, W.J.M. Douglas, Numerical flow and heat transfer under impinging jets: A review, *Annu. Rev. Heat Transfer* 2 (2) (1989) 157–197, doi:10.1615/AnnualRevHeatTransfer.v2.60.
- [147] K. Jambunathan, E. Lai, M.A. Moss, B.L. Button, A review of heat transfer data for single circular jet impingement, *Int. J. Heat Fluid Flow* 13 (2) (1992) 106–115, doi:10.1016/0142-727X(92)90017-4.
- [148] R. Viskanta, Heat transfer to impinging isothermal gas and flame jets, *Exp. Therm. Fluid Sci.* 6 (2) (1993) 111–134, doi:10.1016/0894-1777(93)90022-B.
- [149] B.W. Webb, C.-F. Ma, Single-phase liquid jet impingement heat transfer, in: J.P. Hartnett (Ed.), *Adv. Heat Transfer*, Academic Press, New York, NY, USA, 1995, pp. 105–217, doi:10.1016/S0065-2717(08)70296-X.
- [150] B. Han, R.J. Goldstein, Jet-impingement heat transfer in gas turbine systems, *Ann. N. Y. Acad. Sci.* 934 (1) (2001) 147–161, doi:10.1111/j.1749-6632.2001.tb05849.x.
- [151] N. Zuckerman, N. Lior, Impingement heat transfer: Correlations and numerical modeling, *J. Heat Transfer* 127 (5) (2005) 544–552, doi:10.1115/1.1861921.
- [152] N. Zuckerman, N. Lior, Jet impingement heat transfer: Physics, correlations, and numerical modeling, *Adv. Heat Transfer* 39 (C) (2006) 565–631, doi:10.1016/S0065-2717(06)39006-5.
- [153] B. Weigand, S. Spring, Multiple jet impingement - A review, *Heat Transfer Res* 42 (2) (2011) 101–142, doi:10.1615/HeatTransRes.v42.i2.30.
- [154] A. Dewan, R. Dutta, B. Srinivasan, Recent trends in computation of turbulent jet impingement heat transfer, *Heat Transfer Eng* 33 (4–5) (2012) 447–460, doi:10.1080/01457632.2012.614154.
- [155] A. Sarkar, N. Nitin, M.V. Karve, R.P. Singh, Fluid flow and heat transfer in air jet impingement in food processing, *J. Food Sci.* 69 (4) (2004) CRH113–CRH122, doi:10.1111/j.1365-2621.2004.tb06315.x.
- [156] G.M. Carlomagno, A. Ianiro, Thermo-fluid-dynamics of submerged jets impinging at short nozzle-to-plate distance: A review, *Exp. Therm. Fluid Sci.* 58 (2014) 15–35, doi:10.1016/j.expthermfluidsci.2014.06.010.
- [157] C.F. Ma, Y.P. Gan, Y.C. Tian, D.H. Lei, T. Gomi, Liquid jet impingement heat transfer with or without boiling, *J. Therm. Sci.* 2 (1) (1993) 32–49, doi:10.1007/BF02650835.
- [158] J.H. Lienhard, Liquid jet impingement, *Annu. Rev. Heat Transfer* 6 (6) (1995) 199–270, doi:10.1615/AnnualRevHeatTransfer.v6.60.
- [159] H.H. Cho, K.M. Kim, J. Song, Applications of impingement jet cooling systems, in: *Cooling Systems: Energy, Engineering and Applications*, Nova Science Publishers, Inc., New York, NY, USA, 2011, pp. 37–67.
- [160] M. Molana, S. Banooni, Investigation of heat transfer processes involved liquid impingement jets: A review, *Braz. J. Chem. Eng.* 30 (3) (2013) 413–435, doi:10.1590/S0104-66322013000300001.
- [161] J. Mohammadpour, A. Lee, Investigation of nanoparticle effects on jet impingement heat transfer: A review, *J. Mol. Liq.* 316 (2020) 113819, doi:10.1016/j.molliq.2020.113819.
- [162] D.H. Wolf, F.P. Incropera, R. Viskanta, Jet Impingement Boiling, *Adv. Heat Transfer*, 1993, pp. 1–132, doi:10.1016/S0065-2717(08)70005-4.
- [163] L. Qiu, S. Dubej, F.H. Choo, F. Duan, Recent developments of jet impingement nucleate boiling, *Int. J. Heat Mass Transfer* 89 (2015) 42–58, doi:10.1016/j.ijheatmasstransfer.2015.05.025.
- [164] S. Fan, F. Duan, A review of two-phase submerged boiling in thermal management of electronic cooling, *Int. J. Heat Mass Transfer* 150 (2020) 119324, doi:10.1016/j.ijheatmasstransfer.2020.119324.
- [165] S. Ishigai, M. Mizuno, Boiling heat transfer with an impinging water jet (about the critical heat flux), *Prepr. JSME* 740–16 (1974) 139–142.
- [166] M. Katsuta, Boiling heat transfer of liquid film: 6th report, Test fluid is Freon R-113, in: *14th Natl. Heat Transf. Symp. Jpn.*, 1977, pp. 154–156.
- [167] M. Monde, Burnout heat flux in saturated forced convection boiling with an impinging jet, *Heat Transfer - Jpn. Res.* 9 (1980) 31–41.
- [168] M. Monde, Burnout in high heat-flux boiling system with an impinging jet: 3rd Report, Extension of a generalized correlation of burnout heat flux, *Trans. Jpn. Soc. Mech. Eng. Ser. B* 46 (406) (1980) 1146–1155, doi:10.1299/kikaib.46.1146.
- [169] T. Kamata, S. Kumagai, T. Takeyama, Boiling Heat Transfer to an Impinging Jet Spurred into a Narrow Space, *Trans. Jpn. Soc. Mech. Eng. Ser. B* 53 (485) (1987) 188–192, doi:10.1299/kikaib.53.188.
- [170] T. Kamata, S. Kumagai, T. Takeyama, Boiling heat transfer to an impinging jet spurred into a narrow space (part II. Space with a limited end), *Heat Transfer - Jpn. Res.* 17 (4) (1988) 1–11.
- [171] C.S.K. Cho, K. Wu, Comparison of burnout characteristics in jet impingement cooling and spray cooling, in: *Proc. Natl. Heat Transfer Conf.*, ASME, Houston, TX, USA, 1988, pp. 561–567.
- [172] S.S. Kutateladze, *Heat Transfer in Condensation and Boiling*, State Scientific and Technical Publishers of Literature on Machinery, 2nd ed., Leningrad, Moscow, 1952.
- [173] M. Ishimaru, J.K. Kim, T. Aihara, T. Shimoyama, Boiling heat transfer characteristics due to a micro-impinging jet of LN₂, in: *Proc. 28th Natl. Heat Transf. Symp. Japan*, 1991, pp. 730–732.
- [174] W. Nakayama, D. Copeland, Heat transfer from chips to dielectric coolant: enhanced pool boiling versus jet-impingement cooling, *J. Enhanced Heat Transfer* 1 (3) (1994) 231–243, doi:10.1615/JEnhHeatTransf.v1.i3.50.
- [175] M. Monde, Y. Mitsutake, Critical heat flux in forced convective subcooled boiling with multiple impinging jets, *J. Heat Transfer* 118 (1) (1996) 241–243, doi:10.1115/1.2824051.
- [176] M. Monde, Y. Mitsutake, K. Inamitu, Critical heat flux in forced convective subcooled boiling with multiple impinging jets: Effect of subcooling, *Trans. Jpn. Soc. Mech. Eng. Ser. B* 61 (585) (1995) 1750–1753, doi:10.1299/kikaib.61.1750.
- [177] C. Kamata, Experimental study on boiling heat transfer to an impinging jet on a hot block, Kagaku Kogaku Ronbunshu 23 (4) (1997) 526–531, doi:10.1252/kakoronbunshu.23.526.
- [178] C. Kamata, Experimental study on boiling heat transfer with an impinging jet on a hot block, *Heat Transfer - Asian Res* 28 (5) (1999) 418–427, doi:10.1002/(SICI)1523-1496(1999)28:5<418::AID-HTJ7>3.0.CO;2-O.

- [179] A.A.O. Tay, Hong Xue, C. Yang, Cooling of electronic components with free jet impingement boiling, in: Proc. 8th Intersoc. Conf. Therm. Thermomech. Phenom. Electron. Syst., IEEE, San Diego, CA, USA, 2002, pp. 387–394, doi:[10.1109/ITHERM.2002.1012482](https://doi.org/10.1109/ITHERM.2002.1012482).
- [180] W.R. Gambill, J.H. Lienhard, An upper bound for the critical boiling heat flux, *J. Heat Transfer* 111 (3) (1989) 815–818, doi:[10.1115/1.3250759](https://doi.org/10.1115/1.3250759).
- [181] Y. Mitsutake, M. Monde, H. Ueda, Y. Yoshida, Upper limit of forced boiling with an impinging jet: Challenge to achieve critical heat flux beyond 200 MW/m² with highly subcooled liquid, *Trans. Jpn. Soc. Mech. Eng. Ser. B* 69 (681) (2003) 1242–1247, doi:[10.1299/kikaib.69.1242](https://doi.org/10.1299/kikaib.69.1242).
- [182] D.W. Zhou, C.F. Ma, Local jet impingement boiling heat transfer with R113, *Heat Mass Transfer* 40 (6–7) (2004) 539–549, doi:[10.1007/s00231-003-0463-7](https://doi.org/10.1007/s00231-003-0463-7).
- [183] R. Cardenas, P. Mani, V. Narayanan, Submerged jet impingement boiling of saturated water under sub-atmospheric conditions, in: Proc. ASME 2010 8th Int. Conf. Nanochannels, Microchannels, Minichannels, ASME, Montreal, Quebec, Canada, 2010, pp. 343–351, doi:[10.1115/FEDSM-ICNMM2010-30749](https://doi.org/10.1115/FEDSM-ICNMM2010-30749).
- [184] R. Cardenas, Submerged jet impingement boiling thermal management, Ph.D. Thesis, Oregon State University, OR, USA, 2011.
- [185] R. Cardenas, V. Narayanan, Heat transfer characteristics of submerged jet impingement boiling of saturated FC-72, *Int. J. Heat Mass Transfer* 55 (15–16) (2012) 4217–4231, doi:[10.1016/j.ijheatmasstransfer.2012.03.063](https://doi.org/10.1016/j.ijheatmasstransfer.2012.03.063).
- [186] R. Cardenas, V. Narayanan, Critical heat flux during submerged jet impingement boiling of saturated water at sub-atmospheric conditions, in: Proc. ASME 2011 Pacific Rim Tech. Conf. Exhib. Packag. Integr. Electron. Photon. Syst., ASME, Portland, Oregon, USA, 2011, pp. 95–106, doi:[10.1115/IPACK2011-52043](https://doi.org/10.1115/IPACK2011-52043).
- [187] D. Mikielewicz, T. Muszyński, J. Mikielewicz, Model of heat transfer in the stagnation point of rapidly evaporating microjet, *Arch. Thermodyn.* 33 (1) (2012) 139–152, doi:[10.2478/v10173-012-0007-y](https://doi.org/10.2478/v10173-012-0007-y).
- [188] N. Bin, W. Jie, L. Jun, D. Hongwu, Experimental investigation to boiling heat transfer on a heated surface with multiple impinging jets, *Adv. Mater. Res.* 663 (2013) 477–482, doi:[10.4028/www.scientific.net/AMR.663.477](https://doi.org/10.4028/www.scientific.net/AMR.663.477).
- [189] C. de Brún, R. Jenkins, T.L. Lupton, R. Lupoi, R. Kempers, A.J. Robinson, Confined jet array impingement boiling, *Exp. Therm. Fluid Sci.* 86 (2017) 224–234, doi:[10.1016/j.expthermflusci.2017.04.002](https://doi.org/10.1016/j.expthermflusci.2017.04.002).
- [190] G.D. Naidu, S. Khandekar, Boiling microjet impinging cooling at subatmospheric pressures: Visualization and heat transfer characteristics, *Interfacial Phenom. Heat Transfer* 6 (4) (2018) 437–449, doi:[10.1615/InterfacPhenomHeatTransfer.2019030188](https://doi.org/10.1615/InterfacPhenomHeatTransfer.2019030188).
- [191] S. Ishigai, S. Nakanishi, T. Ochi, Boiling heat transfer for a plane water jet impinging on a hot surface, in: Proc. Int. Heat Transfer Conf. 6, Begell House Inc., Toronto, Canada, 1978, pp. 445–450, doi:[10.1615/IHTC6.860](https://doi.org/10.1615/IHTC6.860).
- [192] S. Nakanishi, S. Ishigai, T. Ochi, I. Morita, Cooling of a hot surface by a plane water jet, *Trans. Jpn. Soc. Mech. Eng. Ser. B* 46 (404) (1980) 714–724, doi:[10.1299/kikaib.46.714](https://doi.org/10.1299/kikaib.46.714).
- [193] M. Furuya, A. Inoue, R. Tanno, Critical heat flux and convection heat transfer with a planar liquid jet impinging on flat and concave surfaces, *Heat Transfer - Jpn. Res.* 24 (7) (1995) 637–650.
- [194] H. Robidou, H. Auracher, P. Gardin, M. Lebouché, L. Bogdanić, Local heat transfer from a hot plate to a water jet, *Heat Mass Transfer* 39 (10) (2003) 861–867, doi:[10.1007/s00231-002-0335-6](https://doi.org/10.1007/s00231-002-0335-6).
- [195] L. Bogdanic, H. Auracher, F. Ziegler, Two-phase structure above hot surfaces in jet impingement boiling, *Heat Mass Transfer* 45 (7) (2009) 1019–1028, doi:[10.1007/s00231-007-0272-5](https://doi.org/10.1007/s00231-007-0272-5).
- [196] M. Monde, Y. Katto, Study of burn-out in a high heat-flux boiling system with an impinging jet: Part 2, Generalized nondimensional correlation for the burn-out heat flux, *Trans. Jpn. Soc. Mech. Eng.* 43 (373) (1977) 3408–3416, doi:[10.1299/kikai1938.43.3408](https://doi.org/10.1299/kikai1938.43.3408).
- [197] J.H. Lienhard, R. Eichhorn, Peak boiling heat flux on cylinders in a cross flow, *Int. J. Heat Mass Transfer* 19 (10) (1976) 1135–1142, doi:[10.1016/0017-9310\(76\)90146-0](https://doi.org/10.1016/0017-9310(76)90146-0).
- [198] J.H. Lienhard, M.Z. Hasan, Correlation of burnout data for disk heaters cooled by liquid jets, *J. Heat Transfer* 101 (2) (1979) 383–384, doi:[10.1115/1.3450984](https://doi.org/10.1115/1.3450984).
- [199] M. Katsuta, Boiling heat transfer of liquid film: 7th report, Critical heat flux of impinging jet of liquid with surfactant, *Prepr. JSME* (1978) 68–70 780–18.
- [200] M. Monde, H. Kusuda, O. Nagae, Critical heat flux of saturated forced convective boiling with an impinging jet, in: Proc. 19th Natl. Heat Transf. Symp. Japan, 1982, pp. 469–498.
- [201] S. Kumagai, Y. Sano, T. Kamata, S. Suzuki, R. Kubo, Boiling Heat Transfer to an Impinged Jet in Cooling a Hot Metal Slab, *Trans. Jpn. Soc. Mech. Eng. Ser. B* 60 (570) (1994) 609–613, doi:[10.1299/kikaib.60.609](https://doi.org/10.1299/kikaib.60.609).
- [202] Y. Katto, Critical Heat Flux, in: J.P. Hartnett, T.F. Irvine (Eds.), *Adv. Heat Transfer*, Academic Press, New York, NY, USA, 1985, pp. 1–64, doi:[10.1016/S0065-2717\(08\)70284-3](https://doi.org/10.1016/S0065-2717(08)70284-3).
- [203] T.L. Bergman, A.S. Lavine, F.P. Incropera, D.P. Dewitt, *Fundamentals of Heat and Mass Transfer*, 8th ed., John Wiley & Sons, Inc., New York, NY, USA, 2017.
- [204] T. Inoue, N. Kawae, M. Monde, Effect of subcooling on critical heat flux during pool boiling on a horizontal heated wire, *Heat Mass Transfer* 33 (5–6) (1998) 481–488, doi:[10.1007/s002310050219](https://doi.org/10.1007/s002310050219).
- [205] R. Cardenas, V. Narayanan, A correlation for critical heat flux in submerged jet impingement, in: Proc. ASME 2012 Heat Transfer Summer Conf., ASME, Rio Grande, Puerto Rico, USA, 2012, pp. 473–486, doi:[10.1115/HT2012-58376](https://doi.org/10.1115/HT2012-58376).
- [206] R. Cardenas, V. Narayanan, A generalized critical heat flux correlation for submerged and free surface jet impingement boiling, *J. Heat Transfer* 136 (9) (2014) 091501, doi:[10.1115/1.4027552](https://doi.org/10.1115/1.4027552).
- [207] X. Quan, L. Dong, P. Cheng, A CHF model for saturated pool boiling on a heated surface with micro/nano-scale structures, *Int. J. Heat Mass Transfer* 76 (2014) 452–458, doi:[10.1016/j.ijheatmasstransfer.2014.04.037](https://doi.org/10.1016/j.ijheatmasstransfer.2014.04.037).
- [208] Z. Zhao, Y. Peles, M.K. Jensen, Water jet impingement boiling from structured-porous surfaces, *Int. J. Heat Mass Transfer* 63 (2013) 445–453, doi:[10.1016/j.ijheatmasstransfer.2013.03.085](https://doi.org/10.1016/j.ijheatmasstransfer.2013.03.085).